Electronic Theses and Dissertations

8-2014

Electrochemical and microfabrication strategies for remotely operated heavy metal sensor networks for water analysis : the dual challenges of calibration-less measurement and sample pretreatment.

Mohamed M. Marei
University of Louisville

ELECTROCHEMICAL AND MICROFABRICATION STRATEGIES
FOR REMOTELY OPERATED HEAVY METAL SENSOR NETWORKS
FOR WATER ANALYSIS:
THE DUAL CHALLENGES OF CALIBRATION-LESS MEASUREMENT
AND SAMPLE PRETREATMENT

By

Mohamed M. Marei

B.S., University of Cincinnati, 2006
M.S., University of Cincinnati, 2009

A Dissertation
Submitted to the Faculty of the
College of Arts and Sciences of the University of Louisville
in Partial Fulfillment of the Requirements
for the Degree of

Doctor of Philosophy

Department of Chemistry
University of Louisville
Louisville, Kentucky

August 2014

ELECTROCHEMICAL AND MICROFABRICATION STRATEGIES
FOR REMOTELY OPERATED HEAVY METAL SENSOR NETWORKS
FOR WATER ANALYSIS:
THE DUAL CHALLENGES OF CALIBRATION-LESS MEASUREMENT
AND SAMPLE PRETREATMENT

By

Mohamed M. Marei

B.S., University of Cincinnati, 2006
M.S., University of Cincinnati, 2009

A Dissertation Approved On

August 8, 2014

By the following Dissertation Committee:

_____
Dissertation Director
Richard P. Baldwin, Ph.D.

_____
Robert S. Keynton, Ph.D.

_____
Craig A. Grapperhaus, Ph.D.

_____
Francis P. Zamborini, Ph.D.

DEDICATION

This dissertation is dedicated to my beloved son

Elias M. Marei

aka blueb

Born March 15, 2014

who stole my heart on that very first day

hope you grow up strong

and sing your own song

ACKNOWLEDGEMENTS

ABSTRACT

ELECTROCHEMICAL AND MICROFABRICATION STRATEGIES
FOR REMOTELY OPERATED HEAVY METAL SENSOR NETWORKS
FOR WATER ANALYSIS:
THE DUAL CHALLENGES OF CALIBRATION-LESS MEASUREMENT
AND SAMPLE PRETREATMENT

Mohamed M. Marei

August 8, 2014

Current heavy metal monitoring in water utilizes sophisticated instrumental methods at centralized laboratories. For many applications, a preferable approach is the deployment of remote sensor networks. To this end, electrochemical methods in conjunction with microfabricated sensors potentially offer the required sensitivity and practical advantages including inexpensive sensors, reduced need for manual operation, reduced energy requirements, and also takes advantage of existing technologies such as communications networks for real-time data acquisition. The remote sensor platform developed herein consists of a photo-lithographically patterned gold electrode on SiO_2 substrate within a custom stopped-flow thin-layer cell (TLC). Metal concentrations were evaluated by anodic stripping coulometry (ASC), where it was possible to pre-concentrate all dissolved metals from the finite TLC volume in about a minute. Unlike previously reported ASC approaches which rely on either linear sweep voltammetry or chronopotentiometry, the ASC variant described herein utilizes a potential step to

simultaneously strip all deposited metals. The use of a double potential step ASC method also allowed *in situ* blank subtraction without the need for a separate blank solution. To achieve selectivity, several deposition potentials are used to pre-concentrate only those metals which can be reduced at a given potential. This method is demonstrated to be capable of measuring 500 ppb As(III) to better than 10% error even in the presence of high interferent levels (1.3 ppm Cu^{2+}, 500 ppb Cd^{2+}, 500 ppb Pb^{2+}, and 5 ppm Zn^{2+}). Similar performance was possible for As(III) spiked Ohio River water after pH adjustment. For more negatively reduced metals, dissolved oxygen (DO) reduction interferes with stripping analysis. An indirect in-line electrochemical DO removal device (EDOR), utilizing a silver cathode to reduce DO in a fluidically isolated chamber from the sample stream, was therefore developed. This device is capable of 98 % DO removal at flow rates approaching 50 µL/min with power consumption as low as 165 mW hr L^{-1}. Besides our specific stripping application, this device is well suited for Lab on Chip (LOC) applications where miniaturized DO removal and/or regulation are desirable.

TABLE OF CONTENTS

viii

LIST OF TABLES

LIST OF FIGURES

LIST OF EQUATIONS

CHAPTER I

INTRODUCTION AND BACKGROUND

1.1 Foreword

In beginning this work, an analytical chemistry dissertation, it is arguably most useful to begin with a description of what analytical chemistry is and what its aims are, or perhaps should be. The experimentally practicable chemistry sub-disciplines are always named, and rightly so, after the compounds they study (e.g., biochemistry, inorganic chemistry, etc.) or the concepts and processes they apply to understand phenomena (e.g., physical chemistry). Using this naming convention as a guide, it is self-evident that analytical chemistry is best described as the *chemical analysis* of materials to achieve qualitative chemical identifications or sensitive quantitative measurements. Naturally, this requires that chemical analysis involve the separation of species in addition to their detection. The diverse separation and detection requirements of different samples have resulted in the development of myriad instruments and techniques. However, the techniques and instruments of chemical analysis are only *tools* to achieve the desired outcome – *practical, sensitive, and selective measurements*. The work in this dissertation is focused on the development of more practical heavy metal sensors for use in environmental monitoring applications. The enhanced practicality arises from the concept

of truly remote sensors, which can simultaneously monitor many sites without any intervention by an operator. Accordingly, the dual challenges of signal calibration and sample pretreatment, which are typically performed by the operator, are the focus of this work. These challenges are shown to be satisfactorily addressable by electrochemical methods in conjunction with miniature (i.e., microfabricated) sensors since these offer important practical advantages.

1.2 Practical, Sensitive, Selective Measurements

In terms of sensitivity, modern analytical methods are capable of routine measurements of trace quantities of many analytes. There are even instances where the detection of a single analyte molecule is at least technically possible [1-2]. In terms of selectivity, it is possible to sort and separate species by methods such as chromatography and mass spectrometry and multi-dimensional combinations thereof prior to detection. In some instances, the use of analyte specific probes such as antibody assays and the more recent development of synthetic nucleic acid sequences known as aptamers allows direct detection of analytes in complex mixtures without prior separation [3-4]. Alternatively, it may be possible to use selective methodologies (which are insensitive to interferents) for direct detection of analytes in complex mixtures [4-5]. Note that the term selectivity is used here over the term specificity, according to the IUPAC recommendation, and is defined as the extent to which particular analytes can be determined under given conditions in mixtures or matrices, simple or complex, without interferences from other components [7].

Modern analysis is thus capable of both *sensitive* and *selective* measurements, and performance in those regards can be evaluated objectively. The *practicality* of an analysis is, however, more complicated to evaluate since it is an amalgamation of many criteria including the desired accuracy and speed of analysis, the number of samples, the required frequency of analysis, instrument and reagent cost, personnel training, reagent safety, disposal of waste, etc. The complexity of these criteria does sometimes allow sophisticated instruments operated by specialized personnel to be, in fact, the most practical solution. This may be the case in a centralized laboratory where the flexibility of doing many types of analysis is important and highly trained personnel are available.

The practicality of the conventional analysis approach described above, however, is especially diminished when the number of samples or the frequency of analysis exceeds a given threshold. This loss of practicality may be due to the increased costs of instruments, reagents, or personnel. Even in the absence of these constraints and if all the costs are met, it is perhaps more important to consider the *type* of the measurements being provided. Large numbers of samples, of course, arise from the sampling of a large number of sites over extended periods of time. Thus, the central laboratory approach to analysis must also address the issues of sample collection, sample stabilization to prevent changes in the species to be measured, and transportation to the laboratory. And even when these additional requirements are met, the resulting measurement is a *snapshot* which reflects the level of a given species or parameter at a particular time and place.

1.3 Increasing Snapshot Frequency: Portable Analysis

One effort to increase the frequency of snapshots has been to develop portable analyses which can be performed in the field. Portable analyses essentially bring the lab to the sample rather than bringing each sample to the central laboratory. One of the primary obstacles has been the development of suitable *sensors* – i.e., sufficiently simplified, inexpensive, and reliable methodology and instrumentation. Indeed, the entire fields of lab on a chip (LOC) and micro total analysis systems (µTAS) have emerged to address the need for such practical sensors for decentralized analysis. Although decentralized sensing has potentially limitless utility, the most useful applications are arguably in the fields of biomedical point-of-care (POC) diagnostics and environmental monitoring. Not surprisingly, both fields share the challenge of a large number of dispersed samples that make routine centralized analysis impractical. Point-of-care diagnostics conducted by a technician at the doctor's office or, preferably, by the patients at home allows for more rapid response to medical conditions which require prompt treatment, and offers the potential of reducing healthcare costs.

1.3.1 An Example: The Blood Glucose Meter

One of the great successes of modern decentralized analysis has in fact been in the field of biomedical POC diagnostics. The blood glucose meter (BGM) is a testament to the utility of portable, inexpensive sensors which can simultaneously provide practical, sensitive, and selective measurements; and this achievement certainly merits more than passing mention in this work. Regular self-monitoring of blood glucose levels is now standard practice for millions of diabetics who are estimated to comprise as much as 5%

of the global population **[8]**. Most of the commercial BGMs use miniature sensors in conjunction with electrochemical detection by a portable battery powered potentiostat, as shown in **Figure 1.1**. Nowadays, the most commonly used electrochemical detection schemes are amperometry or coulometry which are used to monitor the current or charge, respectively, in response to the presence of glucose as shown in **Figure 1.2 [9]**. Selectivity is provided by the indirect detection of glucose according to the scheme of **Figure 1.3**: A glucose specific enzyme, most commonly glucose oxidase or glucose dehydrogenase, first oxidizes glucose and the reduced enzyme is re-oxidized by a suitable mediator **[9]**. The reduced mediator generated during enzyme re-oxidation, which reflects blood glucose levels, is subsequently detected at the electrode **[9]**.

Figure 1.1: A) An assortment of electrochemical miniature blood glucose test strips sampling 1 µL or less from several manufacturers **[10]**. **B)** Four generations of portable, battery-powered BGM meters with sampling times of 5 seconds to 2 minutes.
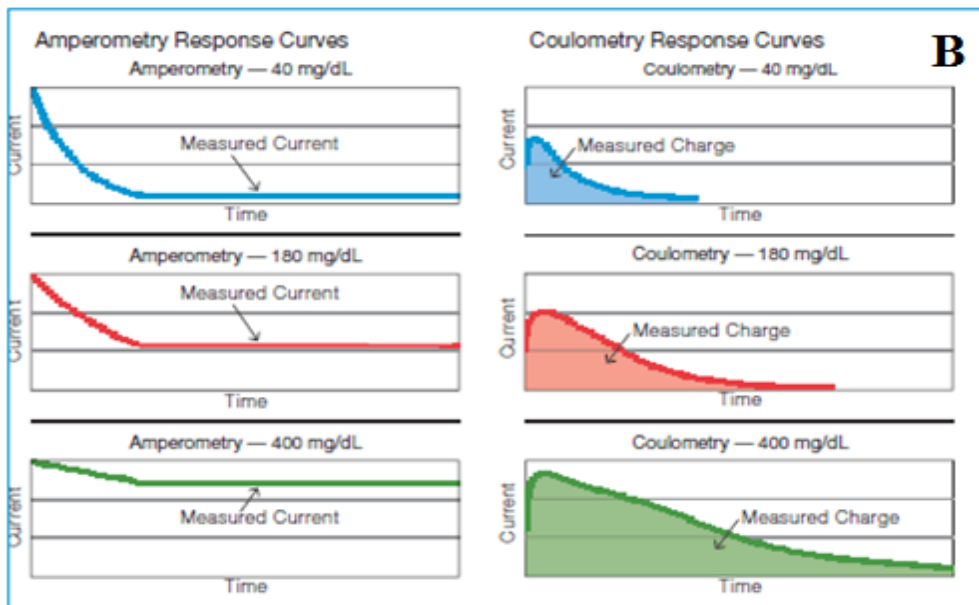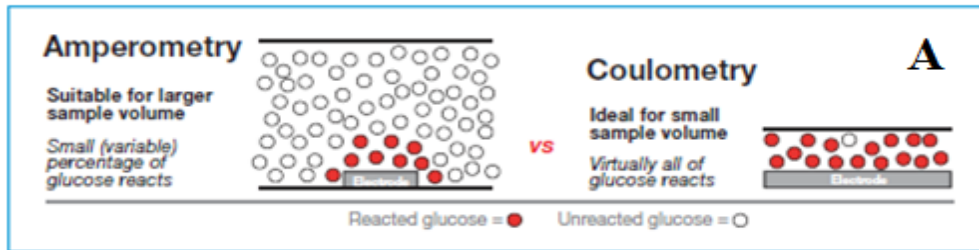
Figure 1.2: A) A sampling of electrochemical detection schemes for blood glucose monitoring. **B)** The raw data response of an amperometric and coulometric BGM. In amperometry, the response is the current measurement at a pre-determined time. In coulometry, the response is the area under the curve. **[9]**
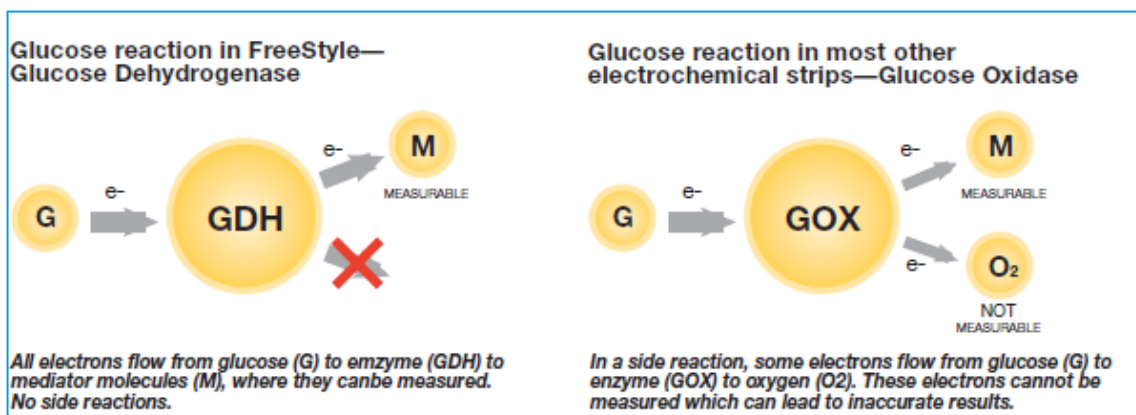
Figure 1.3: A comparison of the commonly employed enzymes in the modern BGM. Contrary to the illustration at right, early BGMs relied on a secondary hydrogen peroxide responsive enzyme to measure the H_2O_2 byproduct of O_2 reduction. **[9]**

1.3.2 Practicality, Sensitivity, and Selectivity of the BGM

The different sensors exhibit a wide variety of approaches to increase stability and enhance selectivity for glucose over interferents such as ascorbic and uric acids. These innovations include the use of different enzyme cofactors, electrode materials, electron mediators, electrode coatings to limit access of interferents, operating potential, and detection mode, along with other improvements which aid reliability. Most of these lie well outside the scope of this work, and excellent reviews are available for the interested reader **[10-11]**. Most important and perhaps most easily overlooked is the elimination of the trained operator in all of these approaches which is of great relevance to the current work. The BGM employs the patient themselves as the operator, and provides simple directions for the use of disposable test strips to reduce trained operator intervention (i.e., doctor visits and lab tests). Also relevant to this work is the BGMs demonstration that electrochemical detection in miniaturized sensors is a 'proven commodity' for decentralized analysis. The choice of electrochemical methods allows for sensitivity since small currents are readily and accurately measurable and selectivity with proper choice of electrode materials and modifications, and it also supports practicality by virtue of its low cost and sensitivity (small samples are possible, if not preferable). Miniature sensors further support practicality due to the cost and reagent savings.

1.4 The Role of the Operator

Although decentralized sensing goes some ways towards increasing the frequency of snapshots, the role of the operator remains essential and should not be overlooked. For the BGM, the patient can actively decide on the frequency of snapshots in their capacity

as the operator. Typically, the operator is responsible for essential tasks such as calibration and, in some cases, sample pretreatment, along with periodic maintenance and troubleshooting. Less obviously, the operator is also needed to collect the sample and introduce it to the sensor and to replace individual sensors after the prescribed number of uses. In the case of POC diagnostics, and the BGM in particular, readily available untrained caregivers or end users themselves are capable of serving as the operator when a few conditions are met.

1.4.1 Calibration and Sample Pretreatment in the BGM

For BGM calibration, stringent quality control has been used to allow a few randomly selected sensors to initially establish a 'calibration code' for the entire batch, which is manually entered or automatically recognized by the pre-programmed handheld potentiostat [10-11]. To reduce complexity, some manufacturers have even eliminated coding entirely and focus solely on stringent quality control so that all sensors respond identically [10-11]. Sample pretreatment is eliminated by built-in sensor selectivity based on enzymatic assays or the use of filtering/trapping layers which limit the access of interferents to the electrode surface [10-11]. To further reduce errors by untrained operators, a variety of additional measures have also been implemented. For instance, the Freestyle sensor, shown in **Figure 1.4**, incorporates additional electrodes, besides those used for analysis, to ensure that the sampled blood volume is consistent since volume is a critical consideration for the coulometric mode of operation of that sensor [9].
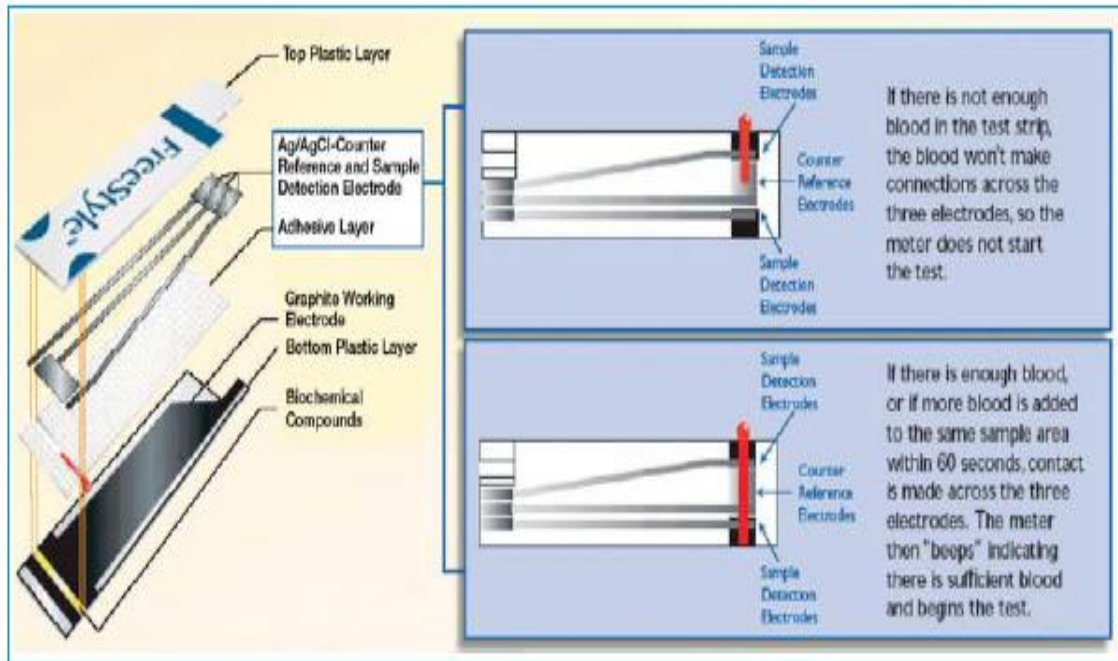
Figure 1.4: Left: Construction of the Freestyle BGM test strip. **Right:** Schematic of the fill electrodes used to ensure consistent sample volumes. **[9]**

1.4.2 Operators in Environmental Monitoring

In environmental monitoring, where decentralized sensing is also of potentially great use, the widely dispersed sampling opportunities cannot be so conveniently attached to an operator. However, there exists an entire class of environmental contaminants which can be monitored electrochemically, namely heavy metals. Thus, a similar approach to the blood glucose meter – electrochemical monitoring using simple, portable, miniature sensors – is capable of increasing the frequency of snapshots. Indeed this is an active research area as demonstrated by the abundance of publications and reviews on portable metal analysis in the recent literature **[12-13]**. Despite these developments, large scale monitoring of many sites over extended periods would still require considerable numbers of technicians, each of whom is armed with a mobile sensor, to visit those sites. Hence, what may be practical in the biomedical POC applications is less useful in environmental monitoring.

1.4.3 Portable vs. Remote Sensors

The distinction between *portable* and *remote* methods is therefore a critical one, in which the former may require only an untrained operator while the latter should require only periodic maintenance. The need for any sort of operator disallows complete avoidance of snapshots, and continuous real-time monitoring thus remains a largely unrealized but nonetheless desirable outcome. In fact, even for the BGM where operators are readily available, recent developments include so called continuous glucose monitoring (CGM) using implantable sensors which autonomously monitor glucose levels with minimal operator intervention **[14]**. These can be connected to a portable belt-

worn potentiostat which can alert the user and possibly even to an insulin pump which automatically responds [14]. In practice, however, most implanted sensors which are exposed to physiological conditions require some calibration (at least twice daily) and sensor replacement (every 6 days) by the wearer to ensure continued accuracy [15]. Hence, despite increased sensor autonomy, there remains a reliance on frequent maintenance by an operator.

1.4.4. Operator Elimination (Calibration and Sample Pretreatment)

The elimination of the operator can be accomplished by eliminating or automating the routine tasks of calibration and sample pretreatment. Outright elimination of the need for calibration is technically challenging since the response of most electrochemical methods is sufficiently unstable so as to require periodic calibration, even under highly controlled laboratory conditions. Another approach to eliminating the need for calibration is stringent quality control of sensors, as in the BGM test strips. This approach is difficult to implement, however, for environmental sensors which must perform measurements under uncontrolled, and perhaps extreme, conditions for extended periods (e.g., temperature, humidity, etc.). Automation of the calibration function is technically feasible by packaging the necessary reference standards and sample handling capability (e.g., pumps, valves, etc.). The practicality of this approach is, however, dubious since cumbersome, complicated devices have greater associated costs and maintenance requirements.

Sample pretreatment is, of course, dictated by the chosen method and analyte matrix. Since the analyte and its matrix are predetermined, the chosen method ought to

therefore minimize and allow for automatable sample pretreatment. Another important consequence of eliminating the operator is the necessity of rugged sensors which can function reliably for extended periods. To further extend sensor lifetime, the use of microfabricated sensors does allow for redundant semi-disposable sensors which can be activated sequentially, in a similar fashion to the semi-disposable sensors employed in CGM. Eliminating the operators of electrochemical sensors also entails addressing their less apparent functions and advantages they bring. These include a host of what are best described as design and engineering challenges: sample handling and transport, low-power remotely operated potentiostat, low-power control hardware (microprocessor), simplified software, wireless communication to transmit data, and access to a continuous power supply, etc.

1.5 Heavy Metals Monitoring

In keeping with the discussion above, electrochemical methods for remote heavy metal sensors appear to be a promising avenue for investigation. The occurrence of heavy metals in environmental waters is a major cause for concern which would benefit from a means for long-term monitoring. This section provides justification of this approach by listing some instances where remotely deployed heavy metal sensors would be useful. These instances include the so called SuperFund sites, municipal drinking waters, and groundwater which is used for drinking or irrigation. Additionally, a brief overview of the most commonly used heavy metal electrochemical detection method is provided.

1.5.1 Heavy Metals Occurrence at the SuperFund Sites, in Municipal Drinking Waters, Ground Waters, and Other Instances

The Comprehensive Environmental Response, Compensation, and Liability Act of 1980 (CERCLA), commonly known as the SuperFund, requires the creation of a National Priorities List (NPL) to serve as a database for sites of known or potential hazardous waste releases **[16]**. The current NPL includes 1321 sites throughout the contiguous United States, as shown in **Figure 1.5**. The SuperFund Amendments and Reauthorization Act of 1986 (SARA) amended CERCLA and requires the Agency for Toxic Substances and Disease Registry (ATSDR) and the EPA to prepare and periodically update a prioritized list of substances that pose the most significant potential threat to human health **[16]**. The prioritized list, shown in **Table 1.1**, includes four metals: As, Pb, Hg, and Cd in the top ten hazardous substances; with As, Pb, and Hg being the first, second, and third prioritized pollutants, respectively **[17]**.

The threat level of a specific hazardous substance is determined not only by its toxicity but also by the potential for human exposure. This exposure is largely determined by the volatility or solubility of pollutants since these are the most likely means of release from contaminated sites. The primary mode of release of As, Pb, Hg, and Cd is via dissolution in runoffs which originate at the SuperFund sites (although mercury may also be released as a vapor) **[18]**. The Onondaga Lake SuperFund Site in New York State is such an example where metals have accumulated in the lake waters from eleven upland sources where industrial waste was stored or discharged **[19]**. This lake flows into the Seneca River, then into the Oswego River, and ultimately into Lake Ontario. Since the mobility of metals from such sites in waters remains a cause for concern, continuous
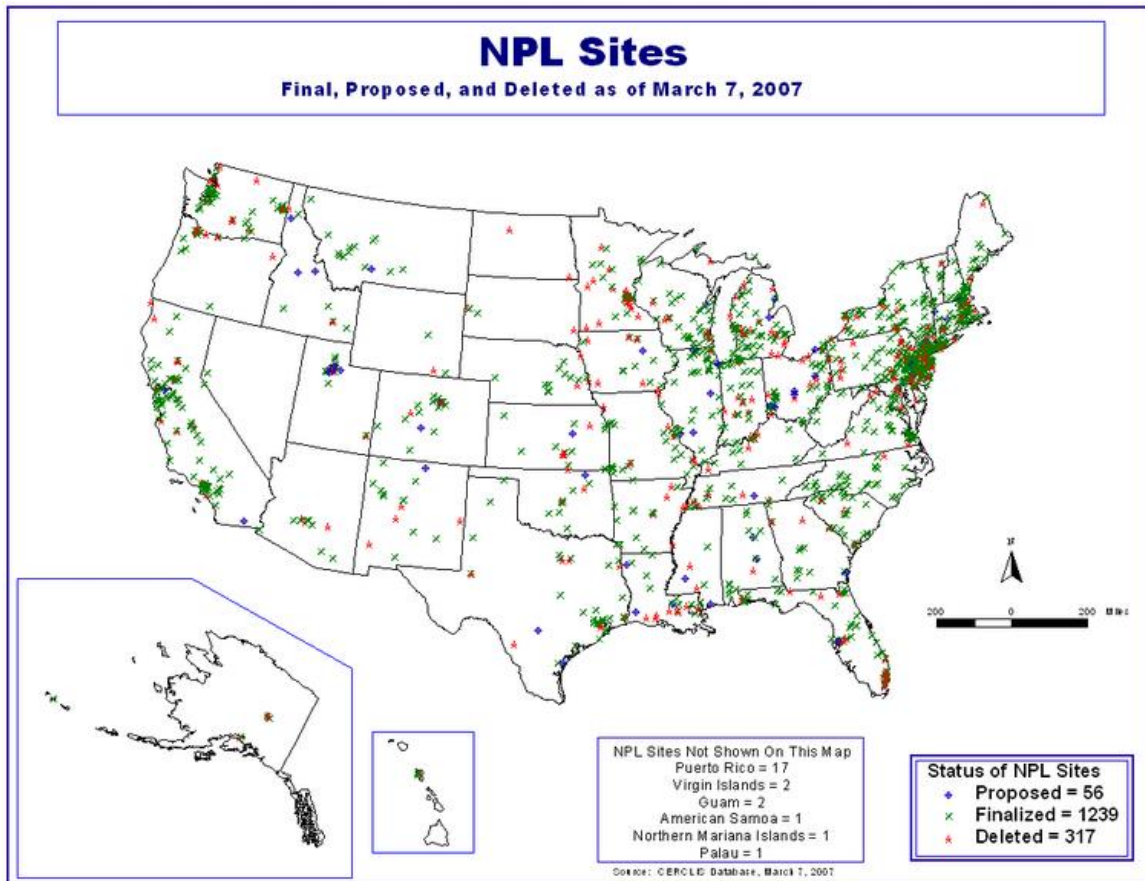
Figure 1.5: The EPA National Priority List Sites as of 2007. **[20]**

2013 Rank	Substance Name	Total Points	2011 Rank	CAS RN	NPL Freq	GMMC Water	GMMC Air
1	ARSENIC	1670	1	007440-38-2	1140	6E-02	8E-05
2	LEAD	1529	2	007439-92-1	1272	1E-01	3E-03
3	MERCURY	1459	3	007439-97-6	832	3E-03	3E-03
4	VINYL CHLORIDE	1360	4	000075-01-4	593	6E-02	9E-03
5	POLYCHLORINATED BIPHENYLS	1344	5	001336-36-3	547	1E-02	1E-03
6	BENZENE	1329	6	000071-43-2	972	6E-02	3E-02
7	CADMIUM	1319	7	007440-43-9	1003	4E-02	1E-04
8	BENZO(A)PYRENE	1305	8	000050-32-8	545	3E-02	3E-04
9	POLYCYCLIC AROMATIC HYDROCARBONS	1280	9	130498-29-2	401	2E-01	1E-03
10	BENZO(B)FLUORANTHENE	1251	10	000205-99-2	405	3E-02	7E-06

Table 1.1: The substance priority list maintained by ATSDR. Total points based on frequency of occurrence at NPL sites, toxicity, and potential for human exposure. Geometric Mean Maximum Concentration for water (mg/l), air (mg/m^3). **[18]**

downstream monitoring of already contaminated sites is highly desirable. In fact, the use of continuous monitoring directly in discharged wastewater and in waters downstream from storage sites may provide early warning and aid in the prevention of future SuperFund sites.

Unsurprisingly, the occurrence of metals in drinking water is even more stringently regulated. A selected list of heavy metal contaminants that are actively regulated by the United States Environmental Protection Agency (EPA) in drinking water along with the maximum levels permitted by the EPA is shown in **Table 1.3 [21-22]**. The table also lists the EPA approved methods for those metals, and with the exception of a single electrochemical method for Pb, most of these rely on sophisticated instruments which are not inherently suited for unattended remote monitoring networks. Although the vast majority of water in the US is adequately treated, the sheer immensity of the drinking water distribution grid gives rise to instances where monitoring of one or more metals is either of great use or is mandated by law. The Louisville Water Company (LWC), for instance, serves a medium sized city and supplies 850,000 people with 124 million gallons of water daily through a 4000 mile network of pipes, where a given water sample may reside in the grid for up to 4 weeks **[23]**. Older sections of pipes which contain lead or lead solder and/or small leaks may also contaminate water with heavy metals. Due to these external factors, many water companies, including LWC, can only reasonably guarantee safe levels of heavy metals for freshly treated water as it leaves the pumping station **[24]**. The common use of copper and the historical use of Pb pipes and solder has given rise to circumstances where monitoring can guide ongoing costly Pb removal and renovations to where they are needed most.

These considerations have led to the EPA mandated lead and copper rule which requires that testing for these contaminants must be conducted at a prescribed number of customer taps **[25]**. Due to financial and manpower constraints, the number of samples collected is typically less than 0.1% of available taps; and sampling can be as infrequent as every 2-3 years **[26-27]**. For instance, the LWC 2010 water quality report cites samples collected and analyzed in 2008, where 4 of 53 samples exceeded the 15 ppb action level for lead **[26]**. The 2011 water quality report showed that 5 of 52 sites exceeded the lead action level **[27]**. Despite the small sample size, the fact that 5-10% of the tested taps showed larger than recommended Pb concentrations was not the worst case. In one case, discovered by random sampling, the lead concentration was 2770 ppb and was tracked to defective equipment (a broken meter vault) **[26]**. Alarmingly, very serious contamination events may exist for long periods prior to discovery by mere random sampling. The lead and copper rule requires even more frequent testing, according to the schedule in **Table 1.2**, of every school and child care facility since Pb is especially harmful to rapidly growing children **[28, 34]**.

In contrast to metropolitan grids where at least some monitoring takes place, private water wells which supply drinking water to over 15 million US households are not regulated by the EPA **[29]**. These under-reported communities are at higher risks for heavy metal consumption, particularly arsenic. Arsenic is common in the earth's crust and enters ground water naturally by dissolution of minerals, although human activities also introduce arsenic to surface water **[30]**. As a result, a significant portion of groundwater wells in the Northeast, the Midwest, parts of Texas, and the West have arsenic levels which exceed the EPA MCL of 10 ppb **[31]**. Arsenic in water used for

drinking also adversely affects millions of people world-wide, particularly in under-developed regions such as Bangladesh and Nepal [32]. Besides drinking water, there have also been reports of elevated levels of arsenic and other heavy metals in a variety of crops including apples, rice, leafy vegetables, etc. [33]. In these instances, decentralized sensors can play a key role to monitor irrigation waters and/or surrounding watersheds for evidence of soil contamination.

School or Child Care Facility Daily Population Served	Number of Lead and Copper Tap Sample Sites		Number of WQP Tap Sample Sites	
	Standard	Reduced	Standard	Reduced
10,001 - 50,000	60	30	10	7
3,301 - 10,000	40	20	3	3
501 - 3,300	20	10	2	2
101 - 500	10	5	1	1
≤ 100	5	5	1	1

Table 1.2: School and child care facility EPA recommended sampling frequency and required number of water samples for Pb and Cu screening. [34]

Analyte	EPA MCL	ASTM International	EPA Methods	Standard Methods	Other Methods
Arsenic	10 ppb	D2972-03B [a] D2972-08B [a] D2972-03C [b] D2972-08C [b] D2972-97B [a] D2972-97C [b]	200.5 rev 4.2 [e] 200.8 rev 5.4 [f] 200.9 rev 2.2 [b]	3113B [b] 3113 B-99 [b] 3114B [a] 3114 B-97 [a]	
Cadmium	5 ppb		200.5 rev 4.2 [e] 200.7 rev 4.4 [g] 200.8 rev 5.4 [f] 200.9 rev 2.2 [b]	3113B [b] 3113 B-99 [b]	
Copper	1300 ppb	D1688-02A [c] D1688-02C [b] D1688-07A [c] D1688-07C [b] D1688-90A [c] D1688-90C [b] D1688-95A [c] D1688-95C [b]	200.5 rev 4.2 [e] 200.7 rev 4.4 [g] 200.8 rev 5.4 [f] 200.9 rev 2.2 [b]	3111B [h] 3111 B-99 [h] 3113B [b] 3113 B-99 [b] 3120B [g]	
Lead	15 ppb	D3559-03D [b] D3559-08D [b] D3559-90D [b] D3559-96D [b]	200.5 rev 4.2 [e] 200.8 rev 5.4 [f] 200.9 rev 2.2 [b]	3113B [b] 3113 B-99 [b]	1001 [i]
Mercury	2 ppb	D3223-02 [d] D3223-95 [d]	245.1 rev 3.0 [d] 245.2 [d] 200.8 rev 5.4 [f]	3112B [d] 3112 B-99 [d]	
Selenium	50 ppb	D3859-03A [a] D3859-03B [b] D3859-08A [a] D3859-08B [b] D3859-98A [a] D3859-98B [b]	200.5 rev 4.2 [e] 200.8 rev 5.4 [f] 200.9 rev 2.2 [b]	3113B [b] 3113 B-99 [b] 3114B [a] 3114 B-97 [a]	
Zinc	5000 ppb*				

Table 1.3: A select list of heavy metals regulated by the EPA and the maximum contaminant levels permissible in drinking water. *Voluntary recommended limit.[a] HGAAS, [b] GFAAS, [c] direct AAS, [d] cold vapor AAS, [e] Axially viewed ICP-AES, [f] ICP-MS, [g] ICP-AES, [h] flame AAS, [i] DPSV. **[21-22]**

1.5.2 Overview of Electrochemical Heavy Metals Monitoring

Heavy metals are naturally suited for monitoring by electrochemical methods. In the US, the laws regulating heavy metals in drinking water are less complex and are, in any case, more stringent than those governing wastewater discharges; the permissible level of heavy metals in wastewater considers criteria such as the type of industry producing the wastewater, the production volume, whether the water is discharged into the environment or to publicly owned treatment works (POTW), and the sensitivity of the local ecosystem. For these reasons, the overall goal for remote heavy metal electrochemical methods ought to be meeting the sensitivity thresholds for drinking water, since this level of performance would very likely also be applicable to wastewaters. This is an especially worthwhile challenge considering that, although some electrochemical methods are listed in EPA guidelines, only one electrochemical method for Pb is approved for the important case of drinking water [35]. Currently, drinking water monitoring for heavy metal contaminants is handled by costly and complex instruments such as inductively coupled plasma atomic emission spectroscopy (ICP-AES), ICP-mass spectrometry, and graphite furnace atomic absorption spectroscopy (GF-AAS) [22]. Paradoxically, these complex instruments, which are confined to central laboratories, can be operated by suitably trained technicians in a 'push button' fashion utilizing standard operating procedures (SOPs).

In comparison, electrochemical methods for heavy metals are capable of equal or even better detection limits, and the required instrumentation is more cost effective for remote sensing. However, the electrochemical heavy metal (i.e., stripping) methods in particular require a higher level of operator experience. This is not due to the any

complexity or difficulty of the techniques but is rather due to the variable nature of the electrode surface/electrolyte interface and the necessity of performing blank subtraction and calibration [36]. This has led to several EPA initiatives to investigate the practicality of electrochemical methods for decentralized analysis of metals; and not surprisingly, these efforts have been focused on the most sensitive of the electrochemical techniques for metals analysis: stripping analysis [37].

1.5.2.1 The Concept of Anodic Stripping

There are many sub-variants of stripping analysis including anodic stripping, cathodic stripping, adsorptive stripping, etc. The most commonly employed scheme for heavy metal detection is anodic stripping, where soluble metal ions are deposited (i.e., reduced) and hence pre-concentrated as elemental metals on the electrode surface according to **Equation 1.1**. In the analytical step, the elemental metals are stripped (i.e., oxidized) from the electrode surface to form, typically, soluble ions (the reverse of **Equation 1.1**).

$$Cu^{2+} + 2\ e^{-} \rightarrow Cu^{0} \qquad \textbf{(Equation 1.1)}$$

The common steps for anodic stripping analyses begin with a cathodic deposition step where metals are pre-concentrated on the electrode surface. The deposition step is usually performed by voltammetric control, although potentiometric depositions can also be used. The deposition step offers relatively few parameters which can be optimized including the deposition potential (or current in the case of potentiometric deposition),

the deposition time, and the stirring rate. The stirring rate is important since, without it, pre-concentration is limited to dissolved analytes within the diffusion layer for a given deposition time. Hence, the deposition time and stirring rate together determine the total volume sampled, and normally seek to pre-concentrate enough dissolved metals on the electrode surface to attain the desired sensitivity. Following the deposition step a rest period may be imposed during which stirring is stopped and the electrode may be placed in a different medium prior to the stripping step. Alternatively, deposition may be immediately followed by the stripping step. The stripping step is the reverse of the deposition step and oxidizes the elemental metals accumulated on the electrode surface and may be performed by either voltammetry or potentiometry. The great sensitivity of stripping analysis arises from the temporal concentration of the signal. It is not atypical to pre-concentrate metals for several minutes *while stirring*, whereas the stripping step *strips* the accumulated metals in as few as hundreds of milliseconds.

1.5.2.1.1 Anodic Stripping by Potentiometry

Anodic stripping analysis has been historically performed on mercury electrodes and can be been performed under potentiometric or voltammetric control. Potentiometric stripping has been most often conducted in one of two approaches. The first is so called potentiometric stripping analysis (PSA) where a dissolved oxidant such as O_2 or Hg^{2+} reoxidizes the plated elemental metals causing measurable changes in the potential as shown in **Figure 1.6 [38]**. In lieu of a chemical oxidant, the second method utilizes an applied anodic current to sequentially strip each of the pre-concentrated metals at its

characteristic potential **[39]**. The potential is again monitored with time and the resulting data is identical to that obtained by PSA.

1.5.2.1.2 Anodic Stripping by Voltammetry

More commonly, the anodic stripping process is performed voltammetrically by scanning the potential to oxidize reduced metals in order, with peaks appearing at the characteristic potential of each metal. The most direct scan method is linear sweep voltammetry (LSV), and an example is shown in **Figure 1.7** where Pb and Cd are anodically stripped (i.e., potential is scanned from negative to positive) in that order from a thin film mercury electrode **[40]**. This figure demonstrates an important feature of stripping voltammetry, where the peak heights are enhanced at higher scan rates. This feature is an important one since it demonstrates that the signal size not only depends on the amount of analyte, but also on the choice of experimental parameters (i.e., scan rate). This is due to the important facet of electrochemical analysis which requires appropriate background subtraction to differentiate the faradaic current from the non-faradaic current **[41]**.
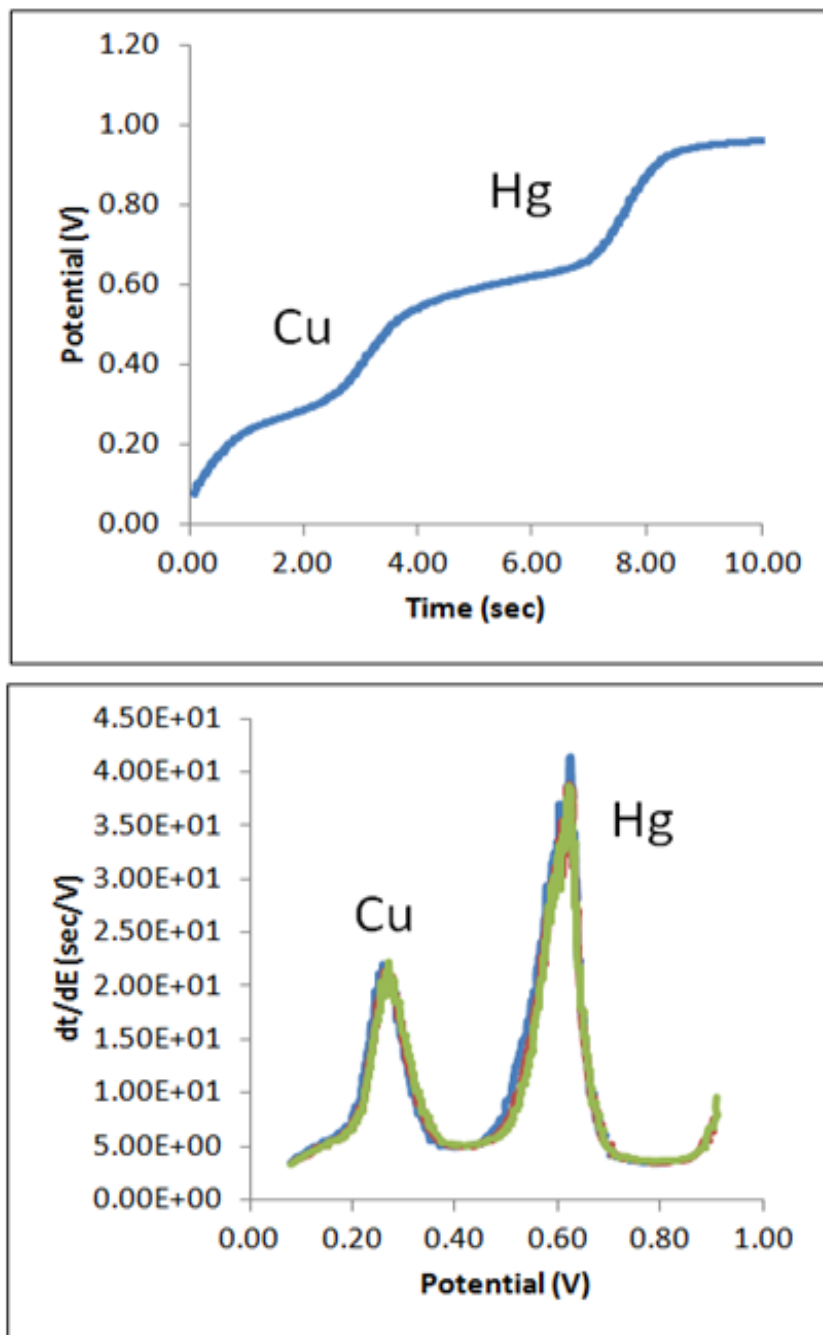
Figure 1.6: Chronopotentiometric stripping analysis of 30 μM Cu^{2+} and 30 μM Hg^{2+}. Applied current +1.0 μA, potential recorded vs. Ag/AgCl reference electrode (3 M NaCl). Bottom panel shows the inverse derivative plot where the plateaus of the left plot are shown as peaks to facilitate estimation of transition times.
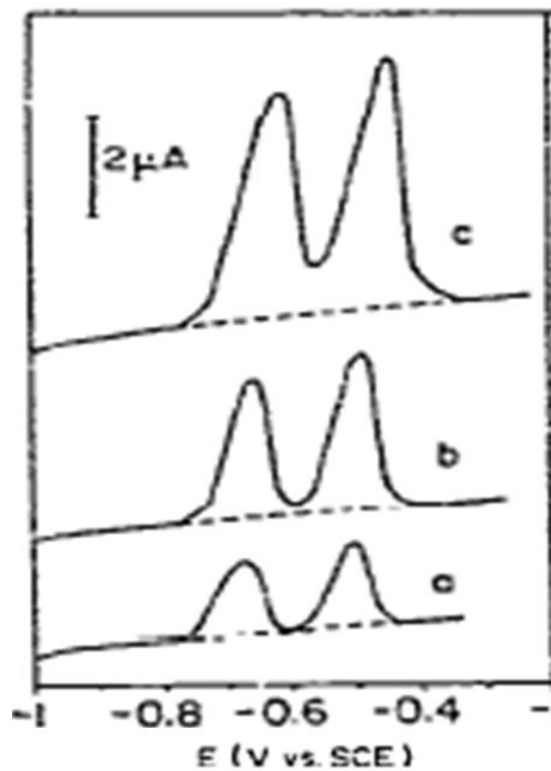
Figure 1.7: The influence of scan rate and peak charge on resolution of LSV (solution volume 200 μL, electrode rotation rate 45 r.p.s, deposition time 17 min). Equal amounts (23.2 μC) Cd and Pb, stripped with scan rates of 5 (a), 10 (b), and 20 mV s^{-1} (c). Dashed lines are baselines. **[40]**

1.5.2.2 Sensitivity and Background Subtraction

Faradaic current is the signal of interest in anodic stripping and arises from the process of stripping the metal deposits. Non-faradaic current by contrast is due to the movement of ions in the process of setting up the double layer in response to a change in potential. Hence, in LSV the main recourse for enhancing the faradaic current is ensuring that the deposition time and/or stirring rate are sufficient to achieve a significant pre-concentration from a large solution volume. And this is in fact the approach taken in **Figure 1.7** where a 17 minute deposition (while stirring!) is used to enhance the analyte peaks.

1.5.2.3 Enhancing Sensitivity by Pulse Voltammetry Methods

An alternative means of enhancing the sensitivity has been the development of a family of techniques known as pulse or step voltammetry. There are a variety of stripping waveforms including normal pulse stripping voltammetry, differential pulse stripping voltammetry, and square wave stripping voltammetry (NPSV, DPSV, and SWSV, respectively). The improved sensitivities arise from the fact that the capacitive current (background) following a potential step decays more quickly than does the faradaic portion **[41]**. The different pulse voltammetry methods have various sensitivities as summarized in **Table 1.4**. Importantly, however, the necessary intermittent sampling after the charging current has dissipated to some pre-determined extent sacrifices a portion of the desirable faradaic current. However, the overall effect of the step stripping techniques is the enhancement of the stripping peaks following shorter depositions, which is certainly useful for many applications.

Technique	Limits of Detection for Pb(II)
Ion selective electrode	10^{-5} M
DC polarography at DME	10^{-6} M
Differential pulse polarography at SMDE	10^{-7} M
Differential pulse ASV at HMDE	10^{-10} M*
DC ASV at mercury film	10^{-11} M*
Square-wave ASV at mercury film	10^{-12} M*

*Deposition for 360 seconds; LOD varies with deposition time. SHMDE = static (hanging) mercury drop electrode

Table 1.4: Summary of several pulse voltammetric methods and detection limits. **[36]**

1.6 Challenges for Remote Heavy Metal Sensors Addressed in this Work

To this point, the need for remote heavy metal sensors for environmental sensors has been overviewed. This overview has included a detailed description of the widely available sampling opportunities where such a sensor can be useful. These examples include monitoring Pb in municipal drinking water, As in groundwater used for drinking and irrigation, and the monitoring of natural waters (lakes and rivers) downstream from SuperFund sites. The overview has also generically established that electrochemical methodologies (in the form of stripping analysis) in conjunction with miniature (microfabricated) sensors offer a promising approach. The overview has also placed a special emphasis on eliminating the need for any operator intervention and enhancing sensor durability.

Elimination of the operator requires minimizing or simplifying the operator intensive tasks of signal calibration and sample pretreatment. To remove the need for any signal calibration, a microfluidic thin layer cell platform where exhaustive coulometry is possible in about a minute is developed and used in conjunction with potential step anodic stripping coulometry. The issue of durability is, in principle, addressable by a combination of two approaches: 1) redundant semi-disposable microfabricated sensors which are activated sequentially and 2) the choice of a method that is inherently tolerant of changes to the ambient conditions and of changes to the sensor (i.e., the electrode surface). The proposed exhaustive coulometric method appears to offer this tolerance to changes to the electrode surface, whereas the stripping offers enhanced sensitivity along with a means to compensate for the background. In regards to sample pretreatment, this includes acidification and removal of humic acids, however, the most challenging step is

arguably the efficient removal of dissolved oxygen. An approach for DO removal, which

has not been previously described for miniature sensors, is described in this work.

Amongst the numerous challenges which remain are the automation and

replication of the amenities of the central laboratory. These amenities include sample

handling and transport, access to a potentiostat, access to a power supply, control

hardware (i.e., a micro-processor), software for data processing, data dissemination, etc.

1.6.1 Calibration Free Measurements of Heavy Metals

The avoidance of calibration essentially requires that every analyte molecule

contributes completely to the signal. The stripping process removes all metals that are

pre-concentrated on the electrode surface, and hence the current over time (i.e., charge) is

equivalent to the deposition process. Hence, a convenient opportunity arises during the

deposition step where the extent of metal pre-concentration can be precisely controlled

(i.e., from a finite known volume). This ensures that the amount of metals measured

during the stripping step correspond to a known volume, allowing the concentration to be

calculated.

1.6.1.1 Faraday's Law of Electrolysis

One of the very few possibilities for calibration free stripping analysis is

coulometry as summarized in Faraday's law of electrolysis (**Equation 1.2**) which states

that the total charge (Q) is related to the amount of analyte (N) and the number of

electrons (n) for a given redox process by the proportionality factor F, known as the

Faraday Constant:

$$Q = n \cdot F \cdot N \qquad \textbf{(Equation 1.2)}$$

$$Q = n \cdot F \cdot V \cdot C \qquad \textbf{(Equation 1.3)}$$

The N term is the product of the sample volume and concentration and Faraday's Law

can be rewritten, as in **Equation 1.3**, to emphasize this fact. Hence the concentration of a

given analyte is easily determinable if electrolysis is 100% complete, reaction

stoichiometry (n) is known, the sample volume is finite (V), and the charge can be

measured **[42]**. The only requirements are that 1) the analyte is electrochemically active

and 2) sample pretreatment methods (e.g., acidification for cationic trace metal analysis)

can be practically achieved in the field. The condition where the sample volume is

completely depleted of the analyte of interest is known as exhaustive coulometry.

1.6.1.2 Coulometry (via Control of the Deposition Step)

Exhaustive coulometry is in fact one of the very few analytical methods which

can be operated in a truly calibration-free fashion **[42-45]**. Unlike the other

electroanalysis methods, coulometric signals are not critically dependent on analyte mass

transport rates **[43-44]** which can vary with temperature, solvent viscosity, etc. In

addition coulometric signals are tolerant of changes to the working electrode surface area

due to fouling, for instance. While partial passivation of the WE surface due to fouling

increases the time required for the analyte to diffuse to the electrode surface, the final

magnitude of the coulometric signal is only dependent on the amount of analyte **[45]**.

These qualities of exhaustive coulometry are fortunate since electrodes for long term infield sensing are likely to become partially fouled with time and are subject to ambient temperature fluctuations.

To avoid very long depositions, a thin layer cell configuration is necessary for flow-by electrodes or alternatively that a porous electrode is used for a flowing sample (where the pores essentially behave as a thin layer cell). Exhaustive electrolysis from thin layer cells is governed by **Equation 1.4 [41, 46]**

$$i(t) = \frac{4nFAC_oD_o}{2h}\sum_{m=1}^{\infty} e^{\left[\frac{-(2\cdot m-1)^2\pi^2 D_o t}{(2h)^2}\right]}$$ 　　　　　(**Equation 1.4**)

where i(t) is the current at a given time, n is the number of electrons governing the redox process, F is the faraday constant, A is the electrode area, D_o is the diffusion coefficient of the analyte, and C_o is the analyte concentration, h is the height of the TLC. However, the time for complete depletion of a TLC, in principle, only depends on the height h, and the diffusion coefficient of the analyte according to **Equation 1.5**

$$\% \ Electrolysis = 100 \cdot \left[1 - e^{\frac{-1\cdot t\cdot \pi^2\cdot D_o}{(2h)^2}}\right]$$ 　　　　　(**Equation 1.5**)

Accordingly for a 75 µm TLC, even a relatively slow diffusing analyte ($D_o = 5 \ X \ 10^{-6}$ cm^2/s) can be effectively depleted (99% electrolyzed) in as few as 20 seconds.

1.6.2 Overview of Anodic Stripping Coulometry

Anodic stripping coulometry is no different than conventional anodic stripping with the exception that an additional constraint is placed on the deposition process. The deposition process, by design, only samples a finite known volume and completely exhausts this volume of dissolved metals which are plated on the electrode surface. The stripping step which is the source of the signal used for analysis, however, may still be performed by potentiometry or voltammetry. Although a comprehensive review of stripping analysis is beyond the scope of the current work, a recent review of on-line (i.e., continuous) metal monitoring methods demonstrates the novelty of the current work **[12]**. The review shows a variety of sampling methods for metals including flow injection analysis and sequential injection analysis and automated monitoring systems for stripping analysis (the various schemes are summarized in **Table 1.5**). Of these approaches, the most relevant to the current work are those which employ a calibration-free (i.e., coulometric) mode of analysis. Examination of the table reveals that only one voltammetric method and one potentiometric method satisfy the coulometry requirement: linear sweep voltammetry and chronopotentiometry, respectively. Notably, all of the calibration-free methods are based on flow approaches to pre-concentrate sufficient metals on the electrode surface. Implementation of this requirement, in practice, requires accurate and reliable pump(s) on each sensing platform. A more attractive coulometric approach that is consistent with economical sensing devices is the stopped-flow thin-layer cell described in this work. Because the sample volume is determined only by the cell volume, the quality of the measurement does not depend on a precisely metered flow rate; and the device design ought to be greatly simplified.

Analyte	Matrix	Flow system	Electrode	Detection/stripping mode	Notes
Fe(III)	Seawater	Continuous flow	Hg-coated Au wire	SWAdSV	
Zn(II), Pb(II), Cd(II)	Honey	Continuous flow	MFE on GCE	PSA	
Pb(II)	Standards	Continuous flow	Cyclam-modified graphite felt	DCASV-stripping coulometry	No calibration
Pb(II)	Standards	Continuous flow	1,4,8-tri(carbamoylmethyl) hydroiodide-modified graphite felt	DCASV-stripping coulometry-	No calibration
As	Polluted water samples	Continuous flow	Au-coated GCE	PSA	Speciation As(V), As(III)
Pb(II)	Standards	Continuous flow	Graphite felt	DCASV-stripping coulometry	No calibration
Tl(I)	Rainwater	Continuous flow	BiFE on GCE	SWASV	
Pb(II)	Wastewaters	Continuous flow	MFE on Nafion-coated porous GCE	CCSA-stripping coulometry	No calibration
Sulphides	Tannery wastewater	Continuous flow	Nafion-coated MFE on GC	CCSA	
Sb(III)	Water samples	Continuous flow	Au-tubular electrode	DPASV	Speciation of Sb
As	Soil	Continuous flow	Au-coated porous C electrode	CCSA-stripping coulometry	As speciation – no calibration
As(III)	Tap water	Continuous flow	Au-coated GC	PSA	
Pb(II)	Drinking and tap water	Continuous flow	Au-sputtered SPEs	SWASV	
Hg(II)	Water samples	Continuous flow	Au, Au-coated GCE	DCASV	
Cr(VI)	River water	Continuous flow	HMDE	DPAdSV	
Cu(II), Cd(II), Pb(II), Zn(II), Fe(III)	Water samples	Continuous-flow	GCE	DPASV	
Sn(II)	Human hair, canned fruit juice, water	Continuous-flow, FIA	Epoxy-carbon composite modified with 8-hydroxyquinoline	DPASV	
Compositional analysis	Bismuth telluride thin-films	Continuous-flow	Gold-coated quartz crystal	DCASV	Combined EQCM-ASV
Ni(II)	Fly ash, Co and Zn metals	Continuous-flow	HMDE	SWAdSV	Three-step procedure – medium-exchange
Se(IV)	Water samples	Continuous-flow	HMDE	DPCSV	Speciation of Se
U(VI), Sb(III), Mo(VI), V(V)	Water samples	Continuous-flow	HMDE	DPAdSV	
Cd(II), Pb(II)	Standards	Continuous-flow	MFE on rotograved C	DPASV	
Ce(III)	Urine, water	Continuous-flow	Electropolymerized catechol on GCE	DPASV	
Fe(II), Fe(III)	Wine, water	Continuous-flow	GCE	DPASV	
Cu(II), Pb(II), Zn(II), Ni(II)	Soil extracts	Continuous-flow	HMDE	SWASV SWAdSV	
Sb(III)	Human hair, seawater	Continuous-flow	Poly(pyrogallol)-coated GCE	DPASV	
Mo(VI)	Water samples	Continuous-flow	HMDE	DPAdSV	
Au(III)	Water, Pin-connector	Continuous-flow, FIA	Epoxy-impregnated graphite modified with 2-mercaptobenzoxazole	DPCSV	Medium-exchange
Zn(II), Cd(II), Pb(II), Cu(II)	Water samples, geological and biological meterials	Continuous-flow	MFE on GC powder electrode MFE on Nafion-coated GC powder electrode	CCSA-stripping coulometry	No calibration
Ag(I)	Water, rice	Continuous-flow	8-mercaptoquinolone-modified GCE	DPASV	
Hg(II)	Water samples	Continuous-flow	Au disk	CCSA	
As(III) and total As	Water samples	Continuous-flow	Au-plated porous C electrode	CCSA-stripping coulometry	No calibration
Zn(II), Cu(II), Cd(II), Pb(II)	River water	Continuous-flow	MFE on Ir microelectrode arrays	SWASV	
Hg(II)	Table salt	Continuous-flow	Au film on GCE	DPASV	Medium-exchange
Labile Cr(III)	River and lake water	Continuous-flow	HMDE	DPAdSV	
As(III)	Gold sample	Continuous-flow	Au-film on GCE	DPCSV	Medium-exchange
Pb(II), Cd(II), Cu(II)	Water	Continuous-flow	Graphite-epoxy composite electrode	DPASV	
Te(IV)	Water, garlic, urine	Continuous flow, FIA	Poly(3,3'-diaminobenzidine) on Au electrode	DPASV	Medium-exchange
Os(IV)	Water, urine	Continuous flow, FIA	Sol–gel-ceramic-carbon powder-9-phenyl-3-fluorone composite electrode	DPASV	Medium-exchange
Cd(II)	Standards	Continuous-flow	MFE on Pt electrode	SWASV	Microwave heating-resistance to surfactants
Pb(II), Cd(II), Cu(II)	Standards	Continuous-flow	MFE on gel-covered Ir microelectrode array	SWASV	Microfabricated cell with PLM

Analyte	Matrix	Flow system	Electrode	Detection/stripping mode	Notes
Pb(II), Cd(II), Cu(II)	Natural waters	Continuous-flow	MFE on gel-covered Ir microelectrode array	SWASV	Microfabricated cell with PLM
Pb(II), Cd(II), Cu(II)	Natural waters	Continuous-flow	MFE on gel-covered Ir microelectrode array	SWASV	Submersible probe
Cr(VI)	Water	Continuous flow	MFE on GCE	SWAdSV	Remote probe combined with microdialysis
Pb(II), Cd(II), Cu(II), Mn(II)	Natural waters	Continuous-flow	MFE on gel-covered Ir microelectrode	SWASV SWCSV	Submersible probe
Sb(III)	Soils	Continuous flow	MFE on Nafion-coated porous C electrode	CCSA	
Pb(II), Cd(II), Cu(II)	Milk	Continuous flow	MFE on GCE	PSA	
Pb(II)	Soils	FIA	Dithizone-modified CPE	DPASV	
Pb(II)	Blood	FIA	MFE on Nafion-coated GCE	DCASV	
Zn(II), Pb(II), Cd(II)		FIA	MFE on GCE	PSA	Study of adsorption of Zn(II), Pb(II), Cd(II) on diatomite
Cr(VI)	Natural waters, soil	FIA	HMDE	DPAdSV	
Pb(II)	Saliva	FIA	MFE on GCE	DPASV	
Hg(II)	Seawater, tapwater	FIA	Au	PSA	Au from recordable CDs
Se(IV)	Water samples	FIA	Au wire	CCSA-stripping coulometry	No calibration
Pb(II)	Urine, blood	FIA	MFE on GCE	DPASV	
Se(IV)	Riverwater	FIA	HMDE	SWCSV	
Cd((I), Pb(II), Cu(II), Zn(II)	Algae	FIA	HMDE	DPASV	Bi internal standard
Tl(I)	Water, bottom sediments, soil	FIA	MFE on epoxy-resin impregnated graphite or GCE	DPASV	
Se(IV)	Human hair	SIA	MFE on GCE	DPCSV	LOV in the presence of CuCl$_2$
Pb(II), Cd(II)	Water samples	SIA	BiFE on GCE		
Pb(II)	Environmental water samples	SIA	MFE on CPE	DPASV	LOV
Pb(II), Cd(II), Zn(II)	Water samples	SIA	BiFE on SPE	SWASV	
Cd(II)	Environmental water samples	SIA	BiFE om Nafion-coated GCE	DCASV	LOV
Cd(II), Pb(II), Zn(II)	Herbs	SIA	BiFE on carbon nanotibes-modified SPE	SWASV	
Cd(II), Pb(II), Ni(II), Co(II)	Fertilizer, iron ore	FIA–SIA	BiFE on GCE and on Nafion-coated GCE	SWASV, SWAdSV	
Zn(II), Pb(II), Cd(II)	Phosphorite	SIA	BiFE on Nafion-coated GCE	SWASV	
Zn(II), Pb(II), Cd(II)	Wastewater from coatings industry	SIA	HMDE	DPASV	
Cd(II), Pb(II), Zn(II), Cu(II)	Water samples	FIA–SIA	MFE on GCE	SWASV	
Cu(II), Cd(II), Pb(II), Zn(II)	Sediment extracts	SIA	MFE on GCE	DPASV	Use of Ga to alleviate Zn–Cu intermatallic
Metals	Standards	SIA	HMDE	DPAdSV	Mixed ligands
Pb(II), Cd(II)	Tap water	SIA	SbFE on GCE	SWASV	
Hg(II)	Standards	SIA	Poly(4-vinylpyridine) and Kryptofix-222-coated GCE	DPASV	
Pb(II)	Standard	SIA	CPE modified with acetamide phosphonic acid self-assembled monolayer on mesoporous silica	DPASV	
Cu(II), Zn(II), Cd(II), Pb(II)	Phosphorite	SIA	MFE on GCE	SWASV	
Pb(II)	Urine	Multi-commutation	MFE on reticulated vitrous carbon	PSA	SLM enrichement and clean-up
Pb(II)	River water	Multi-commutation	MFE on reticulated vitrous carbon	PSA	Pre-concentration and matrix isolation by SLM
Pb(II)	Gunshot residue	Multi-commutation	BIFE on CPE	DPASV	
Ni(II),Co(II)	Iron	Multi-commutation	MFE on GCE	SWAdSV	
Ni(II)	Seawater	On-board monitor	HMDE	SWAdSV	
Pb(II), Cd(II), Zn(II), Cu(II), Ni(II), Co(II), Cr(VI)	River water	Multi-pump set-up	MFE on GCE	PSA	On-line standard addition
Sn(II)	Lake water	Multi-pump set-up	GCE, polyphenol-modified GCE	DCASV (enrichment)	Tin speciation On-line electrode modification

Analyte	Matrix	Flow system	Electrode	Detection/stripping mode	Notes
Cd(II), Pb(II), Tl(I)	Seawater	Multi-pump set-up	MFE on GCE	DPASV	Hyphenation with ICP-MS
Cd(II), Pb(II)	River waters	Multi-pump and multi-valve set-up	MFE on Ir-microelectrode	SWASV	Microfabricated cell with PLM
Cu(II), Pb(II), Cd(II), Tl(I), Zn(II)	Water	Multi-valve set-up	MFE, BiFE on Nafion-coated GCE	DPASV	Coupled on-line with ICP–MS
U(VI)	Seawater	Multi-valve set-up	MFE on GCE	DPAdSV	Coupled on-line with ICP–MS
Sb(III), Cu(II), Cd(II), Pb(II), Ni(II), Co(II)	Zink plant electrolyte	Process analyzer	HMDE	DPASV DPAdSV	Medium-exchange
Cu(II), Cd(II), Pb(II), Zn(II), Mn(II), As(III)	Standards	Portable analyzer	Au film MFE on Ag	DCASV DCCSV	Electronic tongue device
Pb(II)	Standards	Multi-pump set-up	MFE on gel-covered Ir-microelectrode	SWASV	Hollow-fiber SLM
Pb(II), Cd(II)	Standards	Multi-pump set-up	MFE on gel-covered Ir-microelectrode	SWASV	Hollow-fiber SLM
Cu(II), Cd(II), Zn(II), Pb(II)	Natural waters	Automated monitor	HMDE	SWAdSV SWASV	On-line sample pre-treatment UV
Cd(II), Pb(II)	Tapwater, tea	BIA	BiFE on fibrogen-coated CPE	SWASV	
Pb(II)	Gunshot residues	BIA	HMDE	DPASV	
Cr(VI)	Drinking water	BIA	MFE on GCE	SWAdSV	
Zn(II), Pb(II), Cd(II), Cu(II)	Standards	BIA	MFE on polymer-coated GCE	SWASV	
Zn(II), Pb(II), Cd(II), Cu(II)	Industrial and river water	BIA BIA	MFE on polymer-coated MFE	SWASV	
Cd(II), Pb(II), Zn(II)	Standards	BIA	MFE on random carbon-fiber microelectrode arrays	SWASV	
Cd(II), Pb(II)	Water samples	BIA	MFE on GC	SWASV	On-line SPE with Chelex 1000 (interference removal-sensitivity enhancement)
Pb(II), Cd(II)	Ecotoxicological test media	BIA	MFE on Nafion-covered GCE	SWASV	
Ni(II)	Standards	Electro-osmotic flow	MFE on SPE	SWAdSV	Microfluidic chip with electrokinetic injection
Ni(II), Co(II)	Standards	Continuous flow	BiFE on carbon-fiber-loaded plysterene	SWAdSV	Microfluidic polymer chip with integrated conducting polymer electrodes
Cu(II), Pb(II)	Standards	Continuous-flow	Carbon-fiber-loaded polysterene	SWASV DCASV	Injection-moulded microfluidic devices with integrated electrodes
Pb(II), Cu(II), Cd(II)	Industrial and lake water	Continuous-flow	SPE	DPASV SWASV	Microfluidic devices fabricated by injection-moulding
Hg(II), Cu(II)	Standards		Au SPE	SWASV	Micro-analytical system based on low temperature confined ceramics (LTCC) technology
Pb(II), Cd(II)	Soil, ground water, culture media		Microfabricated Bi electrodes (e-beam evaporation)	SWASV	Microfluidic devices with integrated electrodes
Se(IV)	Standards		MFE on GCE Cu-modified MFE on GCE	DPCSV	Robotic system
Cu(II), Pb(II), Cd(II), Zn(II), Ni(II), Co(II), U(VI), Rh	Lake water		HMDE	DPASV DPAdSV	Robotic system
Ni(II)	NiTi Shape Memory Alloys		BiFE on GCE	DPAdSV	Robotic system

Abbreviations: MFE, mercury-film electrode; BiFE, bismuth-film electrode; SbFE, antimony-film electrode; GCE, glassy carbon electrode; CPE, carbon paste electrode; SPE, screen-printed electrode; HMDE, hanging mercury drop electrode; DCASV, linear sweep anodic stripping voltammetry; DPASV, differential-pulse anodic stripping voltammetry; SWASV, square wave anodic stripping voltammetry; DCCSV, linear sweep cathodic stripping voltamme-try; DPCSV, differential-pulse cathodic stripping voltammetry; SWASV, square wave cathodic stripping voltammetry; DCAdSV, linear sweep adsorptive stripping voltammetry; DPAdSV, differential-pulse adsorptive stripping voltammetry; SWAdSV, square wave adsorptive stripping voltammetry; PSA, potentiometric stripping analysis; CCSA, constant-current stripping analysis; MS, mass spectrometry.

Table 1.5: Summary of on-line stripping methods for metal analysis. **[12]**

1.6.2.1 ASC: Potentiometric Approaches

The literature for anodic stripping coulometry is highly developed for the chronopotentiometric stripping variants. These methods typically rely on flow through electrodes with a geometry optimized to allow exhaustive deposition of a metal from a flowing sample where the total volume analyzed is recorded **[47]**. Subsequently, an anodic current is applied while the potential is monitored and the result is typically a plot of potential vs. time which exhibits a series of waves and plateaus as typified in **Figure 1.6**. Subsequent mathematical treatment can then be used to convert this plot into an inverse derivative plot where the area of each peak is equivalent to the individual transition times for each metal (**Figure 1.6**), and this analysis method is known as differential potentiometric stripping analysis **[48]**. Since a known current is used in the oxidation, the total charge passed can be calculated and the concentration calculated using Faraday's Law. This basic method was used extensively by Beinrohr et al. and Pierce et al. for a variety of metals with excellent detection limits **[49-50]**.

1.6.2.2 ASC: Voltammetric Approaches

Notably, there are very few reports of coulometric uses of voltammetric methods. Historically, the voltammetric methods which have attracted the most attention have been the step methods. The chief problem with these step methods is that despite their sensitivity, they require calibration with standards since correction for the non-faradaic component necessarily throws out a portion of the signal (since it is difficult to find a perfect balance where the retained portion of the capacitive current happens to equal the lost portion of the faradaic current). In fact, one of the very few reporting such use of step

methods concludes that double potential step chronocoulometry is the more widely applicable method [**51**].

1.6.3 Blank Subtraction: The Electrode/Electrolyte Interface

The key problem of most electroanalysis methods (including ASC) briefly mentioned above is the subtraction of the non-faradaic background component of the signal. The necessity of this step also has the additional benefit of countering 'drift' that is inherent to most electrochemical systems that arises due to changes at the solid electrode/solution interface **[52]**. One solution to counter this drift is the use of renewable electrodes such as the liquid mercury electrode. However, the use of mercury electrodes in environmental analysis has fallen out of favor for obvious reasons. Another way of correcting for this drift is to dilute the sample into a known electrolyte and compare this response to the pure electrolyte (i.e., to obtain a background in as close a time as possible for every experiment). This approach is obviously of limited practicality for remote sensors, as its employment requires additional device complexity to include the blank electrolyte and the sample handling components to switch between sample stream and blank solutions. Additionally, the speed with which these steps can be performed limits the extent to which transient and difficult to reproduce conditions at the solid electrode/solution interface can be corrected for, which is especially important for trace analysis.

1.6.3.1 Chronopotentiometric ASC Background Subtraction

For chronopotentiometric stripping coulometry, the procedures typically employ large surface area flow through porous electrodes where a significant portion of the applied current is used to charge the double layer as the potential changes **[49-50]**. Therefore, the sampling of large volumes is required (typically 5-20 mL) and few, if any, miniature sensors employing this approach have been reported to date.

1.6.3.2: Subtractive Anodic Stripping voltammetry

An alternative solution to counter 'drift' is so called subtractive stripping voltammetry, which has been most commonly used in conjunction with step stripping methods such as SWSV **[52]**. This technique involves the performance of the blank correcting step in a very short period of time (immediately prior to or following the analytical stripping step). Further, this step can be performed *in situ*; in the same solution containing the metals being measured. The key difference is that no pre-concentration is used in the subtractive step. This approach offers the important advantage of obtaining an appropriate background for the transient and difficult to reproduce conditions at the solid electrode/solution interface. Although the step methods (e.g., SWSV) are difficult to apply coulometrically, the concept of subtractive anodic stripping is readily applicable to techniques that are compatible with coulometry.

1.6.3.3: Linear Sweep Voltammetry

The elimination of chronopotentiometric and step voltammetric methods from immediate consideration thereby leaves LSV. An important consideration in LSV is the

scan rate. The peak heights can in fact be enhanced by increasing the scan rate as shown in **Figure 1.7**. However, the resolution between adjacent peaks is also compromised in this case. Besides, the speed of the maximum scan rate shown is 20 mV s^{-1} and the range shows that each scan would last 35 seconds. Hence the use of LSV directly in a TLC would cause significant pre-concentration during a background scan since the analytical scan itself is only preceded by, at most, several minutes of pre-concentration.

1.6.3.4: Extreme LSV (Potential Step ASV/ASC)

The most practical form of LSV (for ASC in a TLC) is the extreme form where the sweep rate is essentially infinite (i.e., a potential step). Unlike the step methods however where the capacitive current is allowed to dissipate, the signal is collected in its entirety immediately following the potential step (including the non-desirable capacitive component). A secondary step is also performed where the contribution of the capacitive current is measured and subtracted. This approach sacrifices the resolution of the stripping step. However, the rapidity of the analysis allows a different form selectivity to be applied since it is possible to perform the step procedure for many deposition potentials (about 1 minute per deposition potential).

1.6.4 The variants of PS-ASC

There are several possible variants of potential step anodic stripping coulometry. The discussion in this section only considers the stripping process (e.g., single potential step ASC refers to a single stripping step). Although the depositions in this work were also conducted by stepping the potential, these could ostensibly also be performed by

scanning the potential or even by an applied cathodic current. In single potential step

ASC, SPS-ASC, a single potential step is used to strip all pre-concentrated metals

simultaneously. The potential step is performed by stepping the potential from a holding

potential where the metal(s) of interest have been deposited to a sufficiently anodic

potential to oxidize all plated metals. The background correction for this PS-ASC variant

depends on an identical experiment conducted in a metal free electrolyte. Double

potential step ASC, DPS-ASC, is similar to SPS-ASC with the only difference being that

it includes a second identical stripping step which is preceded by a very short deposition

(e.g., 100 msec). This additional step allows for only very limited (i.e., negligible) pre-

concentration of dissolved metals from the TLC onto the electrode surface, and can be

used to estimate the non-faradaic current.

In principle, it is possible for the subtractive step to have a different range than the

analytical step, and this variant is termed multi potential DPS-ASC, MP-DPS-ASC. For

example, the subtractive step may be from -300 mV to 500 mV following a 100 msec

deposition at -300 mV, whereas the analytical stripping signal is from -500 mV to 500

mV following exhaustive deposition at -500 mV. It follows that subtracting the two

signals ought to directly provide the difference in the faradaic signal (assuming the two

non-faradaic components are very similar in magnitude). However, this variant provides

only limited information the contributions of the faradaic and non-faradaic components

for each of the steps, and is not suitable for the method validation and proof of concept

experiments. Although of potential use in the future, this variant of ASC is not used in

this work.

The sequential form of MP-DPS-ASC, termed SEQ-MP-DPS-ASC, essentially combines two separate DPS-ASC experiments. In the first, it seeks to determine the net stripping signal between two potentials (e.g. 0 mV and 500 mV) by employing two separate pulses preceded by exhaustive deposition and a brief deposition, respectively. Subtraction yields the total faradaic current (i.e., the concentration of Metals 1 and 2, for instance) which are deposited and stripped between the potentials of 0 mV and -500 mV. The same sequence is then repeated to obtain the faradaic signal for a more cathodic deposition potential (e.g., -500 mV and 500 mV) where the total signal is due to the combined Metals 1 and 2, along with Metal 3. Comparison of the two steps allows indirect measurement of the concentration of Metal 3.

1.6.5 Sample Pretreatment Considerations

One impediment to remote monitoring is of course sample pretreatment which is easily performed in a laboratory. As noted in the above discussion, the sample pretreatment method is dependent on the specific analyte, the sample matrix, and the analytical method. In practice, only the analytical method may be chosen and the chosen method of ASC along with the majority of electrochemical analyses techniques for heavy metals share two pretreatment steps (acidification and dissolved oxygen removal) [53-54]. The first step is typically a digestion and/or acidification of the sample to extract and/or activate the heavy metals. The acidification step serves two purposes. Most water samples contain so called 'humic acids', which exist as negatively charged species at near neutral pH, and form complexes with cationic heavy metal species (e.g. Pb, Cd) [55-56].

The second reason for acidification is to inhibit the formation of insoluble metal hydroxides during the stripping step **[57]**.

1.6.5.1 Acidification and Humic Acid Removal

Acidification of the sample is a relatively minor problem since the sample volumes are very small and it is in principle feasible to include a concentrated acid reservoir in the remote instrument along with a micro-mixer to introduce to the sample. Another limitation of electrochemical sensors in the field is electrode fouling over time, since the signal is usually dependent on electrode area. Once again, the class of analytes that causes electrode fouling are the humic acids **[58]**. One of the advantages of coulometric analysis is that in the event of partial electrode fouling, it simply takes longer for analyte molecules to reach the electrode surface. However, the removal of humic acid has been reported using a variety of miniaturizable techniques including electrochemical oxidation and UV digestion **[59-60]**.

1.6.5.2 DO Removal is the Most Challenging Step

The most challenging step for heavy metal analysis in the field is the interference of dissolved oxygen or its H_2O_2 reduction product on the stripping analysis of some metals including Pb and Cd **[61-62]**. A brief review of the literature on oxygen removal prior to analysis reveals several approaches, few of which are suitable for remote deployment. The development of such a system capable of dissolved oxygen removal with minimal sample alteration is therefore highly desirable. A promising approach where dissolved oxygen is reduced to water on Ag electrodes has been reported but direct

exposure of the sample allows plating of some metals on the electrode surface **[63]**. Approaches for indirect DO removal have also been reported and these are based on flowing the sample through DO permeable silicone tubing which is submerged in an oxygen depleted reservoir **[64]**. To date, the combination of these two approaches has not been reported. However, this combination would seem to offer much for remote DO removal.

1.7 Overview of Requirements for Remote Heavy Metal Sensors

The overall goal of this work is to demonstrate the concrete progress towards heavy metal sensor networks with the requisite sensitivity, selectivity, and practicality for decentralized remote analyses of drinking waters, wastewater effluents from industry and agriculture, and even rivers and lakes. The development of this sensor draws its advantages from the fields of microelectronics fabrication and electrochemistry. This approach offers many advantages in the way of practicality including miniaturized and inexpensive sensors, potential for real-time data acquisition, reduced need for manual operation, and reduced energy requirements. It also takes advantage of advances in miniaturized instruments such as miniature remote potentiostats, control circuitry, communications, etc. Due to the complexity and interdisciplinary nature of this approach, an overview of the entire system has been included as **Figure 1.8**.
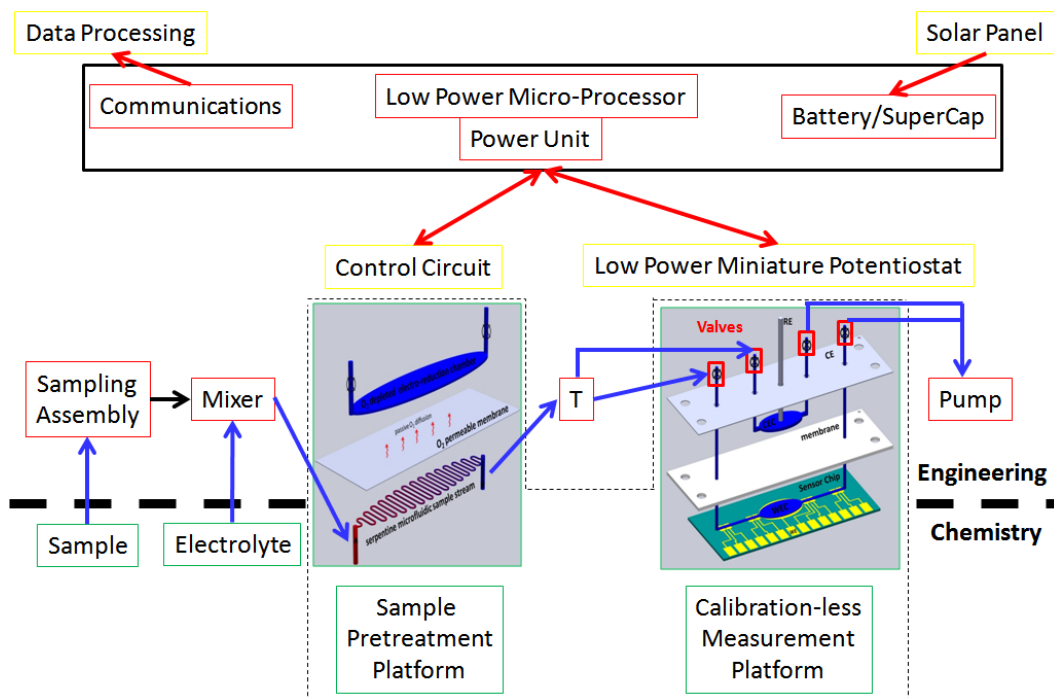
Figure 1.8: Overview of the remote heavy metal sensor. The portions contained within the dashed lines indicate the focus of this dissertation. Green outlines indicate major progress of a component, yellow outlines indicate preliminary work, and red outlines indicate as yet to be addressed components.

1.8 Overview of Dissertation

A select list of key issues has been compiled in **Table 1.6** to frame the

developments which are described in this work. In Chapter 2, the development and

evaluation of a microfabricated platform suitable for calibration free determination of

metals by ASC is described. This platform consists of a stopped-flow, thin-layer, three-

electrode electrochemical cell (a microfabricated gold working electrode, pyrolytic

graphite counter electrode, and custom miniature Ag/AgCl reference electrode). In

Chapter 3, the application of this sensor to measurements of arsenite in the presence of

the interferents Cu, Pb, Cd, and Zn by SEQ-MP-DPS-ASC is described. In Chapter 4, a

device for the indirect removal of dissolved oxygen from microfluidic sample streams is

developed and evaluated. Finally, Chapter 5 summarizes the current status of the remote

heavy metal sensor in terms of its sensitivity, selectivity, and practicality. This discussion

also includes a description of future directions of this research that are aimed at further

improvements in sensitivity and selectivity; and a brief description of the remaining

challenges which will hopefully inspire future developments.

Chapter	Specific Aim	Status
2	Microfabricated Stopped-Flow Thin-Layer Cell of Known Volume	Addressed
2	Anodic Stripping Coulometry for Metals (Cu and Hg)	Addressed
3	*In situ* Background Subtraction (DPS-ASC and SEQ-MP-DPS-ASC)	Addressed
3	Sensitivity and Selectivity of As^{III} in the Presence of Cu, Pb, Cd, and Zn	Addressed
4	Sample Pretreatment (Oxygen Removal)	Addressed
5	Sensitivity & Selectivity (Approaches for Further Enhancement)	In Progress
5	Durability and Practicality Considerations: Remote Miniature Potentiostat, Automated Sample Handling, Communications, Powering the Remote Sensor, etc.	In Progress

Table 1.6: The specific aims for developing a remote heavy metals sensor for water
analysis and the current development status.

CHAPTER II

MICROFABRICATED STOPPED FLOW THIN LAYER

CELL FOR ANODIC STRIPPING COULOMETRY

2.1 Overview

Remote unattended sensor networks are increasingly sought after to monitor the drinking water distribution grid, industrial wastewater effluents, and even rivers and lakes. One of the biggest challenges for application of such sensors is the issue of in-field device calibration. With this challenge in mind, we report here the use of anodic stripping coulometry (ASC) as the basis of a calibration-free microfabricated electrochemical sensor (CF-MES) for heavy metal determinations. The sensor platform consisted of a photo-lithographically patterned gold working electrode on SiO_2 substrate, which was housed within a custom stopped-flow thin-layer cell, with a total volume of 2-4 μL. The behavior of this platform was characterized by fluorescent particle microscopy and electrochemical studies utilizing $Fe(CN)_6^{3-/4-}$ as a model analyte. The average charge obtained for oxidation of 500 μM ferrocyanide after 60 seconds over a 10 month period was 176 μC, corresponding to a volume of 3.65 μL (RSD=2.4%). The response of the platform to copper concentrations ranging from 50-7500 ppb was evaluated, and the ASC results showed a linear dependence of charge on copper concentrations with excellent reproducibility (RSD ≤ 2.5%) and accuracy for most concentrations (≤ 5-10% error). The

platform was also used to determine copper and mercury mixtures, where the total metallic content was measurable with excellent reproducibility (RSD $\leq$ 4%) and accuracy ($\leq$ 6% error).

2.2 Introduction

At present, water quality monitoring for heavy metal contaminants is usually handled by costly and relatively complex instruments such as ICP-MS, GC/LC-MS, and AAS [1]. These instruments provide a high level of performance in terms of sensitivity and selectivity but require operation by trained personnel, usually in a central laboratory [2]. This approach also relies on selected "grab sampling" where samples are collected on-site and then transported to the lab for analysis. The result, of course, is a "snapshot" of the water quality at a particular time and place which may not be representative of other times and places in the over-all system. Alternatively there are numerous portable instruments, often electrochemical in nature, which permit measurements to be made in the field [3-7]. This is a promising approach, particularly in view of the rapid advances in fabrication of micro total analysis systems [8]. However, these are normally operated by a suitably trained technician and still offer the same type of periodic "snapshot" monitoring provided by the grab sampling approach. This is an important limitation, and clearly it would be desirable to develop a sensing system that enables continuous, on-site operation on a 24/7 basis with minimal direct operator intervention.

At present, there do exist some commercially available instrument systems intended for continuous water monitoring [9]. These systems, which are usually intended for use in monitoring drinking water distribution grids, are typically large in size and relatively expensive and require direct access to a conventional electrical power source.

Furthermore, the analytical measurements carried out are usually non-specific in nature –

e.g., conductivity, turbidity, etc. – and therefore provide little or no direct insight into the

presence of individual metal species. As a consequence, this approach does not seem to

offer a very attractive solution for real-time sensing of heavy metals in drinking or

wastewater systems.

It seems that a more promising approach is the development of simple yet reliable

sensors that can be constructed in large quantity, with a high degree of reproducibility,

and at an affordable cost. Such devices could be placed permanently on-site to create an

appropriate sensor network and interfaced to a wireless communications network for

control and monitoring purposes [10-11]. In order for this goal to be practically

achievable, advances are required in numerous technical areas. However, the focal point

of such a measurement network is, of course, the sensor itself which needs to be able to

operate accurately and reliably for extended periods but independently without the need

for constant maintenance or direct supervision. Unfortunately, most analysis methods for

metals fail to meet this critical requirement. Even if miniaturized and field-deployable,

nearly all instruments require considerable attention from a suitably skilled technician for

proper operation. For example, virtually all analytical instrumentation, including

electrochemically based devices, require frequent calibration, even when located in a

pristine laboratory setting [2, 12]. When deployed for long measurement periods in an

uncontrolled field environment (temperature, humidity, etc.), calibration issues may be

overwhelming.

With this in mind, we have chosen to investigate a well-known but infrequently

used electroanalysis technique – coulometry – that, in principle, should not require

calibration **[12]**. Nearly all electroanalysis methods are sensitive to a variety of variables

such as temperature, pH, electrolyte concentration, and electrode area and therefore

provide reliable quantitative information only if these variables are suitably controlled

and the experiment is adequately calibrated by comparison to standard solutions of

known concentration. This is certainly true for nearly all commonly employed

voltammetric and potentiometric measurement schemes. The exception to this are

coulometric measurements in which a sample is electrolyzed and the resulting electrical

charge (current Integrated over time) is determined. Such processes are described by

Faraday's Law, first proposed by Michael Faraday in 1834:

$$Q = n \cdot F \cdot N \qquad \textbf{(Equation 2.1)}$$

where Q is the measured charge in coulombs, n is the # of electrons involved in the redox

process, F is the Faraday constant (96,485 coulombs/mole), and N is the number of moles

of sample species electrolyzed. An alternative form of the equation is:

$$Q = n \cdot F \cdot C \cdot V \qquad \textbf{(Equation 2.2)}$$

where C represents the analyte concentration and V the sample volume. Clearly, n and F

are constants for any given redox process. So, as long as the redox reaction (n) is known,

the sample volume (V) is known, and the electrolysis has proceeded to 100% completion,

the associated charge is an absolute measure of the analyte concentration – regardless of

prevailing experimental conditions. The only requirements are that 1) the analyte is

electrochemically active and 2) sample pretreatment methods (e.g., acidification for cationic trace metal analysis) can be practically achieved in the field. EPA regulated contaminants that can be monitored electrochemically include lead, mercury, cadmium, arsenic, chemical oxygen demand, and many others. Variations in temperature or pH or even changes in electrode area due to fouling are irrelevant to the determination as long as the electrolysis is given sufficient time to proceed to completion.

Some coulometry-based analysis concepts have been reported in recent years. In particular, Bakker's group has demonstrated how coulometric methodology may be used to transform ion-selective electrode measurements that are conventionally potentiometric in nature [13-14]. For example, application of a constant current to appropriate ion-selective membranes can be used to deliver coulometrically controlled amounts of various ions for either calibration or titration purposes. Alternatively, application of a suitable potential at an ion-selective membrane and measurement of the current over time (or charge) associated with the resultant ion uptake can produce a calibration-free ion-selective sensor that may be attractive for remote monitoring purposes [15].

A coulometric variation on traditional anodic stripping voltammetry (ASV) was reported for metal analysis by Beinrohr's group in the early 1990s [16-19] and, more recently, by Geneste [20-21] and Pierce [22] as well. In this approach, the sample solution is passed through a porous flow-through electrode possessing a large surface area. When a reducing potential is applied, metals are collected via electrodeposition; and, as in conventional ASV, they can be stripped off and determined after a suitable accumulation period. In all of these cases, the integrated stripping current gave the total charge associated with the sample volume that had flowed through the electrode

(assuming 100% electrodeposition); and a potentially calibration-free analysis was possible. Although it is possible that this anodic stripping coulometry (ASC) method might be suitable for on-site remote sensing applications, we are not aware of any such reports as yet. Furthermore, because of the requirement to maintain a fixed and very well known sample flow rate in this approach, implementation in practice would require an accurate and reliable pump or flow meter if flow is natural e.g., capillary action, gravity, etc.) on each sensing platform.

We believe that a more attractive coulometric approach that is consistent with the production of relatively economical sensing devices is the stopped-flow thin-layer cell. Because the sample volume is determined only by the cell volume, the quality of the measurement does not depend on a precisely metered flow rate; and the device design ought to be greatly simplified. Recently, our group has completed "proof-of-concept" work on such calibration-free coulometric approach **[23]**. Specifically, we have reported a μL-volume, thin-layer coulometric cell that allows total sample electrolysis to be achieved with a high degree of reproducibility in less than a minute. This cell consisted of isolated working and counter electrode chambers where the working electrode was microfabricated by photo-lithographically patterning a Si wafer with a Au film that covered the entire bottom of the cell. For a model analyte (such as $Fe(CN)_6^{3-/4-}$), this first-generation device was shown to track the analyte concentration over a very wide range and to yield reliable sub-ppm determinations over periods of weeks without the need for direct calibration. In the present work, we describe further developments in the coulometric analysis technique. In particular, we report device improvements

implemented in order to provide higher quality coulometric performance and application of the approach to measurement of metals.

2.3 Experimental

2.3.1 Chemicals

Copper and mercury standard AAS solutions (1000 ppm), potassium nitrate, nitric acid, and sodium chloride were all purchased from Sigma-Aldrich (Milwaukee, WI); potassium ferrocyanide was obtained from VWR International (Batavia, IL), and agarose was purchased from Difco Laboratories (Detroit, MI). All chemicals were of the highest available purity and were used without further purification. Deionized water was used to prepare all solutions, and potassium ferrocyanide solutions were prepared daily before use.

2.3.2 Sensor Chip Containing the Working Electrode

Fabrication of the sensor chips was conducted in the cleanroom facility of the University of Louisville Micro/Nano Technology Center. The gold sensing electrodes were patterned on SiO_2 coated wafers using an image reversal photolithographic liftoff technique. Briefly, this process consisted of thermally oxidizing a 100 mm silicon wafer to form a ~500 nm oxide insulating layer. The SiO_2 layer was then coated with a positive photoresist and selectively exposed in a MA6/BA6 mask aligner (Suss MicroTec, Garching, Germany) to yield the negative of the desired pattern. Subsequently, gaseous NH_3 assisted image reversal in a 310TA oven (Yield Engineering Systems, Livermore, CA) was used to improve liftoff and yield patterned wafers with exposed oxide only in

the electrode regions. A buffered oxide etch produced a ~210 nm recessed region in the oxide layer. These recessed regions were then filled by two successive sputtering steps (conducted without breaking vacuum) utilizing the multi-target PVD 75 sputtering machine (Kurt J. Lesker Co., Jefferson Hills, PA). The final electrode consisted of a thin nickel adhesion layer (100 Å) covered by a layer of gold (2100 Å), which served as our thin-film gold working electrode. A final liftoff step then removed the excess metal deposits atop the remaining sacrificial photoresist, exposing the final patterned wafer. The edges of the metal filled recesses were checked by a Dektak 8 surface profilometer (Veeco Instruments Inc., Plainview, NY), and the surface roughness was less than 10 nm in all cases. Each wafer contained 13 sensor chips which were then separated by dicing to yield the individual 1.3 cm X 3 cm sensor chips (**Figure 2.1 inset**).

2.3.3 Flow Cell

The flow cell consisted of the sensor chip, two polycarbonate fixtures, two rubber gasket layers, and a membrane. Drawings for the top and bottom fixtures were prepared using Computer Aided Design (CAD) software (Solidworks, Dassault Systèmes SolidWorks Corp., Waltham, MA) and were milled from translucent polycarbonate by a commercial prototyping service (FirstCut, Proto Labs Inc, Maple Plain, MN). A trench in the bottom fixture allowed for precise positioning of the sensor chip, and four alignment pins (short 1/16th inch stainless steel rods) between the two polycarbonate fixtures served as guides for precise placement of the remaining components during assembly. The drawings for the gasket and membrane layers were also prepared using CAD software (AutoCAD, Autodesk, Inc., San Rafael, CA) and cut using a precision 40W CO_2 mini

laser cutter/engraver (Epilog Laser, Golden, CO). Assembly of these components together yielded a three electrode, membrane separated, dual compartment cell with independent flow paths for each compartment (**Figure 2.1**). Here we refer to the lower compartment containing the working electrode as the analysis compartment, and the upper compartment containing the counter and reference electrodes as the auxiliary compartment.

The volume of the lower (analysis) compartment was defined by the sensor chip's central 8 mm X 5 mm elliptical electrode (which served as the working electrode) on the bottom, the elliptical hole in the lower gasket along its sides, and the membrane (SelRO MPF-34, Koch Membrane Systems, Inc., Wilmington, MA) at the top. The lower gasket was made of 125 μm (± 75 μm) thick ultra-pure silicone rubber, and the elliptical hole in the center sat atop the sensor chip's elliptical electrode, masking the edges for an active area of 8 mm X 4 mm. This central hole was flanked by two 8 mm long X 0.5 mm wide holes which channeled flow to pre-cut holes in the layers above. The volume of the upper (auxiliary) compartment was defined by the same SelRO membrane on the bottom, the upper gasket (8 mm X 4 mm hole in 500 μm (± 75 μm) thick ultra-pure silicone rubber flanked by two 1 mm X 0.5 mm holes to channel flow upwards as before) along its sides, and the top fixture. This upper compartment also contained the counter and reference electrodes, which were inserted through access holes in the top fixture.

Two types of counter electrodes (CE) were employed. The first CE consisted of two ultra-pure (99.985%) 1 mm diameter gold wires (Alfa Aesar, Ward Hill, MA) in the bottom face of the top fixture connected together to form a single electrode. This CE was made by inserting a length of the gold wire through two pre-machined access holes in the
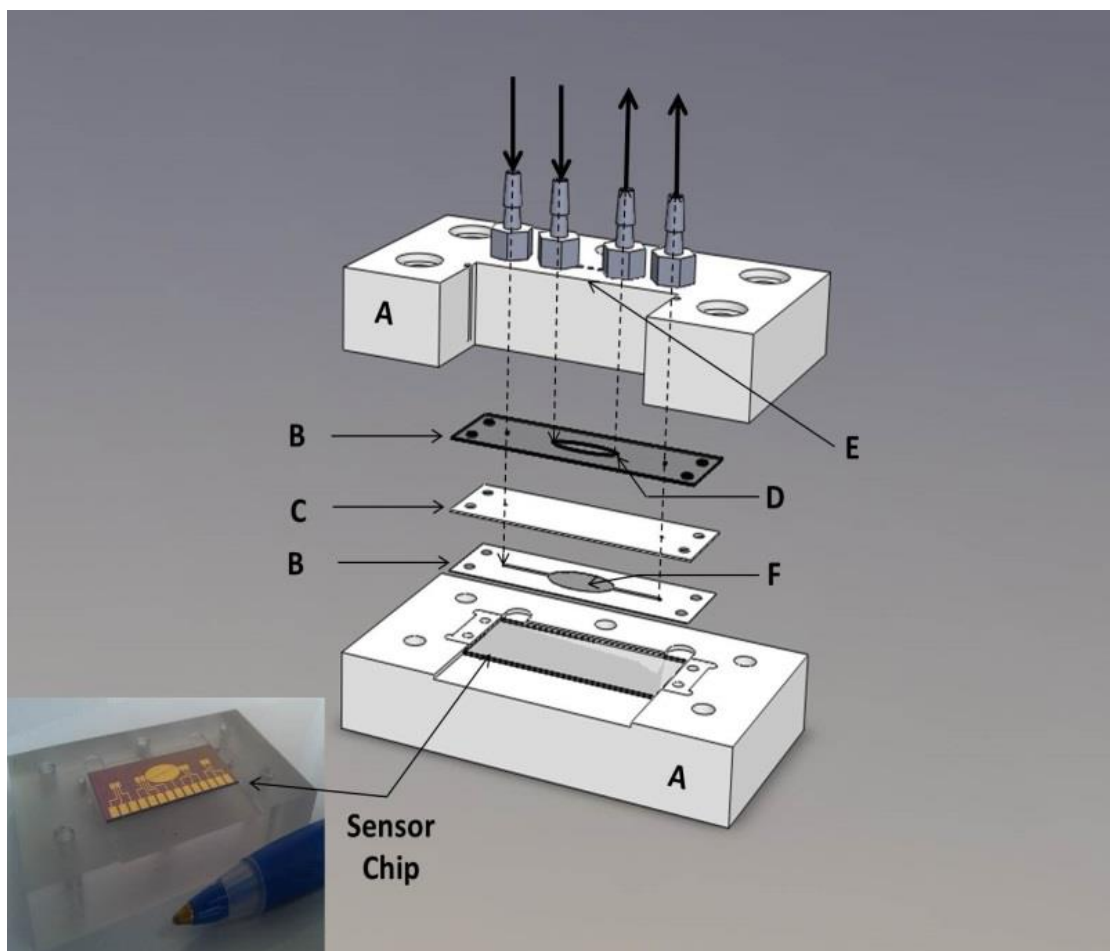
Figure 2.1: The platform consists of two polycarbonate fixtures (A), two rubber gasket layers (B), analyte impermeable membrane (C), counter and reference electrode compartment and access holes (D&E), and 2-4 µL working electrode analysis compartment (F). Assembly yields a three electrode dual compartment cell with independent flow paths. **Inset:** Photo of elliptical Au working electrode on SiO_2 chip, bottom fixture, and a pen for scale.

top fixture. The second type of CE consisted of a flat 100 μm thick pyrolytic graphite sheet (Panasonic Electronic Components, Secaucus, NJ) incorporated as an additional layer between the top gasket and top fixture. This custom cut pyrolytic graphite sheet (PGS) included holes for the alignment pins and flow paths of the layers above and beneath it, and an additional 0.8 mm diameter hole in the center aligned with the access hole for the miniature reference electrode (RE). In order to ensure stopped flow during electrochemical experiments, rigid connections were used to connect the inlets and outlets of the top fixture to closeable valves. These valves served to isolate the microfluidic analysis cell from the flexible Tygon tubing used to connect it to the sample and waste reservoirs. Fittings, tubing, rubber gaskets, syringes, and valves for sample handling were all composed of inert plastics and rubbers and were obtained from Cole-Parmer (Vernon Hills, IL) and/or McMaster Carr (Aurora, OH). The expected volume of the analytical compartment based on the design dimensions was 2-4 μL, depending on the thickness of the gasket used. The exact volume was established for each set of experiments using known concentrations of electroactive species such as $Fe(CN)_6^{3-/4-}$ or Cu^0/Cu^{2+}.

2.3.4 Reference Electrode

For all experiments in the cell, we utilized a custom-made Ag/AgCl miniature reference electrode. The end of a 3-4 cm length of ultra-pure (99.997%) 100 μm diameter silver wire (Alfa Aesar) was soldered to a larger wire for easier handling and then cleaned by successive sonication in 1 M HNO_3 and deionized water. Chlorinating the clean silver wire was conducted vs. a similar length of 500 μm diameter Pt wire in 1 M

NaCl using a two electrode configuration. A function generator (Model 4011A, B&K Precision Corp., Yorba Linda, CA) was used to generate a 560 mV, 40 msec on/60 msec off pulse that was applied for 60-70 min. A rectifier diode (1N4001, Vishay Semiconductor) was placed in series with the electrodes to suppress any reverse (non-oxidizing) current. The square wave was monitored with an oscilloscope (Model DS1052E, Rigol Technologies Inc., Oakwood Village, OH), and a digital multimeter (Model 34410A, Agilent Technologies Inc., Santa Clara, CA) was connected via a LabVIEW (National Instruments, Austin, TX) control program to monitor the unidirectional current flow over time. Reverse current during the "off" period was negligible, while the typical average current during the "on" period was 300-400 μA initially and gradually increased to 400-500 μA after 60-70 minutes. The chlorinated silver wires were stored in deionized water until needed. To assemble the reference electrode, 3 M NaCl was drawn into a 41 mm long X 0.8 mm O.D. glass capillary (Drummond Scientific Co., Broomall, PA) until it was about 3/4th full, then the bottom of the capillary was pressed into solidified 3% w/v agarose gel in 3 M NaCl to form a ~0.25 inch frit. The chlorinated wire was then inserted into the top of the capillary and sealed with Torr Seal insulating epoxy (Varian Vacuum Technologies, Lexington, MA). The fritted end was immersed in 3 M NaCl while the epoxy dried and thereafter stored in that solution when not in use. The prepared electrodes exhibited less than 10 mV drift over an 18 hour period relative to commercial Ag/AgCl reference electrodes (Bioanalytical Systems, West Lafayette, IN).

2.3.5 Fluorescent Particle Microscopy

For microscopy, the CNC machining tool marks were removed from the bottom polycarbonate fixture by chemical and mechanical polishing until the fixture was optically clear. For this study, the assembled flow cell was identical to that described above, except that the sensor chip was replaced by a transparent glass slide of identical dimensions (Fisher Scientific, Pittsburgh, PA). The Fluoro-Max R0200 2 μm polystyrene fluorescent particle solution (Thermo Fisher Scientific Inc., Waltham, MA) was prepared by adding 2-3 drops to 50 mL deionized water until the particle density was visually suitable. The visualization utilized a Nikon Eclipse Ti-U inverted microscope (Nikon Instruments Inc., Melville, NY) equipped with a green light source for excitation of the particle immobilized dye (λ_{ex}=542 nm, λ_{em}=612 nm), and a suitable filter for isolating the emitted light. Videos and snapshots were captured using a Pico Sensicam QE camera (PCO AG, Kelheim, Germany). After filling the cell, repositioning the microscope platform and fine-tuning the focus (approximately a 30 second process), the camera was used to record the particle movements at 9.1 frames per second. A total of 46 frames, recorded 30 to 60 seconds after filling the cell, were then combined into a single composite image where streaks represent the movement of particles over a 5 second span in real-time. The particles which did not move, presumably immobilized on the walls of the compartment, reflect the elliptical shape of the compartment.

2.3.6 Electrochemical Measurements

Electrochemical measurements were carried out using a BASi Epsilon potentiostat (Bioanalytical Systems, West Lafayette, IN). For ferrocyanide, the basic

experiment consisted of using a syringe to fill the working electrode compartment with

500 μM ferrocyanide in 0.1 M KNO_3. To ensure that the electrode surface was

sufficiently pre-conditioned prior to each run, a potential of -100 mV was applied and

held for 10 seconds, followed by a 400 mV potential applied for 130 to 600 seconds to

exhaustively oxidize the ferrocyanide to ferricyanide. Background correction was

performed by conducting an identical experiment in the absence of ferrocyanide (0.1 M

KNO_3 only). The analyses of Cu and Hg were conducted in a 10 mM HNO_3/10 mM NaCl

supporting electrolyte and also utilized a 10 second pre-conditioning step (at the stripping

potential) followed by a reducing potential step at 0 mV for exhaustive deposition of the

metals.

For early experiments, the background was obtained in a separate experiment in

which the cell was filled with blank solution. However, in order to simplify the

background correction process and minimize possible changes in electrode area over

time, later experiments utilized an *in situ* background correction which was performed in

the sample solution by stripping with and without pre-concentration of the metal on the

electrode surface. The potential step sequence was 850 mV for 10 seconds to pre-

condition the electrode surface, 0 mV for 60 seconds to exhaustively reduce the metals

onto the electrode surface, 850 mV for 640 msec during which the metal stripping signal

was recorded, 850 mV for an additional 60 seconds to allow the metals to diffuse back

into the cell, 0 mV for 20 msec where metal deposition was minimal, and finally to 850

mV for 640 msec to obtain the background stripping signal. In all cases, the experiments

were performed in triplicate for each sample, resulting in 3 current vs. time plots for each

sample and/or blank. A LabVIEW program was created to integrate the current-time

curves and calculate the total charge passed following the potential steps.

2.4 Results and Discussion

2.4.1 Micro-Coulometry Cell Performance

In our earlier work [**23**], we reported the development of a proto-type micro-

coulometry platform for calibration-free measurements and characterized its performance

using $Fe(CN)_6^{3-/4-}$ as a model analyte. This device consisted of a µL-volume thin-layer

cell with isolated working and counter electrode chambers. The actual working electrode

consisted of a sputtered Au layer that was photo-lithographically patterned and covered

the entire bottom of the elliptical cell (25.6 mm^2). Thus, for the approximately 80 µm

thick cell employed, the length of time required for complete electrolysis, once the

working electrode compartment had been filled with sample and an appropriate potential

was applied, was approximately 15 sec. The electrolysis charge was found to track the

$Fe(CN)_6^{3-/4-}$ concentration over a very wide range (50-10,000 µM); and, most important,

the approach gave stable and reproducible results for extended periods without the need

for any calibration or other operator adjustments. The elliptical shape of the cell also

promoted complete replacement of the cell contents, as indicated by excellent run-to-run

reproducibility.

However, despite these positive outcomes, closer examination of the coulometry

experiments indicated significant problems in cell performance. In particular, although

the electrolysis currents were relatively short-lived as expected, it was found that these

currents never completely reached the appropriate background and in fact persisted at low

levels for extended time periods. Consequently, the corresponding charge failed to reach a fixed level (representing total oxidation/reduction of the $Fe(CN)_6^{3-/4-}$ sample) but rather continued to increase slowly but steadily long after the cell should have been exhausted. For example, even though diffusion considerations suggested that electrolysis should be complete within tens of seconds, the accumulated charge continued to increase for several minutes and reached levels much higher than could be accounted for simply by the quantity of $Fe(CN)_6^{3-/4-}$ that had been injected into the cell (e.g., total charge 140% of expected after 1 min).

In view of these findings, the first problem that needed to be addressed in the current study was to improve the absolute coulometric performance of the measurement platform. The fact that the observed currents were always so long-lived and the measured charges for all $Fe(CN)_6^{3-/4-}$ concentrations consistently exceeded the expected values suggested that the effective electrolysis volume was larger than the actual physical volume of the cell and that this volume was augmented by unanticipated analyte mass transfer during the electrolysis. This could be due to such factors as analyte diffusion into the cell **[24-25]**, leakage of sample solution, or residual flow after filling the sample compartment. In order to investigate these possibilities, we turned to a fluorescence particle microscopy (FPM) approach in order to visualize directly the microfluidic processes that were occurring in the device during a typical analysis.

The details of the FPM experiments are provided in the Experimental Section. Very briefly, the microfabricated sensor chip was removed and replaced by a transparent glass slide to permit viewing of the cell from below by an inverted microscope. The $Fe(CN)_6^{3-/4-}$ sample solution was replaced by one that contained a suspension of 2 μm

fluorescent-tagged polystyrene particles, but the cell filling procedure was carried out via manual syringe loading in exactly the same manner as usual. During the first 30 seconds, visual observations qualitatively indicated the flow was very fast initially and thereafter gradually slowed to a steady state value within 15-30 seconds. **Figure 2.2A** shows a composite FPM image constructed from dozens of individual photos taken between 30 and 60 sec after a typical sample injection. In this image, recorded at the outlet of the electrolysis cell, the vertical streaks represent the movement of individual fluorescing particles during this period. Clearly, the sample solution was not static as desired but rather showed a long-term and relatively steady flow through the cell. By measuring and averaging the lengths of several streaks, the average linear flow rate was estimated to be nearly 4000 μm min^{-1} – which corresponds to a volume flow rate on the order of 0.30 μL min^{-1}. Considering that the total volume of the electrolysis cell was only 2-4 μL, it was apparent that this level of residual sample flow could easily account for the surplus current and charge noted above.

In an attempt to address this problem, all flow paths into and out of the cell (which previously had consisted of 1/8th inch I.D. Tygon tubing) were replaced by rigid plastic connectors. In addition, manual valves that could be closed after sample injection were inserted into the sample flow stream as close as possible to the device in order to isolate the cell to the greatest extent possible. When these simple measures were implemented, the residual sample flow was drastically decreased. As seen in **Figure 2.2B**, FPM imaging revealed that the steady-state flow was reduced by a factor of 4 (to 0.07 μL min^{-1}). Most critically, the resulting coulometric performance showed an immediate and drastic improvement. As shown in **Figure 2.3**, the experimentally measured charge for

$Fe(CN)_6^{3-/4-}$ closely matched the theoretically calculated charge over a much longer time period than before. Because the residual flow was not completely eliminated, the accumulated charge did increase slowly over time, but at a much slower rate than for the previous device.
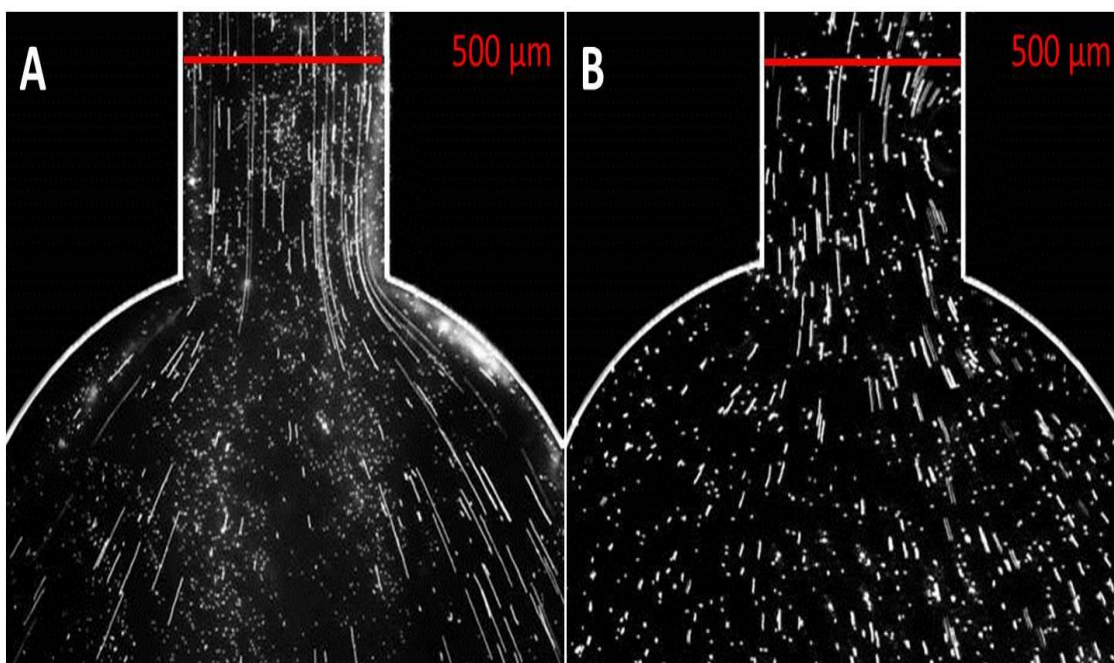
Figure 2.2: Fluorescent particle microscopy through transparent bottom fixture (sensor chip replaced with glass of identical dimensions). Particle movements recorded at 9.1 fps, 46 frames composited to show particle movement over a 5 second span. A: Open valves, linear flow in channel: 3970 µm min^{-1}. B: Closed valves, linear flow in channel: 882 µm min^{-1} (0.07 µL min^{-1} volumetrically).
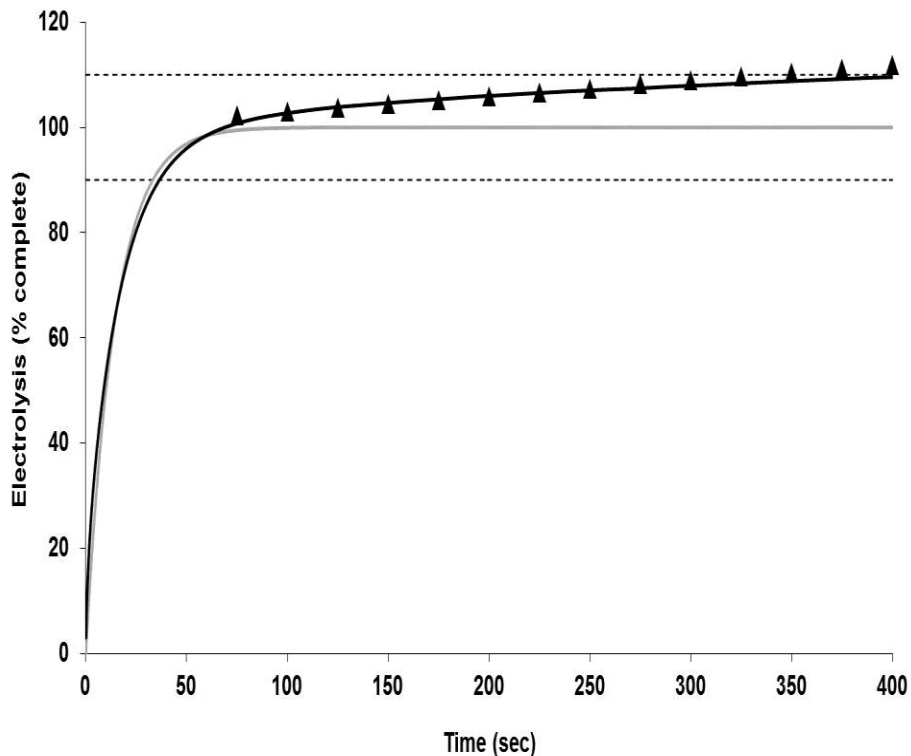
Figure 2.3: Theoretical response of micro-coulometric cell (grey line), experimental result (black line), and ±10% of theoretical (dashed lines), and flow model based on 0.07 µL min⁻¹ of Figure 2.2B (triangles). Experimental data from charge accumulated during oxidation of 500 µM ferrocyanide in 0.1 M KNO_3, background corrected and normalized. Oxidation at 0.4 V after 10 second electrode pre-conditioning at -0.1 V vs. Ag/AgCl, background correction obtained by subtraction of identical experiment with electrolyte only.

At times up to 2 minutes, there was practically no difference from the calculated charge; and even at electrolysis times up to 7 minutes, far exceeding that required for diffusion across the thin-layer cell, the measured charges remained within 10% of the expected/theoretical value. Further, the divergence of the experimental charge from the calculated charge appeared to be satisfactorily explained by accounting for the steady flow of fresh analyte at 0.07 µL min^{-1} (triangles of **Figure 2.3**).

With the improved cell approaching stopped-flow conditions, it was possible to determine experimentally the cell volume by using ferrocyanide solutions of known concentrations. This would represent a good measure of the inherent reproducibility of the electrolysis operation over an extended period of time as shown in **Table 2.1**. The average charge obtained for the oxidation of 500 µM ferrocyanide after 60 seconds over a 10 month period was 176 µC, corresponding to a volume of 3.65 µL, with an RSD of 2.4%. Each day, the platform was 'freshly' assembled with different individual components (e.g., sensor chips, gaskets, electrodes). Even the major modification of the platform layout, for example, by addition of an extra layer (PGS counter electrode) did not affect the calculated cell volume (Days 291, 292, and 308), compared to the calculated volumes when the built-in gold counter electrode was used (Days 1, 5, and 105). The experimentally obtained charges and calculated volumes above also showed the coulometric performance of the cell, with the excess charge after 130 seconds being, on average, only 5% higher than the charge at 60 seconds. Although improvements directed toward improving the coulometric performance of the device are being planned, the quality of these measurements was deemed adequate to allow the desired application to metal monitoring to be initiated.

Day	Charge after 60 Sec (μC)	Calculated Volume (μL)
1	180 (1.4%)	3.73
5	179 (4.0%)	3.71
105	172 (1.3%)	3.56
291	170 (2.0%)	3.53
292	179 (1.3%)	3.71
308	177 (0.8%)	3.65
Avg.	176 (2.4%)	3.65 (2.4%)

Table 2.1: Experimentally calculated cell volumes on different days. Experimental details were the same as Figure 2.3. For each day, values in parentheses are the RSDs of three measurements, whereas the RSD next to the average values are for the six days.

2.4.2 Applications to Metal Analysis/Anodic Stripping Coulometry

Obvious targets for electrochemically based analysis methods are the heavy metals, many of which are well known for their characteristic electroactivity. These species are of potential importance in practically relevant applications such as the monitoring of drinking and waste water systems. One fundamental difference in the analysis of metal analytes, compared to solution analytes such as ferri-/ferrocyanide, is the deposition of the reduced metal onto the electrode surface. In classic metal stripping experiments, the dissolved metal ion is pre-concentrated onto the electrode surface during a long lasting deposition step performed at a sufficiently negative potential to result in accumulation of a metallic deposit on the electrode surface. The deposition step, typically carried out in a bulk solution, is often accompanied by a stirring of the solution to enhance the transport of ions to the electrode surface, thereby enhancing the pre-concentration effect. The most common stripping process involves some form of anodic potential sweep (linear or pulsed) where the metal deposits accumulated on the electrode surface during the deposition step are removed at a characteristic potential and the resulting currents are recorded.

This is, of course, the basis for the familiar ASV trace analysis technique. The peak sizes (areas or heights) of the resulting voltammogram can then be used to determine the metal concentration by comparison to prepared standards. The peak size is dependent on numerous factors including the electrode area and history, deposition time, stirring rate, and the potential sweep parameters. Therefore, calibration is always necessary; and we are not aware of any reports of calibration-free methods based on voltammetric stripping techniques. By analogy, the method specifically examined here

might be termed anodic stripping coulometry (ASC). As with ASV, both deposition and stripping cycles are possible. The basic differences are that, with ASC, the amount of sample is fixed by the thin-layer cell volume and the length of time required for complete electro deposition is relatively short. Because the sample volume is intentionally restricted to a few μL, the very low concentration levels accessible by ASV are unlikely to be accessible with ASC. However, by fixing the volume, one ought to achieve an absolute, calibration-free measurement.

Figure 2.4 illustrates a typical square-wave voltammogram (SWV) obtained for a sample solution containing both Cu^{2+} and Hg^{2+} placed in the thin-layer micro-coulometry cell described above. (These metals were chosen because they are reducible at fairly positive potentials at the Au working electrode and therefore allowed us to avoid the concomitant reduction of O_2 and H_2O.) The voltammogram showed the expected redox processes: Hg^{2+} reduction at approximately 600 mV and Cu^{2+} reduction at 275 mV (vs. Ag/AgCl) as well as the corresponding oxidations of the deposited metals on the return SWV scan. The oxidation, or "stripping", peaks of trace B are larger than the reduction, or "deposition", peaks of trace A due to the pre-concentration effect that occurs for each metal once its reduction potential has been reached. In fact, the reduction waves observed corresponded to the "underpotential deposition" (UPD) peaks related to the very first metal monolayer deposited onto the Au surface, which appears at a somewhat more positive potential than the subsequent "bulk" deposition occurring after the Au surface has been saturated. From the outset, we decided to focus on the UPD condition because, in view of the our small cell volume and large working electrode area, it was expected that sub-monolayer coverage would be exceeded only at very high Cu^{2+} or Hg^{2+}
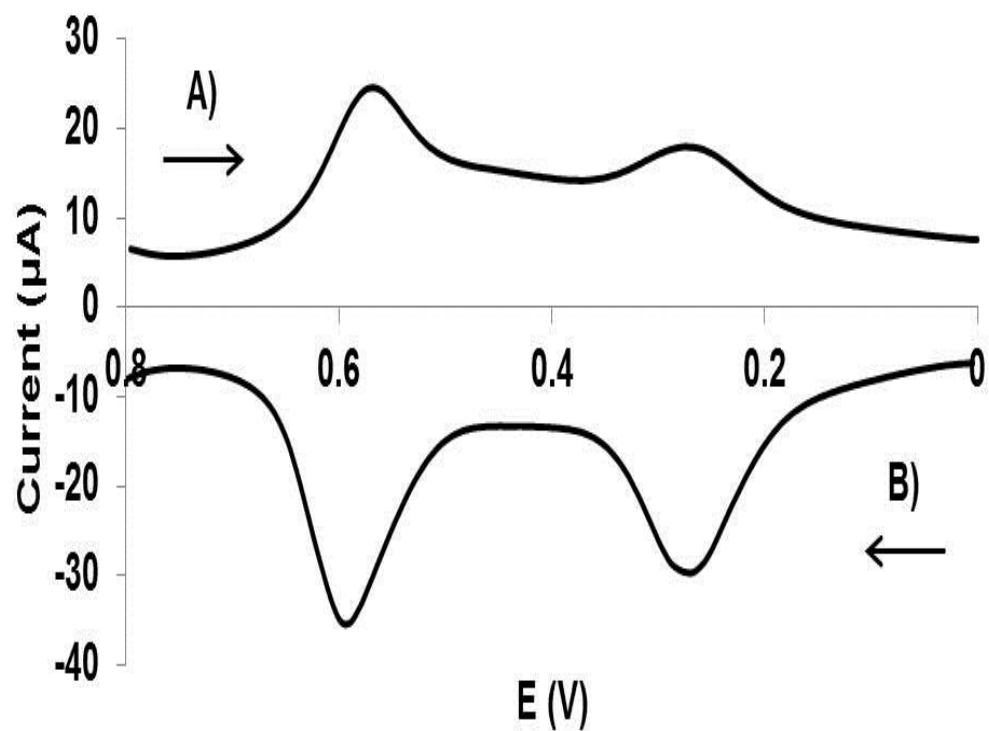
Figure 2.4: Square wave voltammogram in the micro-coulometry cell of 1.5 ppm Cu^{2+}/5 ppm Hg^{2+} in in 10 mM HNO_3/10 mM NaCl, pH 2.20 ($f = 15$ Hz, $E_p = 25$ mV, $E_s = 4$ mV, 2 second quiet time preceded deposition before immediate return scan). A) Deposition trace showing reduction of Hg^{2+} followed by Cu^{2+}. B) Stripping trace showing oxidation of metallic Cu followed by metallic Hg.

concentrations. For example, calculations indicate that, for our specific cell, copper

concentrations up to 20 ppm would yield sub-monolayer coverage [**26**]. By contrast, the

maximum allowable Cu concentration in drinking water is only 1.3 ppm and that for most

other heavy metals is much less than this. In addition, UPD conditions produced

simplified voltammograms where (1) there was only one reduction peak and one

oxidation peak for each metal, (2) intermetallic alloys were less likely to form [**27**], and

(3) the Au electrode surface was likely to show less run-to-run hysteresis and therefore

greater long-term reproducibility [**28**].

Initial ASC experiments, shown in **Figure 2.5**, examined the i-t behavior

obtained for electrolysis of a sample solution that contained only Cu^{2+}. Each experiment

consisted of two phases. First, the potential was stepped to 0.0 V where the Cu^{2+} was

efficiently reduced to Cu^0 and the corresponding current was recorded over time. As seen

in **Figure 2.5A**, the background corrected currents, whose levels were directly related to

the Cu^{2+} concentration employed, decreased smoothly after the potential step, reaching

the background after approximately 15 seconds. Next, as shown in **Figure 2.5B**, the

potential was stepped back to 0.45 V to oxidize the deposited Cu^0 back to Cu^{2+}. Again,

the currents (after background correction) were proportional to the Cu concentration in

the starting sample. In this case, however, the currents were both much larger in

magnitude and much shorter-lived, now decaying very rapidly and reaching the

background level after only 500 msec. The slower decay of the deposition signal was, of

course, determined by the diffusion of copper ions across the cell to the electrode surface

and matched well what would be expected for the 73 μm thick cell used in this set of

experiments. However, the stripping signal for the surface-confined copper, whose
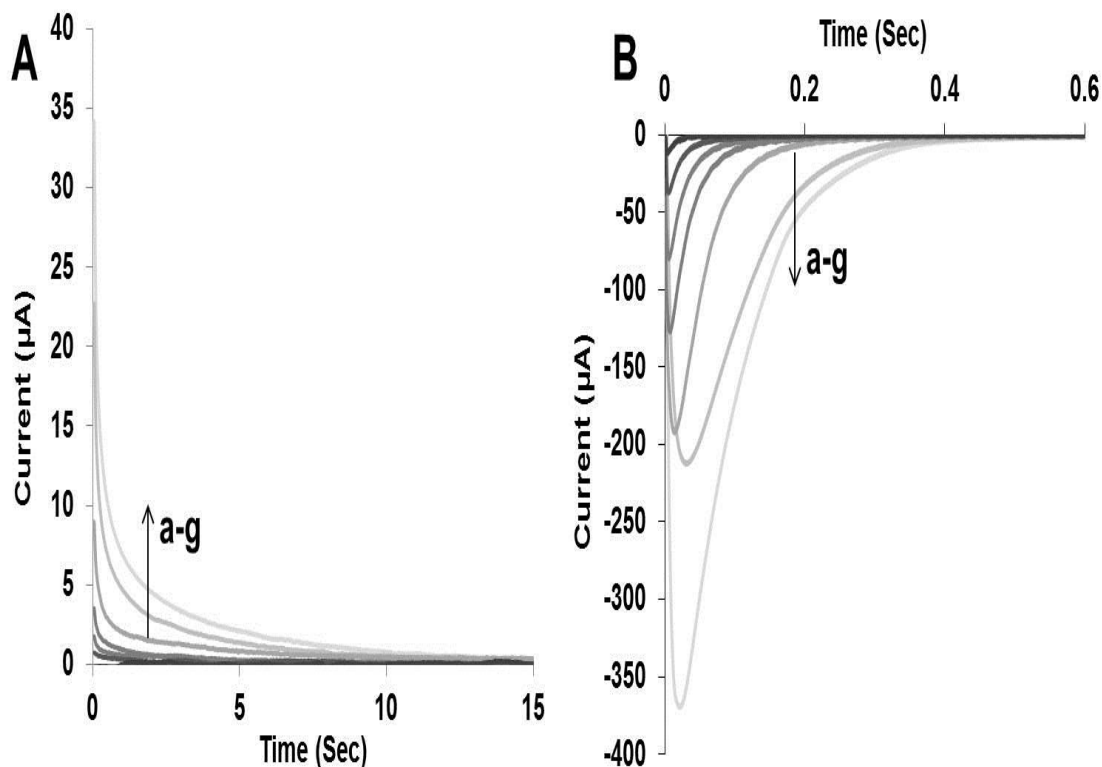
Figure 2.5: Anodic stripping coulometry experiment for copper concentrations of 0.05 ppm (a), 0.2 ppm (b), 0.5 ppm (c), 1 ppm (d), 2.5 ppm (e), 5 ppm (f), and 7.5 ppm (g) in 10 mM HNO_3/10 mM NaCl, pH 2.20. **A)** Background corrected deposition traces of first 15 seconds shown (total deposition time was 60 seconds). **B)** Background corrected current time traces for subsequent stripping. Depositions were performed at 0 mV for 60 seconds and stripping at 450 mV for 640 msec vs. Ag/AgCl reference electrode (3 M NaCl) and using PGS CE. Each trace represents the average of 3 trials of each $[Cu^{2+}]$ minus the average of 3 blank trials performed immediately prior to each concentration.

oxidation is no longer diffusion dependent, exhibited much faster charge accumulation. For all concentrations studied, the magnitude of the stripping charge was essentially finished in less 500 msec (with the measured charge increasing by <2% after an additional 140 msec). For both the deposition and stripping experiments, the corresponding charges could be obtained by integration of these i-t curves. When this was done, the coulometry data shown in **Table 2.2** and the calibration curves shown in **Figure 2.6** were obtained.

Several aspects of the ASC results in **Table 2.2** were noteworthy. First, for both the deposition and stripping cycles, the total charges were directly related to the Cu^{2+} concentrations over the entire range studied – from 50 ppb up to 7500 ppb which is consistent with an absolute measurement such as exhaustive coulometry of a fixed sample volume. Second, for any given Cu^{2+} concentration, the total charge seen for the deposition and stripping cycles was always essentially the same which is consistent with a chemically reversible electrode process such as Cu^0/Cu^{2+}. Third, the accuracy and the precision of charge data obtained for the stripping cycle were consistently superior to the similar data for the corresponding deposition cycle. For the stripping experiments, the charges were much more reproducible, with RSDs generally less than 1%, even for the lowest concentrations employed. More important, the charges measured for the stripping cycle also matched the charges expected for the cell volume and Cu^{2+} concentrations much more closely – usually within 10% – than was the case for the corresponding deposition measurements where the discrepancy with the expected charge was sometimes 50% or more.

This last feature of the ASC data – namely, the obviously higher quality of the stripping data compared to the deposition data – was somewhat surprising. We believe that this improvement is likely due to the much shorter time scale of the stripping step in ASC compared to that of the deposition: 500 msec vs. 15 sec. While the signal measured in each of these cycles should be identical in magnitude, it occurs over a much shorter time window for the stripping step; and therefore, there may be much less noise included in the measurement. This is a somewhat different situation than ASV where improved detection is obtained by the use of an extended electro deposition period to increase the signal directly. Despite the dissimilarity of the deposition processes, ASV and ASC both favor the stripping step to produce higher quality data.

The lowest Cu^{2+} concentration employed in this study was 50 ppb (or 0.8 μM), but it was apparent that the limit of detection (LOD, signal/noise = 3) was somewhat lower. We chose not to try to optimize this aspect of ASC at this time because the LOD will clearly be determined by the specific characteristics of the ASC platform in use (in particular, the cell/sample volume and electrode area) and the specific application being targeted (i.e., the particular metal). Nevertheless, it seems likely that LOD values in the low ppb range should be achievable without drastic changes in cell design. At the same time, it is important to realize that the immediate goal of our ASC sensors is not to rival the ultra-trace level quantitation capabilities of conventional ASV but rather to make possible stand-alone sensing devices for use in sensor networks capable of providing reliable semi-quantitative monitoring capabilities suitable for early warning or emergency purposes.
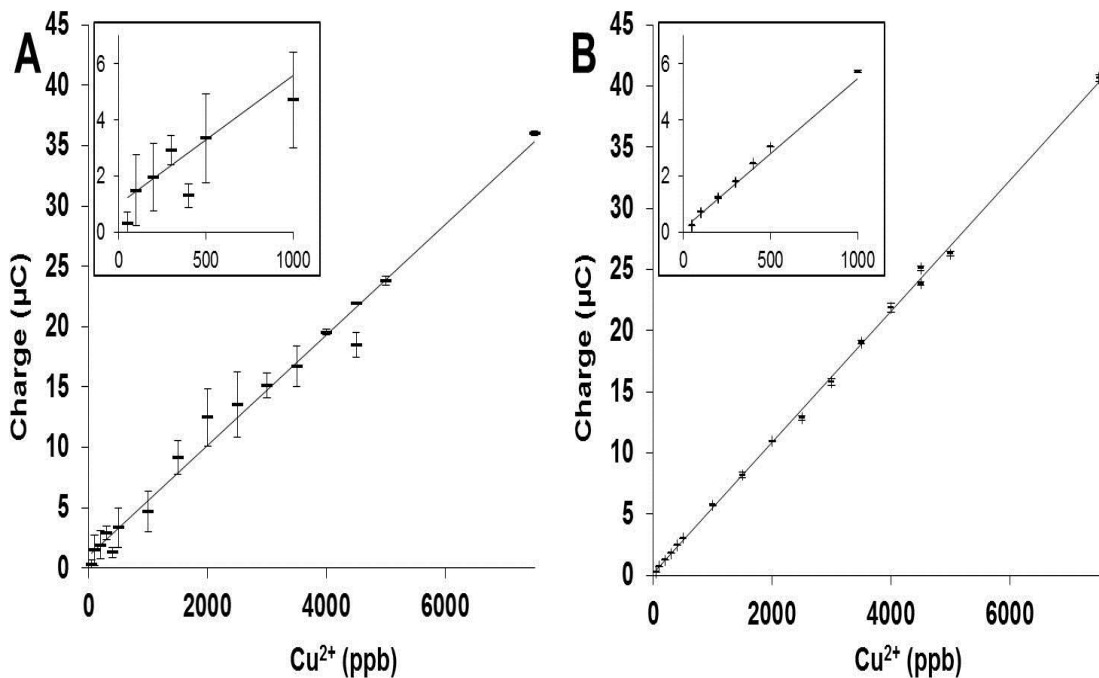
Figure 2.6: Background corrected charges for Cu^{2+} concentrations of 50 ppb to 7.5 ppm in a solution of 10 mM HNO_3/10 mM NaCl, pH 2.20. **A)** Charges of deposition cycles from Figure 2.5A (0-15 seconds). **B)** Charges of stripping cycle from Figure 2.5B (0-640 milliseconds). Error bars represent the standard deviation (n=3).

Concentration (ppb)	Calculated Charge (µC)	Deposition charge (µC)	Percent of Calculated	Stripping Charge (µC)	Percent of Calculated
7500	41.7	36.0 (0.5%)	86	40.7 (0.7%)	98
5000	27.8	23.9 (1.6%)	86	26.3 (0.7%)	95
4500	25.0	22.0 (0.5%)	88	23.8 (0.6%)	95
4000	22.2	19.5 (1.2%)	88	21.9 (1.6%)	98
3500	19.5	16.7 (10.1%)	86	19.0 (0.7%)	98
3000	16.7	15.1 (6.5%)	91	15.8 (1.6%)	95
2500	13.9	13.5 (19.9%)	97	12.8 (1.4%)	92
2000	11.1	12.5 (19.1%)	112	10.9 (0.5%)	98
1500	8.3	9.2 (15.0%)	110	8.2 (2.5%)	98
1000	5.6	4.7 (36.0%)	85	5.7 (0.9%)	103
500	2.8	3.3 (47.6%)	120	3.0 (0.3%)	109
400	2.2	1.3 (33.8%)	58	2.4 (0.3%)	109
300	1.7	2.9 (17.9%)	175	1.8 (0.2%)	106
200	1.1	1.9 (62.3%)	174	1.2 (0.8%)	109
100	0.6	1.5 (85.6%)	266	0.7 (0.6%)	125
50	0.3	0.3 (127.6%)	110	0.2 (0.3%)	81
4500	25.0	18.5 (5.6%)	74	25.1 (0.6%)	100

Table 2.2: Background corrected experimentally determined charges for the deposition and stripping cycles for 50-7500 ppb Cu^{2+}. Deposition charges calculated after a 15 second reduction and stripping charges after 640 msec of oxidation (RSD indicated in parentheses n=3). Calculated charges are based on 1.83 µL cell and $2e^-$ process for copper reduction and oxidation. Experimental conditions were the same as Figure 2.5.

2.4.3 Metal Mixtures

It is unlikely that, in practice, many real samples such as drinking water or waste water would contain only a single metal ion. Rather, it is far more likely that, even if the analyst might be interested in only a single specific metal in his or her sample, other metals that are subject to electro deposition and stripping would be present in the sample as well. Therefore, a logical next step in characterizing the ASC method was to start to investigate samples that consisted of mixtures of metal ions. Of course, unlike ASV, where a potential scan is employed during the stripping cycle and individual metals give rise to peaks at characteristic potentials, the current ASC method employs just a single potential step for stripping. Thus, the resulting i-t curves provide insight only into the total quantity of metals that were electrodeposited from the sample and give no direct information with regard to exactly which metals had been present in the sample. In order to obtain such qualitative information, a more complex stripping approach would be required.

The first mixture examined contained both Cu^{2+} and Hg^{2+}. The SWV in **Figure 2.4** shows the i-E behavior of these metals under the prevailing experimental conditions and that both metals can be electrodeposited at 0.0 V (vs. Ag/AgCl). After exhaustive deposition, the metals were subsequently stripped from the electrode surface by a potential step to 850 mV, and the resulting i-t stripping curves for both Cu^{2+} alone and a Cu^{2+}/Hg^{2+} mixture are shown in **Figure 2.7**. In both cases, the i-t curves shown are just those for the stripping of the Cu or Cu/Hg deposit since this measurement cycle has the greater analytical utility. The behavior seen in **Figure 2.7A** for Cu^{2+} by itself was exactly as expected: an exponentially decreasing anodic current that reached the background

level within 100 msec; and, as shown in **Table 2.3**, integration of this amperogram yielded charges that closely matched the value expected for this concentration and sample volume. Corresponding results for the Cu^{2+}/Hg^{2+} mixture, shown in **Figure 2.7B** and **Table 2.3,** also displayed the expected short-lived oxidation current and allowed accurate determination of the total metal concentration present. However, close examination of the i-t curve for the mixture showed that the stripping current for the Hg deposit was slightly slower than that for Cu. The reason for the difference in time dependence, which was always seen for Cu/Hg mixtures, is not known at this point but presumably is due to slower electron-transfer kinetics for the Hg oxidation or to a specific interaction of the Hg with the Au electrode surface such as amalgam formation.

In order to evaluate the capabilities of ASC for long-term calibration-free sensing applications, the above analyses of Cu^{2+} and Cu^{2+}/Hg^{2+} samples were repeated several times over a period of more than 2 weeks. The results obtained, along with the values expected for the concentrations used, are summarized in **Table 2.3**. As always, the measured charges were highly reproducible for any single set of replicate measurements, with RSD's of only a few percent. In addition, the charges showed good accuracy over the entire 2-week period, with errors usually much less than 1-3%. Although a 5-10% error in a conventional laboratory analysis might be considered large, we regard this level of performance as very good considering that these results did not depend on the use of any standards or on any run-to-run adjustments of the measurement platform and that the target of our ASC method is on-line metal measurement as part of a continuous "early warning" system.
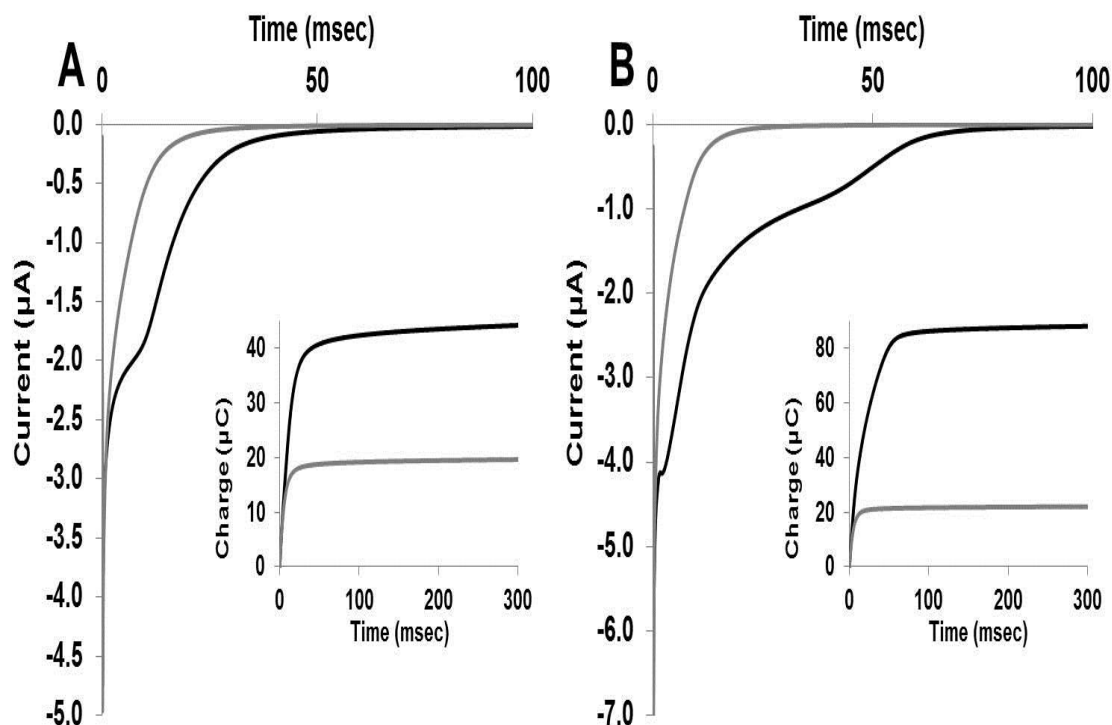
Figure 2.7: Simultaneous determination of copper and mercury using *in situ* background correction. **A)** 30 µM Cu^{2+}. **B)** 30 µM Cu^{2+} and 50 µM Hg^{2+}. Electrolyte consisted of 10 mM HNO_3 and 10 mM NaCl, pH 2.20. Depositions were performed at 0 mV for 60 seconds and stripping at 850 mV for 320 msec (vs. Ag/AgCl reference electrode and using PGS CE). Each trace represents the average of 3 metal trials (black) and 3 metal free electrolyte trials (grey). Insets show the corresponding charge-time curves.

Day	30 µM Cu^{2+} (RSD)	Error from Expected	30 µM Cu^{2+} / 50 µM Hg^{2+} (RSD)	Error from Expected
1	21.4 µC (0.4%)	1.9%	55.2 µC (3.3%)	1.6%
2	22.3 µC (0.5%)	6.0%	57.6 µC (2.1%)	2.7%
18	21.0 µC (1.1%)	0.1%	54.6 µC (1.8%)	2.6%

Table 2.3: ASC background corrected results for Cu^{2+} and Cu^{2+}/Hg^{2+} mixtures over several weeks (RSD in parentheses n=3). The expected charges were 21 µC for copper and 56 µC for the copper/mercury mixture.

2.5 Conclusions

Although coulometry is a well-established electrochemical technique that has long been used in the investigation of electrode processes, it has not routinely been employed as a quantitative analysis tool. The reason for this is that coulometry is neither highly sensitive nor highly selective in nature and therefore possesses some distinct limitations for trace analysis of complex samples. Nevertheless, this study demonstrated clearly that coulometry, particularly in the form of ASC, offers some unique advantages. Most important, by carrying out exhaustive electrolysis in a µL-volume thin-layer cell, it is possible to make an absolute quantitative determination of the concentration of electroactive analytes. As long as the cell volume is fixed, the determination does not require the use of any standards and can be viewed as essentially "calibration free". This uncommon feature of ASC makes the approach extremely attractive for applications requiring continuous on-site monitoring where immediate operator intervention is not feasible. Further, the ASC method should also be relatively insensitive to prevailing environmental conditions, such as temperature, which are not possible to be controlled in the field without direct operator input.

By means of the microfabricated ASC device described here, we were able to begin exploring potential applications of this technique for the determination of individual metals and mixtures and were able to achieve rapid detection at sub-ppm levels by making use of the very fast stripping process that follows the much slower electro deposition step. Numerous issues remain to be investigated before practical applications for unattended on-site metal analysis by ASC will be feasible – e.g., electrode materials other than Au, more advanced stripping waveforms, inclusion of

elementary sample treatment steps. Nevertheless, we believe this new analysis approach

is promising and that the current study represents a useful advancement of this

methodology.

CHAPTER III

ASC OF ARSENIC (III)

WITH IN SITU BLANK SUBTRACTION

3.1 Overview

The prevalence of arsenic in ground water and the large number of potential water sources used for drinking and irrigation makes remote widespread monitoring highly desirable. The ideal approach should be highly independent of operator intervention (i.e., automatable), not require any sort of calibration or blank electrolyte for background correction. Additionally, the approach ought to be selective for the most toxic of the arsenic species and tolerate possible interference by other metals. We describe such an approach here that is based on our previously developed microfabricated platform for determination of metals by potential step anodic stripping coulometry. Further, we also report the use a double potential step ASC (DPS-ASC) variant for *in situ* background correction, which does not require the use of a separate blank solution. To measure As(III) in the presence of other metals, (sequential multiple potential) SEQ-MP-DPS-ASC is used to correct for the contribution of Pb, Cd, and Cu to the stripping signal. The coulometric response is shown to linear for As(III) standards between 100-1000 ppb (errors <10% and RSD <5%). In the presence of interferents, 500 ppb As(III) is

measurable to better than 10% error even in the presence of high interferent levels (1.3 ppm Cu^{2+}, 500 ppb Cd^{2+}, 500 ppb Pb^{2+}, and 5 ppm Zn^{2+}). Similar performance was also possible for As(III) spiked Ohio River water after pH adjustment. An artificial component of the signal arising from the DPS-ASC method itself is also shown to be partially addressable by the SEQ-MP-DPS-ASC method.

3.2 Introduction

Human exposure to arsenic from groundwater used for drinking has been linked to numerous health problems, including skin diseases and a variety of cancers **[1],** and adversely affects the health of millions of people worldwide. For example, the Chinese Ministry of Health screened 445,000 wells in 20,000 villages between 2001 and 2005 and found 5% and 13% contained arsenic levels greater than 50 ppb and 10 ppb, the old and current World Health Organization and EPA recommended limits, respectively **[2-3]**. Despite the view that this problem is particularly associated with underdeveloped regions **[4]**, naturally occurring arsenic in groundwater also represents a concern in rural regions of developed countries. For instance, it has been determined that a significant portion of groundwater wells in the northeast, midwest, and west regions of the USA have arsenic levels that exceed 10 ppb **[5]**. In addition, accidental release from industrial waste ponds can lead to elevated arsenic levels in local waters, and a variety of health scares relating to contamination of crops grown with arsenic contaminated waters or soils continues to be an issue **[6]**.

Current EPA approved methods for As monitoring in drinking water include ICP-AES, ICP-MS, GF-AAS, and HG-AAS **[7-12]**. The cost and complexity of these methods

clearly limit their widespread application, and any large-scale As monitoring program based on these approaches would require a sustained and coordinated effort for sample collection and transportation to centralized laboratories. However, arsenic geochemistry and transport processes are complex in nature, and reports indicate that As levels even in individual wells can vary significantly with time. Therefore, both the periodic sampling possible via the above methods and even occasional on-site testing with portable instrumentation fail to provide an ideal system for As monitoring. In fact, the main lasting impact of the large scale study above is a recently reported predictive model for China that is based on parameters such as soil texture, wetness, salinity, and current understanding of the geochemical arsenic mobilization processes in groundwater [13].

Rather, there is a need for sensing devices that enable continuous in-the-field As monitoring. In practice, such sensors need to have adequate sensitivity to detect relevant As species at or near dangerous levels, sufficient selectivity to render complex sample treatment procedures unnecessary, and high enough reliability to permit long-term operation without the need for frequent hands-on operator intervention. Beyond this, the devices also ought to be able to be fabricated reproducibly in large enough quantity and at low enough cost to enable the development of extensive sensor networks. In contrast to the AAS, AES, and MS methodologies, electrochemical (EC) methods would seem to possess many of the above qualities and therefore offer real potential for remote monitoring applications. One of the critical characteristics of EC-based analysis systems is that EC cells can usually be scaled down in size dramatically without incurring any loss in performance. This feature has made the use of modern microfabrication techniques very attractive for the construction of electroanalysis devices; and, as a

consequence, the mass production of miniaturized electrochemical sensors that would be required to create sensor networks has potentially become cost effective **[14]**.

Recently, our group has begun to explore the use of anodic stripping coulometry (ASC), involving the exhaustive electrolysis of a fixed-volume sample, to provide accurate stripping measurements that are effectively calibration free and thus seem to be ideally suited for in-the-field metal sensing applications **[15]**. In this work, our goal is to extend the ASC approach to As analysis. In particular, the sensor system presented here is specifically intended to enable the monitoring of inorganic As(III) or arsenite. Arsenic can exist in a variety of oxidation states including arsenide (As^{3-}), elemental arsenic (As^{0}), arsenite (As^{III}), and arsenate (As^{V}). The most common species of arsenic in ground and surface waters are the inorganic forms of As^{III} and As^{V}, which occur as the oxo-anions AsO_3^{3-} and AsO_4^{3-} and can be protonated to different extents depending on pH **[16]**. Elemental arsenic is nearly non-existent in surface and groundwater while the organic forms are rare and more commonly found in foods where they are readily eliminated by the human body and pose little toxicity risk **[17]**. Of the inorganic forms, As(III) is the more prevalent species in anoxic environments such as groundwater where entry most frequently occurs by dissolution of arsenic rich soil deposits **[17]**. Furthermore, As(III) is reported to be 25-60 times more toxic than As(V), and hundreds of times more toxic than organic As species **[19-21]**. While it would, of course, be ideal to have the capability to determine As in each of its chemical forms, that task would be undoubtedly require the instrument resources of a full analytical laboratory.

However, we believe that development of a practical in-the-field As(III) sensor would represent a useful step forward.

There already exists a substantial body of knowledge regarding As(III) electrochemistry. Both voltammetric and potentiometric stripping techniques have been reported for As, and there is widespread agreement on the utility of the gold electrode for its determination [22-24].The deposition of As^{III} (as As^0) is reported to be facile on Au, requiring the application of a relatively modest cathodic potential, while As^V reduction is much more difficult and occurs only at applied potentials in the H_2 evolution region [25]. Thus, As^{III} can be pre-concentrated selectively and then subsequently determined by anodic stripping. Despite the relative portability electrochemical methods, all of these methods rely on a technician to physically transport instrumentation and manually sample each site. The technician is responsible for essential functions such as calibration to obtain quantitative results and sample pretreatment and/or additional experiments to mitigate the influence of interferents.

In our previous work, we examined the calibration-free quantitative determination of metals such as Cu^{2+} and Hg^{2+}. Our findings were in accord with Faraday's Law: the absolute charge (in coulombs) associated with the deposition process must equal the charge for the stripping process. Although the signal associated with either the deposition or the stripping process could be employed for absolute quantitative analysis, the use of the stripping signal afforded two important advantages: 1) enhanced S/N and 2) more facile background correction. A limitation of our prior investigation was the utilization of a 'blank' electrolyte to obtain background signals for subtraction of the non-faradaic component of the signal. The requirement of a blank solution necessitates an extra sample

preparation step to mix the sample into a known electrolyte, in addition to the experimental steps to obtain and compare blank and analyte signals. We have therefore also been interested in developing an *in situ* blank correction to eliminate the need for a separate blank solution.

One approach for *in situ* blank correction of is so called subtractive anodic stripping voltammetry (SASV). In this method, two stripping voltammograms are obtained in the same solution (with and without prior pre-concentration of dissolved metals) and subtracted to enhance the various peaks at the characteristic potentials for each metal [26]. SASV is commonly used with pulse or step techniques such as SWSV which sacrifice a portion of the stripping signal to enhance sensitivity; and consequently SASV is not routinely or commonly applied as a calibration-less coulometric method [27]. Hence, the typical SASV analysis still requires the use of standards or standard additions. It should be noted that these methods are not intended for the application we have in mind and are indeed well suited for laboratory analysis where frequent operator intervention is possible. However, the concept of SASV is readily applicable to the potential step anodic stripping coulometry method.

3.3 Experimental

3.3.1 Chemicals

Standard AAS solutions (1000 ppm) were used as the source for arsenite, cadmium, copper, lead, and zinc, and were purchased from Sigma-Aldrich (Milwaukee, WI) along with nitric acid and sodium chloride. All chemicals were of the highest

available purity and were used without further purification. Deionized water was used to prepare all solutions, and arsenic solutions were prepared daily before use.

3.3.2 Sample Preparation

As_2O_3, Cu^{2+}, Pb^{2+}, Cd^{2+}, and Zn^{2+} AAS standard solutions (1000 ppm) were diluted into the supporting electrolyte solution containing 10 mM HNO_3 and 10 mM NaCl to make the indicated concentrations of those metals. For the determination of arsenite in natural waters, we used Ohio River water as a test matrix. The river water was collected in Downtown Louisville into a 1 gallon polypropylene container from the Kentucky side riverbank just upstream of the Big Four Bridge (GPS coordinates: 38°15'47.0"N 85°44'14.3"W) and was refrigerated until used. To prepare samples using the RW, slightly less than 100 mL was decanted from the top of the container (to avoid a small amount of sediment which had settled) and allowed to come to room temperature. The sample was then acidified with approx. 900 μL 1 M HNO_3 to a pH of 2, and NaCl added to a final concentration of 10 mM along with the desired amount of As^{III} before the final volume was adjusted to 100 mL. The resulting solution was then filtered through a 0.45 μm polypropylene syringe filter to remove suspended particles and used directly in the analysis described below.

3.3.3 Coulometric Stopped-Flow Cell and Microfabricated Au Working Electrodes

Fabrication and testing of the coulometric flow cell and sensor chips has been previously described [15]. Briefly, thin film (2100 Å) gold working electrodes atop a thin nickel adhesion layer (100 Å) on SiO_2 coated wafers were patterned by an image reversal photolithographic liftoff technique. Each 1.3 cm X 3 cm sensor chip contained a central 8

mm X 5 mm elliptical electrode, and a patterned 125 µm (± 75 µm) thick ultra-pure

silicone rubber gasket was used to define the 8 mm by 4 mm working electrode

compartment in the center of the electrode (**Figure 3.1**). Otherwise, the flow cell

consisted of two polycarbonate fixtures, rubber gasket layers, 100 µm thick pyrolytic

graphite sheet as counter electrode (Panasonic Electronic Components, Secaucus, NJ),

and a 200 MWCO membrane (SelRO MPF-34, Koch Membrane Systems, Inc.,

Wilmington, MA). An access hole at the top allowed insertion of a custom-made

Ag/AgCl 0.8 mm OD miniature reference electrode (RE), also as previously described

[15]. Assembly yielded a three electrode, membrane separated, dual compartment cell

with independent stoppable flow paths (**Figure 3.1**). The volume of the lower (WE)

compartment was 1.85 µL (4 mm X 8 mm X 75 µm) and the dimensions of the top

compartment were 4 mm X 8 mm X 500 µm. Fittings, tubing, rubber gaskets, syringes,

and valves for sample handling were all composed of inert plastics and rubbers and were

obtained from Cole-Parmer (Vernon Hills, IL) and/or McMaster Carr (Aurora, OH).
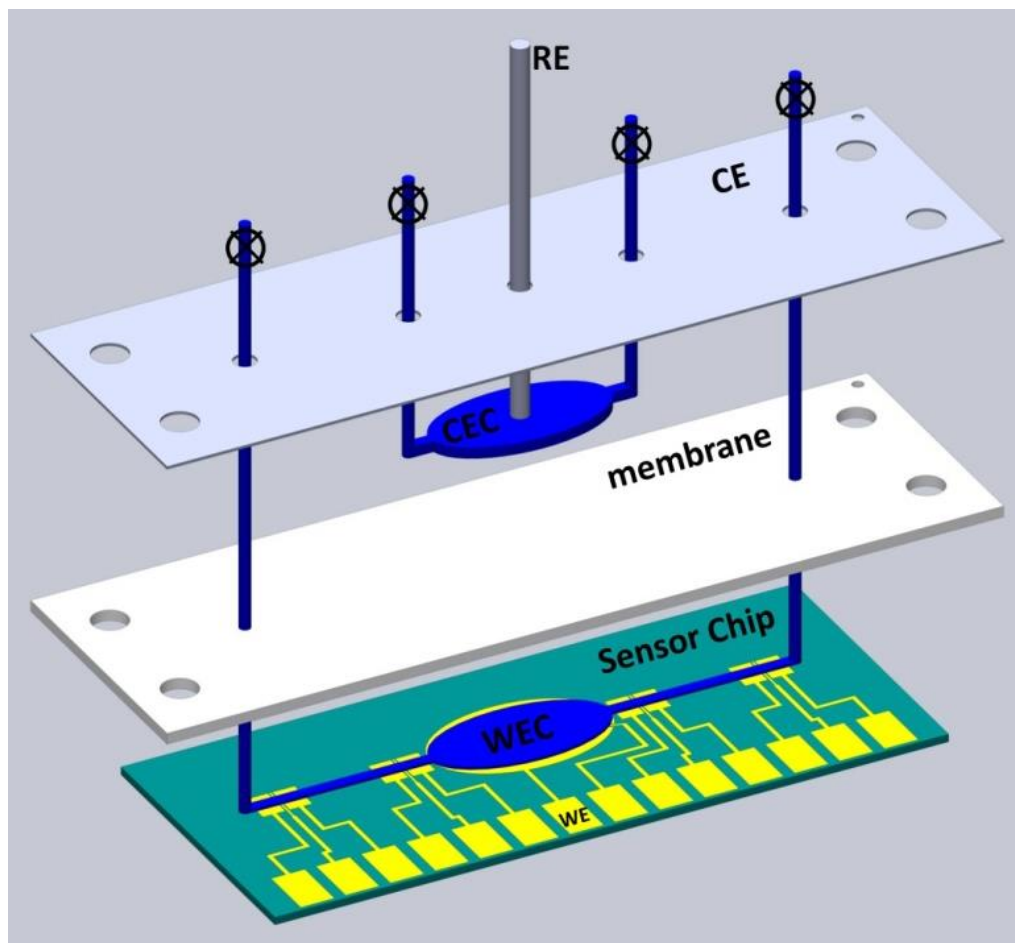
Figure 3.1: Partial schematic of anodic stripping coulometry platform (structural layers omitted for clarity). RE: custom 0.8 mm OD Ag/AgCl reference electrode. CE: pyrolytic graphite sheet counter electrode. CEC: counter electrode compartment (4 mm X 8 mm X 0.5 mm). WEC: working electrode compartment (4 mm X 8 mm X 75 µm). WE: lithographically patterned 5 mm X 8 mm elliptical working electrode and contact pad (remaining electrodes unused in this work). Assembly yields a three electrode dual compartment cell with independent stop-valve controlled flow paths for WEC and CEC.

3.3.4 Electrochemical Measurements

Electrochemical measurements were carried out using a BASi Epsilon potentiostat (Bioanalytical Systems, West Lafayette, IN). With the exception of river water samples, all analyses were conducted in a 10 mM HNO_3/10 mM NaCl supporting electrolyte. In all cases a 10 second pre-conditioning step (at the stripping potential) was followed by the sequence of potentials indicated in **Figure 3.3**. Briefly, this consisted of an *in situ* blank deposition for 100 msec followed by stripping for 320 msec, then deposition for 60 seconds to exhaust the cell volume of all dissolved metals followed by stripping for 320 msec. The deposition potentials were 0 mV for Cu^{2+} deposition, -300 mV for simultaneous Cu^{2+}, Pb^{2+} and Cd^{2+} deposition, and -500 mV for simultaneous As^{III}, Cu^{2+}, Pb^{2+} and Cd^{2+} deposition. The stripping potential was 500 mV in all cases.

3.4 Results and Discussion

3.4.1 Characteristics of As(III) Deposition

Since our aim is in-field calibration-free determination of arsenite, we began by examining the arsenite deposition and stripping processes by CV. Since arsenic deposition is pH dependent, we chose to conduct these initial studies in an electrolyte of known pH (~2). We also chose low arsenite concentrations to ensure that the deposited arsenic on the electrode surface resulted in less than monolayer coverage since metallic arsenic is a semiconductor and does not readily electrodeposit on itself **[28-29]**. The resulting cyclic voltammograms for 2.5 μM arsenite are shown as curve 2 of **Figure 3.2**. Comparing this curve to the electrolyte only CV (curve 1) shows the reduction peak for dissolved oxygen remains nearly unchanged. Although the arsenic deposition peak

cannot be clearly distinguished from the oxygen reduction peak, the notable difference between these two traces is the small arsenic stripping peak at +100 mV. Since the oxygen reduction reaction or its byproducts on Au electrodes has been reported to interfere with stripping analysis for some metals [30-31], we wanted to investigate whether the arsenite stripping response was altered in the absence of oxygen. We therefore purged the arsenite containing sample with N_2 and collected another CV (curve 3). The absence of O_2 allows visualization of the arsenite reduction peak at approximately -300 mV. The size of this peak is comparable to the arsenic stripping peak and also necessary for observation of the latter, indicating that these peaks represent the As^{III}/As^0 redox couple.

These findings were in accord with earlier studies of arsenite, and importantly, showed no evidence of the arsenite peak instability observed by previous investigators [32]. Van den Berg et al. investigated this instability and convincingly showed that generation of HOCl at the counter electrode oxidizes arsenite to arsenate if $E_{dep} <$ -0.5V and/or the chloride concentration is greater than 0.01 M. Van den Berg et al. also described that this effect is exacerbated by the presence of O_2 (whose reduction current at the WE, causes generation of extra Cl_2 at the CE and hence more HOCl). At our chosen conditions of pH~2 and 0.01 M chloride, we do not expect significant contribution of this effect. Additionally, the employment of a membrane to isolate the WE and CE in the ASC platform should further limit the exchange of byproducts between the chambers.
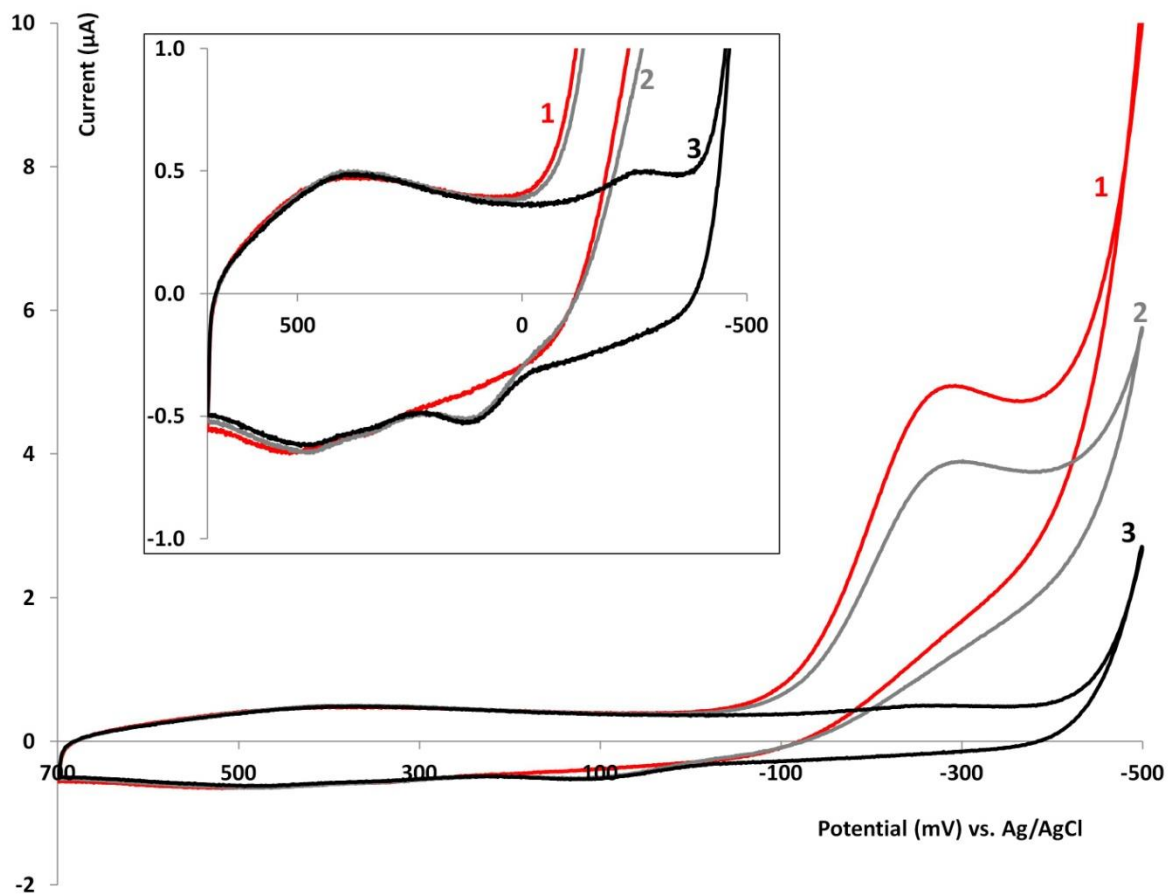
Figure 3.2: Cyclic voltammograms initiated at 700 mV (100 mV/sec scan rate) of 1) 10 mM HNO_3 and 10 mM NaCl supporting electrolyte. 2) 2.5 μM As^{III} in 10 mM HNO_3 and 10 mM NaCl (ambient dissolved O_2). 3) 2.5 μM As^{III} in 10 mM HNO_3 and 10 mM NaCl (after purge and blanket with N_2). **Inset:** Expanded view of +/- 1 μA.

3.4.2 Measuring As(III) Standards by DPS-ASC

All coulometric measurements were performed in the ASC platform of **Figure 3.1**. Our aim was to combine the primary advantage of potential step stripping for absolute coulometric analysis with the primary advantage of SASV, namely *in situ* background correction. We have termed the resulting method, shown in **Figure 3.3**, double potential step anodic stripping coulometry (DPS-ASC). In practice, the DPS-ASC method is very similar to the SASV method described above in that it employs two stripping steps (with and without exhaustive pre-concentration of dissolved metals from the TLC). To experimentally validate this method, we began by conducting the DPS-ASC experiment described in **Figure 3.3** at various arsenite concentrations. In accordance with **Figure 3.2**, we chose a deposition potential of -500 mV and a stripping potential of 500 mV since these would entirely encompass the arsenite deposition and stripping processes. The use of a wide potential window is purposeful in DPS-ASC since a sufficiently positive stripping potential is needed to remove all deposited metals in one step. This ensures the restoration of the gold electrode to its original condition, which is necessary for appropriate subtraction between analytical and background steps. The resulting amperograms for the stripping process with and without exhaustive deposition of the cell contents are overlaid in **Figure 3.4**, and correspond to the two stripping steps of **Figure 3.3**. For each of the arsenite concentrations from 0-1000 ppb, the stripping signal obtained after a brief (100 msec) deposition resulted in negligible metal pre-concentration (<4% of the total dissolved arsenic in the 1.85 μL cell). This 'background' stripping signal is shown as the grey trace of **Figure 3.4** for each concentration and corresponds to the first (grey) stripping signal of **Figure 3.3**. The stripping signal obtained after

exhaustive deposition of the TLC is shown in black and corresponds to the second stripping signal (black) of **Figure 3.3**. The arsenite stripping signal (in coulombs) is therefore equivalent to the difference between the integrated current time curves with and without exhaustive deposition of the cell. The magnitude of this arsenite coulometric stripping signal is visually represented by the crescent shaped area between the signals of **Figure 3.4**.

Plotting the area of these crescents vs. the arsenite concentration resulted in the calibration curve, inset of **Figure 3.4**. Two positive attributes of DPS-ASC that are immediately evident in the calibration curve are its linear response to the arsenite concentration, and of course the low RSD values (~<5%) indicated by the error bars for the individual data points. One aspect of this plot that was unexpected was the non-zero intercept for the blank (electrolyte only) coulometric signal. Independent experiments have demonstrated that this 'signal' is an artifact of the DPS-ASC method. Those experiments show the cause of this artifact is due to the necessary non-identical treatments of the electrode surface prior to each stripping step (100 msec deposition for 'blank; and 60 sec for exhaustive deposition). Although further details are omitted presently, this is an important aspect of DPS-ASC and certainly merits further investigations as described below. Of course, the non-zero intercept complicates the direct application of Faraday's law since the charge obtained at any concentration is partially due to this artifact. However, when this artifact is accounted for by artificially placing the intercept at zero and a cell volume of 1.85 µL is used (as earlier determined by a similar experiment with copper), we find that the absolute accuracy is better than 5%

at concentrations above 500 ppb arsenite, and remains better than 10% for concentrations as low as 100 ppb (**Table 3.1**).

The DPS-ASC experiment was conducted three to five times for each concentration, and the last 3 experiments were always used for the quantitative analysis described above. In between runs, the cell contents were flushed and replaced by a fresh aliquot of sample. Notably, the stripping signals without exhaustive pre-concentration (grey traces of **Figure 3.4A**) were highly reproducible and nearly indistinguishable visually (RSD's < 5%). Similarly the stripping signals after exhaustive deposition were highly reproducible. This reproducibility is somewhat surprising given that the current time plots are obtained in the order indicated by repeating the experiment of **Figure 3.3** (i.e., a deposition and stripping cycle is completed before repeating any particular peak is reproduced). The actual evaluation of the detection limit (LOD) should however be based on the RSD value of the areas for 3 individual crescents representing 3 identical trials, and these RSD values are shown in the fourth column of **Table 3.1**. It thus appears the actual LOD is certainly below 100 ppb and depending on the desired accuracy, the LOQ is also in this range. Nonetheless, this approach does not account for the impact of the non-zero intercept and it is clear that future work should seek to reduce the magnitude of this intercept artifact experimentally. In that regard, investigation of the DPS-ASC method parameters has shown that this intercept can be reduced by making the electrode area smaller and/or the 'blank' deposition time longer than the 100 msec shown in **Figure 3.3**.

96
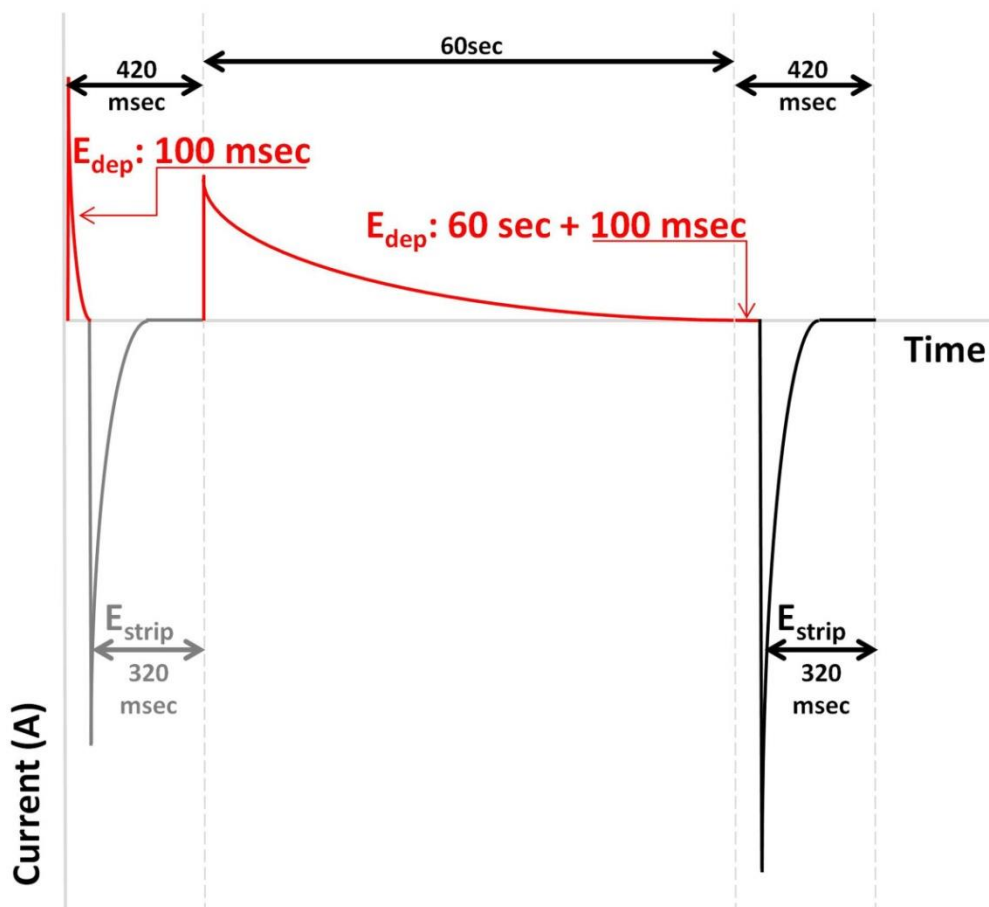
Figure 3.3: Illustration of recorded current during DPS-ASC pulse sequence performed within the ASC platform of Figure 3.1 (not to scale). Experiment always initiated by holding the stripping potential (E_{strip}) for 10 sec (not shown in schematic above). Recording of current initiated upon stepping to deposition potential (E_{dep}) for 100 msec, then stepping to E_{strip} for 320 msec. The potential is then stepped back to E_{dep} for 60.1 sec to exhaustively pre-concentrate all metals on the electrode surface, followed by E_{strip} for 320 msec. E_{dep} was 0 mV for plating Cu^{2+}, -300mV for plating Cu^{2+}, Pb^{2+}, and Cd^{2+} simultaneously, and -500 mV for plating Cu^{2+}, Pb^{2+}, Cd^{2+}, and As^{III} simultaneously. E_{strip} was always 500 mV and reflects the stripping of all plated metals.
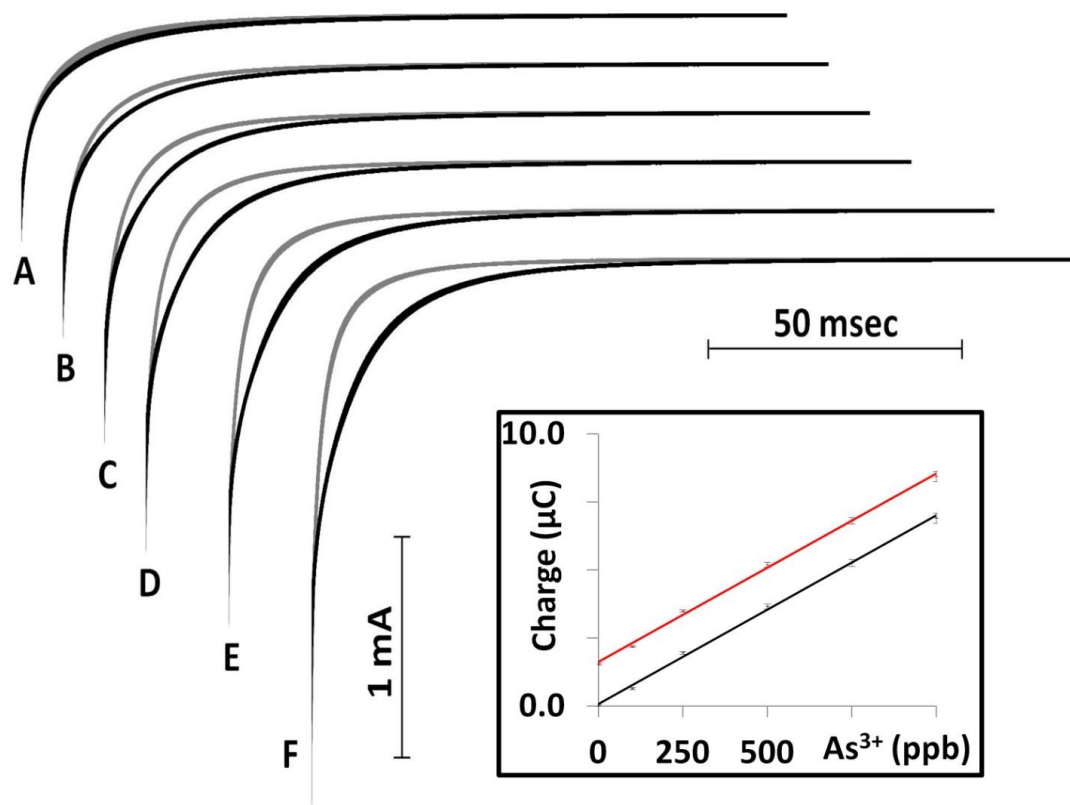
Figure 3.4: DPS-ASC results for As^{III} concentrations of 0 ppb (A), 100 ppb (B), 250 ppb (C), 500 ppb (D), 750 ppb (E), 1 ppm (F) in 10 mM HNO$_3$/10 mM NaCl, pH 2.0. The collected stripping signal for any given concentration (e.g., for F) shows an overlay of the two stripping steps collected during the experiment described in Figure 3.3. **Inset:** Top line: Measured charge in μC for the stripping signals (i.e., area of the crescents at each As^{III} concentration). Bottom line: same as top line, but 'background corrected' so that intercept is zero (see text for discussion). Error bars represent the standard deviation of the crescent areas (n=3).

Arsenite (ppb)	Step 1 Charge (μC) (RSD)	Step 2 Charge (μC) (RSD)	BgC Charge (μC) (Step 2 minus Step 1)	Intercept Corrected Charge (μC)	Expected Charge (μC)	% Error
0	8.73 (3.5 %)	10.27 (2.7 %)	1.54 (2.4 %)	0.00	0.00	-
100	9.20 (0.4 %)	11.38 (0.5 %)	2.19 (1.6 %)	0.65	0.71	-9.0
250	9.60 (0.3 %)	13.10 (0.4 %)	3.50 (1.2 %)	1.96	1.79	9.5
500	10.08 (0.2 %)	15.28 (0.7 %)	5.21 (1.7 %)	3.67	3.57	2.6
750	10.00 (1.4 %)	16.81 (1.5 %)	6.81 (1.8 %)	5.27	5.36	-1.8
1000	9.81 (1.8 %)	18.26 (2.0 %)	8.45 (2.2 %)	6.91	7.15	-3.3

Table 3.1: Numerical values for DPS-ASC results shown in Figure 3.4. 'Strip 1' is the area under stripping amperogram after 100 msec at E_{dep} = -500 mV. 'Strip 2' is the area under stripping amperogram after 60.1 sec at E_{dep} = -500 mV. Indicated RSD's for Strip 1 and Strip 2 are based on the standard deviation and averages of the individual steps from three trials. 'BgC Charge' is the area of the crescent independently calculated for three trials. Corresponding RSD's are calculated by first obtaining the area of the crescents from three independent DPS-ASC trials for each solution, then using the standard deviation of the area of three crescents (i.e., three trials). Measured 'Intercept Corrected Charge' (in red) is based on artificially subtracting the intercept (1.54 μC) from each 'BgC Charge' value, hence the RSD's are identical to the 'BgC Charge'. Expected charge as calculated from Faraday's Law, Q=nFVC, where n=3 for As^{III}/As^{0}, F is the Faraday constant, C is As^{III} concentration, and V is volume (1.85 μL).

3.4.3 Interferences: Selective As(III) Stripping by SEQ-MP-DPS-ASC

The issue of interference by other metals which can be pre-concentrated on the electrode surface and subsequently stripped is a concern for most arsenite studies. Beinrohr et al. found that the stripping peaks for As, Sb, and Pb completely coalesced, and partially overlapped with the Bi peak [33]. They concluded that Sb and Bi were less probable in the analysis of real waters and proposed an additional experimental step to correct for Pb interference [33]. Compton et al. utilized gold nanoparticle modified electrodes to analyze river water (1:1 with 2 M HCl) by LSV and SWV and concluded Cu^{2+} was the only likely interferent [23, 34]. Kounaves et al. also investigated the effect of Hg, Pb, and Cu interference on the arsenite stripping peak in 2 M HCl on Au microelectrode arrays by SWASV [28]. They found significant interference by Pb, Hg, and especially Cu at ppb concentrations similar to the 100 ppb As(III) used [28]. Due to the prevalence of these metals, an approach for the removal of these positively charged metal cations has been described by Swain et al. [35]. In DPS-ASC, the effect of such interferents ought to be correctable by variation of the deposition potential.

As previously demonstrated for mixtures of copper and mercury [15], the potentials chosen for the DPS-ASC experiment can be chosen to encompass the deposition and stripping processes for one or more metals, so that the stripping signal reflects the total concentration of metals within a chosen potential window. Since the most problematic interferents appear to be other metals which can be electrodeposited and accumulated on the electrode surface at potentials preceding the arsenite deposition (e.g., Cu^{2+}, Pb^{2+}, and Cd^{2+}), we investigated the feasibility of arsenite analysis in the presence of these metals. We also included Zn^{2+}, whose deposition potential is well

negative of arsenite to demonstrate that interferents in this category may be ignored entirely in DPS-ASC. Cyclic voltammograms were conducted in the Cu^{2+}, Pb^{2+}, and arsenite spiked electrolyte and the results indicated that a Cu stripping peak is evident when the deposition potential is more negative than 0 mV, and a Pb stripping peak is present when the deposition potential is negative of -300 mV. Separate experiments showed that a stripping peak for Cd was obtained when the deposition potential was less than -100 mV, and that the presence of 5000 ppb Zn^{2+} was not detectable at potentials as negative as -500 mV.

To demonstrate the effect of the above interferents, we conducted a series of DPS-ASC experiments for arsenite solutions spanning 0-1000 ppb, all of which also contained 1300 ppb Cu^{2+}, 500 ppb Pb^{2+}, 500 ppb Cd^{2+}, and 5000 ppb Zn^{2+}. These concentrations were chosen since they are much higher than the concentrations expected in groundwater samples and ought to give a general idea of the feasibility of this approach. The premise of this experiment is that quantitative differentiation between the total arsenite content from that of Cu, Pb, and Cd content could simply be obtained by comparing the DPS-ASC signal when the deposition was carried out at -300 mV (where the stripping signal reflects the sum of Cu, Pb, and Cd) and -500 mV (where the signal reflects these metals in addition to arsenite). The results are shown in **Figure 3.5** where the different bars show the measured charge after depositions at several potentials. In the case of 0 mV, only the signal due to copper is apparent and the measured charge is constant since the copper concentration was a constant 1300 ppb in all the solutions, even as the arsenite concentration of the solutions is changed. Unexpectedly, the signal at -300 mV deposition showed an increasing response (for fixed Cu, Pb, and Cd concentration). The cause of

101

this slope is likely due to some arsenite deposition at this potential (see **Figure 3.2**). The RSD values were however generally excellent (~<5%) as is typical for the DPS-ASC experiment. Further, the slope increase was most pronounced when the deposition potential was -500 mV (sufficient for deposition of arsenite).

Interestingly, the acquisition of this data set allows the application of an alternate background correcting (BgC) method. BgC method 1 (as in **Figure 3.4**) is to simply, and of course artificially, adjust the intercept to a value of zero. In practice, this BgC method was only possible since the stripping signal of an arsenite-free but otherwise identical blank solution was used in that data set. Such a convenient blank solution would of course be unavailable at the time and location of analysis for remotely deployed sensors. We therefore explored background correction using the multiple deposition potentials that the data set of **Figure 3.5** affords. This BgC method essentially subtracts the stripping signals obtained after depositions at -500 mV and -300 mV, respectively. This is possible since the coulometric stripping signal for the -300 mV deposition ought to contain 1) any metals besides arsenic which can be deposited at that potential, and importantly 2) a large portion of the artificial signal which arises due to the use of the DPS-ASC method (even if metals are absent). The subtraction of the two DPS-ASC signals after depositions at -500 mV and -300 mV gives the final coulometric values (blue bars of **Figure 3.5**) which are clearly correlated to the concentration of As(III) in each solution. Encouragingly, comparison of the measured charge (blue bars) to the expected charge (red bars) shows an accuracy of better than 5% for arsenite concentrations above 500 ppb. However, when the ppb lead and cadmium concentrations (500 ppb) exceed the arsenite ppb concentration, the accuracy is compromised (>30%). In

practice, it is unlikely that interferents such as Cu^{2+}, Pb^{2+}, and Cd^{2+} would be present at such high concentrations in natural samples.

In conclusion the DPS-ASC method, Like SASV and traditional stripping voltammetry, shows enhanced sensitivity due to the temporal concentration of the signal. Unlike SASV, the selectivity of DPS-ASC arises from the choice of deposition potential whereas the stripping is performed at positive enough potentials to indiscriminately strip all plated metals. Also unlike SASV, this method is capable of directly providing accurate coulometric determinations without the use of standards. An additional advantage of DPS-ASC is the run to run signal stability (RSD typically less than 5%), which allows meaningful subtraction between signals. Despite these advantages, an important limitation is that the chosen potentials essentially contain all analytes which can be deposited and stripped over a given potential window. The lack of direct information about the individual metal contents is mitigated by the speed of the analysis. Each determination takes about a minute, and therefore the total analysis time is approximately 3 minute per metal (for 3 trials).
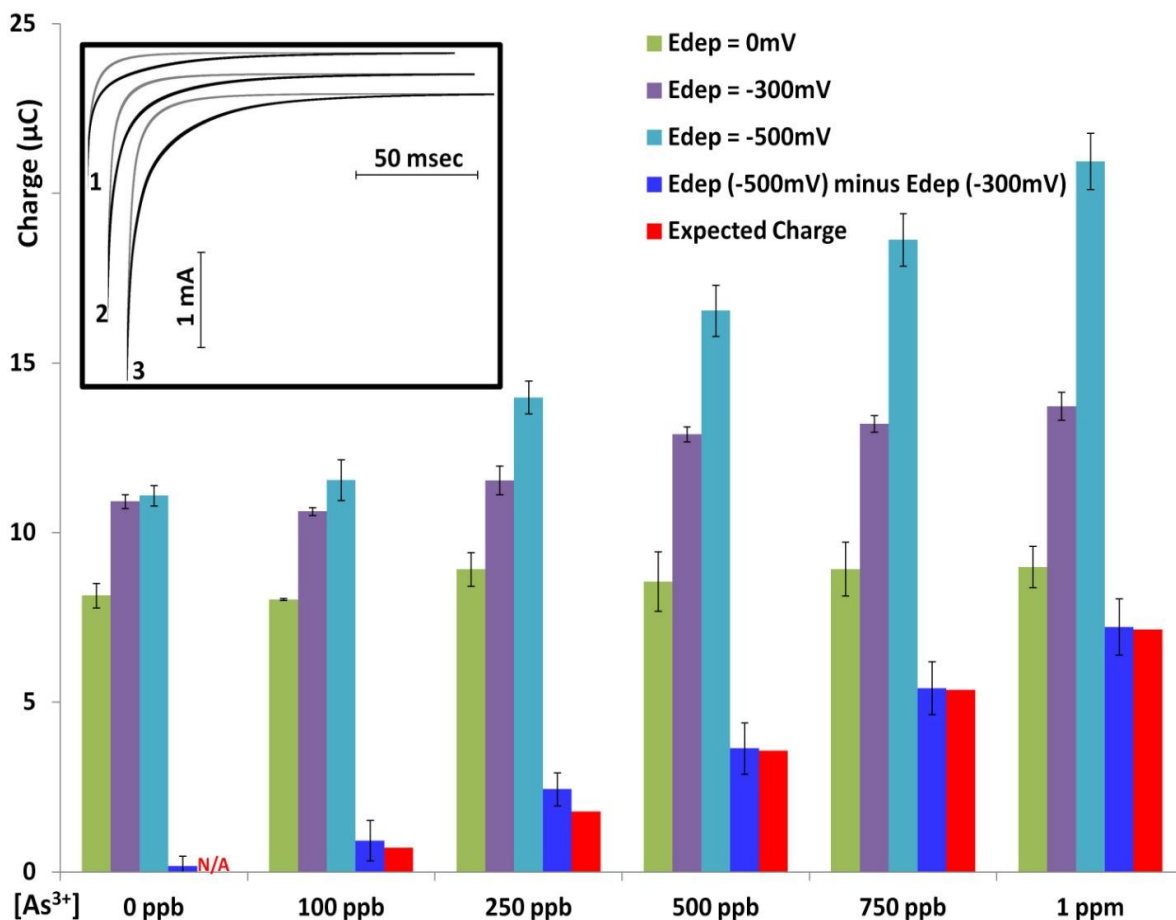
Figure 3.5: SEQ-MP-DPS-ASC results for As^{III} concentrations of 0 ppb (A), 100 ppb (B), 250 ppb (C), 500 ppb (D), 750 ppb (E), 1 ppm (F) in 10 mM HNO_3/10 mM NaCl, pH 2.0 containing 1.3 ppm Cu^{2+}, 500 ppb Pb^{2+}, 500 ppb Cd^{2+}, and 5 ppm Zn^{2+}. Bars indicate measured charge after conducting experiment of Figure 3.3 using an E_{dep} of: 0 mV (Cu^{2+} measurement), -300 mV (simultaneous Cu^{2+}, Pb^{2+}, and Cd^{2+}), and -500 mV (simultaneous Cu^{2+}, Pb^{2+}, Cd^{2+}, and As^{III}) as shown in green, purple, and light blue, respectively. Error bars represent the standard deviation of the crescent area for 3 independent trials. Subtracting the area of crescents obtained after deposition at -300 mV and -500 mV resulted in the charge values of the dark blue bars (Error bars represent standard error propagation of values used for calculation, i.e., light blue bars minus purple bars). The expected charge for the ASC platform at the indicated As^{III} concentrations is represented by the red bars for ease of comparison. **Inset:** Representative results for 1 ppm As^{III} solution showing the raw current-time stripping signal following: 1) E_{dep} = 0 mV, 2) E_{dep} = -300 mV, 3) E_{dep} = -500 mV.

3.4.4 As(III) in Spiked Ohio River Water by SEQ-MP-DPS-ASC

In order to explore the utility of this approach for determinations of arsenite in natural waters, we used natural river water samples that were spiked with arsenite in the 500-1000 ppb range. We chose to conduct this investigation in acidified river water that was adjusted to resemble the electrolyte used in the experiments above (10 mM NaCl, pH ~2). To ensure that the ASC platform behaved as expected, the first trace shows the response for a 500 ppb arsenite sample identical to that shown in **Figure 3.4**. The resulting stripping signals for this sample and three river water samples spiked with 500-1000 ppb, shown as **Figure 3.6**, are qualitatively similar. Background correction utilizing the subtraction method described for **Figure 3.5** (i.e., the stripping after deposition at -500 mV less the stripping signal after deposition at -300 mV) resulted in the numerical values of **Table 3.2**. The accuracy of the standard 500 ppb solution was within 0.5%, while those for the arsenic spiked river water were within 2.6%, 3.0%, and 13.6% for the 500 ppb, 750 ppb, 1000 ppb arsenite spiked treated river water. Clearly, the pretreatment of the river water with NaCl and HNO_3 is a disadvantage. We therefore attempted the same experiment (results not shown) for untreated arsenite spiked river water. Although Van den Berg et al. showed that arsenite can be detected at pH<8, we were not able to obtain coulometric results at the natural pH of arsenic spiked river water even when stripping at +850 mV. This may be consistent with the reported non-optimal anodic stripping voltammetry in the presence of O_2 at low ionic strength (low chloride) **[36]**.
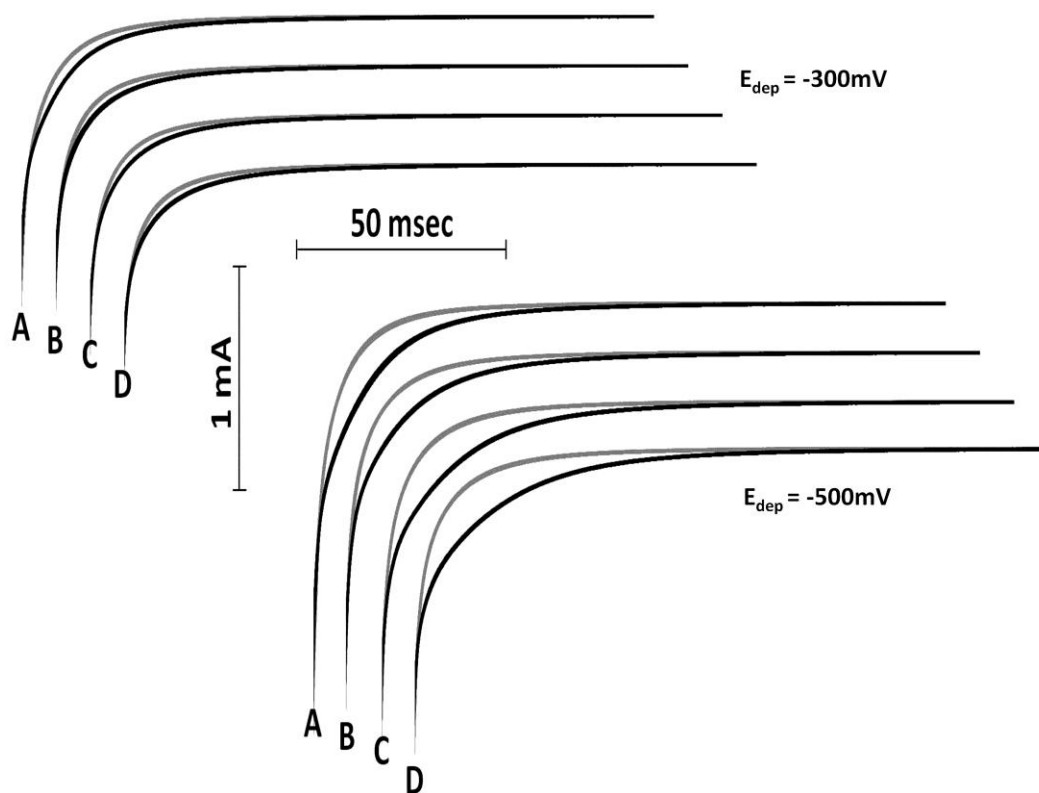
Figure 3.6: SEQ-MP-DPS-ASC results for 500 ppb As^{III} standard in 10 mM HNO_3 and 10 mM NaCl (A), and 500, 750, 1000 ppb spiked river water (plus 10 mM NaCl and HNO_3 to pH~2) (B, C, and D respectively). Measured charge corresponding to As^{III} was obtained by subtracting the area of crescents obtained after deposition at -300 mV and -500 mV for each sample (See Table 3.2 for numerical values).

Arsenite (ppb)	for -300mV deposition			for -500mV deposition			deposition potential adjusted	Expected Charge (μC)	% Error
	Step 1 Charge (μC) (RSD)	Step 2 Charge (μC) (RSD)	BgC Charge (μC) (Step 2 minus Step 1)	Step 1 Charge (μC) (RSD)	Step 2 Charge (μC) (RSD)	BgC Charge (μC) (Step 2 minus Step 1)			
500	9.47 (1.0 %)	11.74 (0.6 %)	2.27 (3.0 %)	11.85 (2.4 %)	17.68 (1.4%)	5.83 (9.2 %)	3.56 (15.2%)	3.57	-0.5
500	7.50 (1.5 %)	9.27 (1.9 %)	1.77 (4.5 %)	10.51 (0.4 %)	15.76 (0.9 %)	5.25 (3.5 %)	3.48 (5.8%)	3.57	-2.6
750	7.53 (0.5 %)	9.29 (0.3 %)	1.77 (1.5 %)	10.41 (1.0 %)	17.37 (0.7 %)	6.96 (1.7 %)	5.20 (2.3%)	5.36	-3.0
1000	7.03 (1.5 %)	8.81 (1.4 %)	1.78 (0.6 %)	9.77 (0.9 %)	17.72 (0.9 %)	7.95 (0.9 %)	6.18 (1.2%)	7.15	-13.6

Table 3.2: Numerical values for SEQ-MP-DPS-ASC results shown in Figure 3.6. 'Strip 1' is the area under stripping amperogram after 100 msec at indicated E_{dep}. 'Strip 2' is the area under stripping amperogram after 60.1 sec at E_{dep}. Indicated RSD's for Strip 1 and Strip 2 are based on the standard deviation and averages of the individual steps from three trials. 'BgC Charge' is the independently calculated crescent area for three trials. Corresponding RSD's are calculated from the standard deviation of the area of three crescents (i.e., three trials). Measured BgC (in red) is based on subtracting crescent 1 from crescent 2, and RSD's were obtained by propagation of the uncertainties used in the calculation.

3.5 Conclusions

We describe a method we have termed multi-potential DPS-ASC, and demonstrate its excellent promise for large-scale de-centralized remote monitoring of arsenite in natural waters for health applications. The technique uses a 1.85 µL sample volume but nonetheless shows promising sensitivity (currently 1-2 orders of magnitude higher than the 1-10 ppb LOD required for practical field use). Further development of this approach should proceed in several directions: 1) adapt the method for natural pH low conductivity media such as river and well waters, 2) expand the method to arsenate in a manner that is consistent with remote monitoring, and most importantly 3) adapt or modify the method to obtain lower LOD's which ought to be applicable to ASC as an approach for remote metal determinations. To lower the LOD, a detailed investigation to optimize parameters such as the electrode area and DPS-ASC waveform is currently underway and we look forward to reporting on these in the near future. Additionally, significant inter-disciplinary advances will be necessary to integrate a remotely deployable potentiostat, sample handling techniques (e.g., pumping/moving the sample), remote data collection and processing before routine field application is feasible.

CHAPTER IV

SAMPLE PRETREATMENT:

DISSOLVED OXYGEN REMOVAL

4.1 Overview

Current water quality monitoring for heavy metal contaminants largely results in analytical snapshots at a particular time and place. We have therefore been interested in miniaturized and inexpensive sensors suitable for long-term, real-time monitoring of the drinking water distribution grid, industrial wastewater effluents, and even rivers and lakes. Amongst the biggest challenges for such sensors are the issues of in-field device calibration and sample pretreatment. Previously, we have demonstrated use of coulometric stripping analysis for calibration-free determination of copper and mercury. For more negatively reduced metals, O_2 reduction interferes with stripping analysis; hence, most electroanalysis techniques rely on pretreatments to remove dissolved oxygen (DO). Current strategies for portable DO removal offer limited practicality due to their complexity and often cause inadvertent sample alterations. We have therefore designed an indirect in-line electrochemical DO removal device (EDOR), utilizing a silver cathode to reduce DO in a chamber that is fluidically isolated from the sample stream by an O_2 permeable membrane (**Figure 4.1**). The resulting concentration gradient supports

passive DO diffusion from the sample stream into the de-oxygenation chamber. The DO

levels in the sample stream were determined by cyclic voltammetry (CV) and

amperometry at a custom thin-layer cell (TLC) detector. Results show removal of 98 %

of the DO in a test sample at flow rates approaching 50 µL/min and power consumption

as low as 165 mW hr L^{-1} at steady state. Besides our specific stripping application, this

device is well suited for LOC applications where miniaturized DO removal and/or

regulation are desirable.
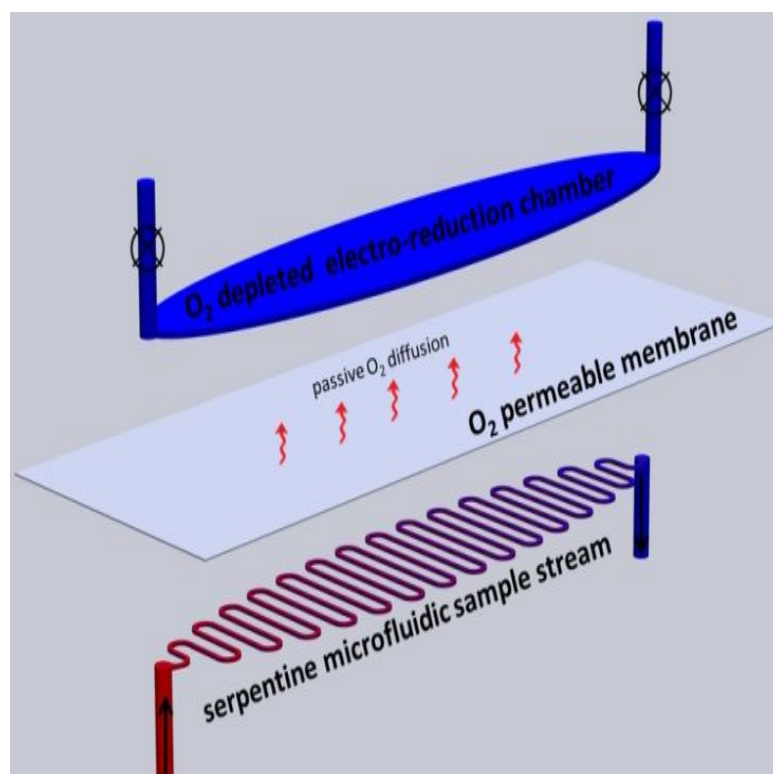
Figure 4.1: Overview of indirect dissolved oxygen removal by passive diffusion.

4.2 Introduction

A unique characteristic of electrochemically based analysis systems is that the electrodes and cells at the heart of such instrumentation can generally be scaled down in size without loss of performance. This feature makes the use of modern microfabrication techniques very attractive for the construction of electroanalysis devices, and in fact the production and use of microfabricated electrochemical devices has become commonplace. Among the new possibilities that this has made feasible is the cost-effective mass production of miniaturized electrochemical sensors.

In our group, we have become interested in the development of microfabricated devices suitable for the creation of sensor networks for long-term remote analysis applications - such as the continuous monitoring of chemical contaminants in drinking water systems. In these situations, the scale and complexity of the system limits a conventional analysis approach to only periodic sampling at limited times and locations. The primary obstacles to making such remote sensors practical are the issues of in-field sample preparation and calibration. To address the latter, our group has recently shown that anodic stripping coulometry (ASC) in microfabricated devices is a promising approach for calibration-free sensing of heavy metals [1]. However, these investigations were not able to address metals such as Pb and Cd which suffer from interference due to oxygen reduction at the potentials needed for electrodeposition [2]. Although portable anodic stripping analyses are widespread, the associated dissolved oxygen (DO) removal step still requires direct operator intervention and thus would be unsuitable for remote automated sensing [3-5]. With the exception of Ag, Ag amalgam electrodes and a few special cases with the Au electrode [6-9], classical stripping analysis of Pb requires a de-

oxygenation step on typical electrode materials such as graphite and mercury **[10-11]**.Consequently, we have become involved in the development of microfabricated electrochemical platforms for on-site removal of DO for use with our ASC devices for metal analysis. In fact, a miniaturized DO removal or regulating apparatus should also be useful for a diverse range of electroanalytical and lab-on-a-chip applications, such as voltammetric detection in capillary electrophoresis, microfluidic cell culturing platforms, and possibly O_2 sensitive microfluidic reactors **[12-15]**.

A review of 'portable' continuous DO removal schemes reveals a variety of chemical and physical approaches. The principal of these include the application of a vacuum, exposure to an O_2 scavenger, and the displacement of DO by purging with an inert gas such as Ar or N_2. Furthermore, the removal can be carried out either directly (e.g., by direct addition of the scavenger or direct degassing with N_2) or indirectly (e.g., by flowing the sample stream through O_2 permeable tubing immersed in O_2 scavenging medium or N_2 atmosphere) **[4-5, 16-19]**. Most of these approaches possess obvious drawbacks for automated remote analysis. The direct addition of oxygen scavenging additives may unintentionally change metal speciation while membrane separated use requires storage of air reactive consumables on the device. And the use of vacuum pumps or purge gas reservoirs, besides being cumbersome and complicated, may also change sample pH by removal of dissolved CO_2 **[17-19]**.

An ideal device for in-line DO removal should be simple to operate over extended time periods and should offer the potential for low cost fabrication and low power requirements. A very attractive, but macro-sized, electrochemical approach was described by Frei et al., where the sample is passed through a porous silver electrode held at a

sufficiently cathodic potential for O_2 reduction [20]. Subsequently, Adanuvor and White studied the reduction of oxygen on silver electrodes in detail and suggested that, in highly basic solution, the O_2 conversion involves the following reaction sequence [21-22]:

$$O_2 + H_2O + 2e^- \rightarrow HO_2^- + OH^- \qquad \textbf{(Equation 4.1)}$$

$$HO_2^- \rightarrow 1/2O_2 + OH^- \qquad \textbf{(Equation 4.2)}$$

We report herein a proof-of-concept study demonstrating the design and evaluation of an indirect electrochemical oxygen removal system. The device described here allows DO in a thin-layer sample stream to proceed via passive diffusion across an oxygen permeable membrane into a second thin-layer chamber where it is electrochemically reduced at a Ag electrode as reported above. Importantly, this indirect approach avoids unintended alterations of the sample stream by the Ag cathode (e.g., deposition of metals) or reactions at the associated counter electrode.

4.3 Experimental

4.3.1 Materials

ACS reagent grade NaOH was obtained from Fisher Scientific (Pittsburgh, PA). KCl, 1000 ppm AAS Pb^{2+} standard, sodium acetate, and acetic acid were obtained from Sigma-Aldrich (Milwaukee, WI). 1.6 mm Au disc and Ag/AgCl electrodes were obtained from BASi (West Lafayette, Indiana). Deionized water was used to make the EDOR de-oxygenation solution (6.5 M NaOH), and the test sample (100 mM KCl) was allowed to

equilibrate with air for at least 24 hours. N_2 and CO_2 gases were from Welder's Supply (Louisville, KY).

Drawings for the fixtures and rubber layers were designed in SolidWorks (Dassault Systèmes SolidWorks Corp., Waltham, MA) and Auto-CAD (AutoCAD, Autodesk, Inc., San Rafael, CA), respectively. The fixtures were milled by a commercial prototyping service (FirstCut, Proto Labs Inc, Maple Plain, MN), and the rubber layers were precision cut by a mini laser cutter/engraver (Epilog Laser, Golden, CO). Rubber layers including the 125 μm thick high purity silicone rubber, valves, PEEK tubing, adapters, and Viton O-rings were from McMaster Carr (Aurora, OH), Cole-Parmer (Vernon Hills, IL), or AAAcme Rubber (Tempe, AZ). High purity (99.95 %) 75 μm thick silver foil was obtained from Alfa-Aesar (Ward Hill, MA), the 200 MWCO SelRO MPF-34 membrane was from Koch Membrane Systems, Inc., (Wilmington, MA), and 100 μm thick pyrolytic graphite sheet was from Panasonic Electronic Components (Secaucus, NJ).

4.3.2 Equipment

A commercial power supply (Model GPR-1810HD, GWInstek Corp., Chino, CA) was used to provide a 1V potential to the EDOR device, and a digital multimeter (Model 34410A, Agilent Technologies Inc., Santa Clara, CA) connected via a LabVIEW (National Instruments, Austin, TX) control program was used to monitor the current. The initial sample DO content was measured by a commercial Clark type O_2 Probe (Milwaukee Instruments Inc., Rocky Mount, NC). Sample flow was controlled by an HPLC pump (Model 222C, Scientific Systems, Inc., State College, PA). A BASi Epsilon

potentiostat (Bioanalytical Systems, West Lafayette, IN) was used to monitor the DO at the TLC detector.

4.3.3 Electrochemical Dissolved Oxygen Remover

Operationally, the EDOR device consisted of two adjacent fluidic chambers separated by a 125 μm thick O_2 permeable silicone rubber sheet (**Figure 4.2**). The choice of this O_2 permeable membrane was based on its practicality for prototype construction and high O_2 permeability coefficient, 19685 $cm^{3.}mm/m^2 \cdot day \cdot atm$ [**23**]. The sample chamber was a serpentine channel 250 μm deep, 400 μm wide, and 345 mm long. These dimensions were chosen so that sample residence time was >10 times the diffusion time ($\sqrt{2Dt}$) at a flow rate of 10 μL/min. On the other side of the silicone rubber separator was the de-oxygenation chamber which included a porous silver cathode and graphite anode. This chamber was subdivided into three elliptical thin-layer compartments with independent inlet/outlet ports with valves. Opening/closing of the six valves in different combinations ensured complete filling of each thin-layer sub-chamber by syringe.

Device construction was accomplished using a 'layer-by-layer' approach with PVC fixtures at the top and bottom with fluidic inlet/outlets for the de-oxygenation chamber and sample stream, respectively. Sandwiched in between were alternating layers of rubber gaskets precision patterned with channels and aligned holes to direct flow through each layer and to the layers beneath. A perforated silver cathode and graphite anode were incorporated as additional layers between the rubber sheet layers to facilitate a good fluidic seal. A diagram of the complete 14 layer device and additional details regarding its fabrication are available (**Figure 4.6**).
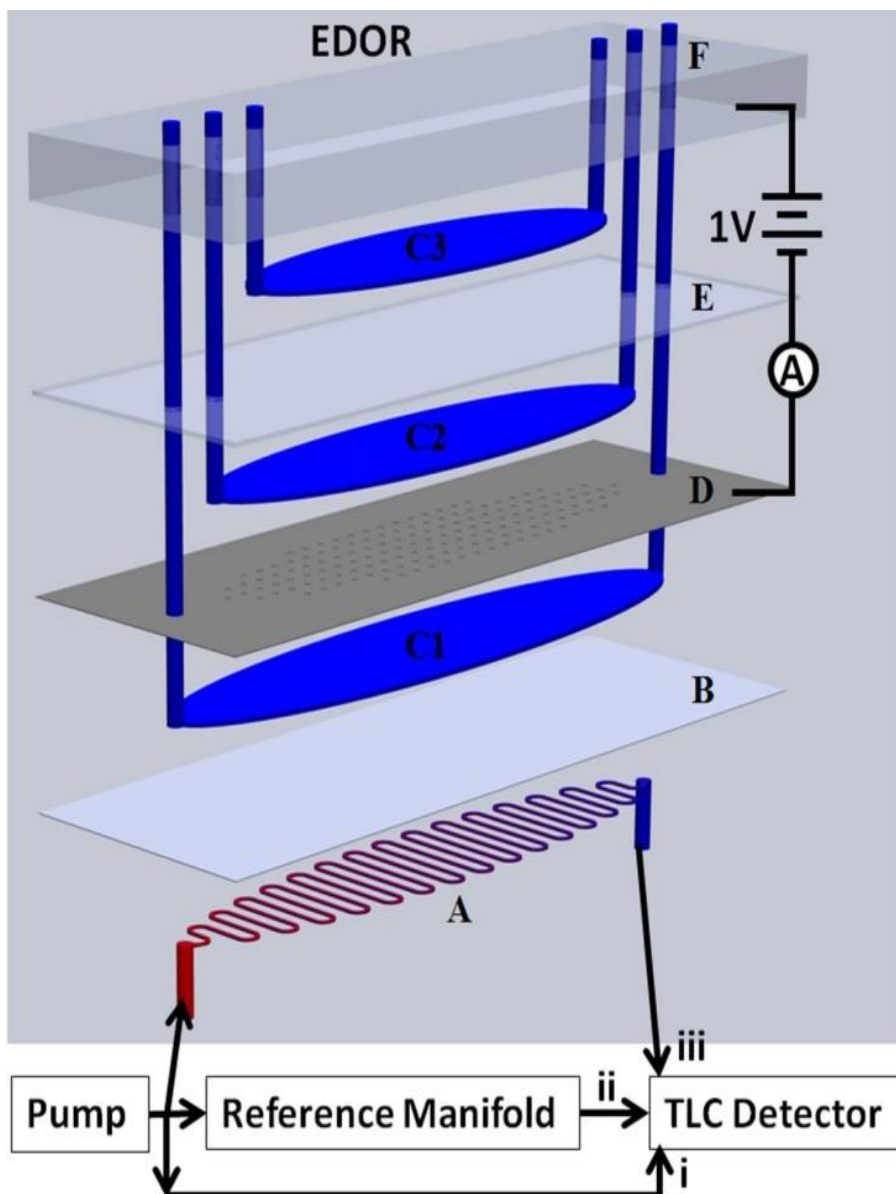
Figure 4.2: Experimental setup and functional schematic of EDOR prototype (structural layers omitted for clarity). A: Serpentine micro fluidic sample stream (250 μm deep X 400 μm wide X 345 mm long). B: O_2 permeable silicone rubber (125 μm thick). C1-C3: O_2 reduction chamber divided into three thin-layer elliptical sub-chambers (C1: 15 mm X 65 mm X 0.5 mm, C2: 15 mm X 55 mm X 0.5 mm, C3: 15 mm X 45 mm X 0.5 mm). D: Perforated silver sheet cathode. E: Insulating membrane. F: Graphite anode.

4.3.4 TLC Detector

The sample stream of **Figure 4.2** was directed to a custom built TLC where residual DO could be electrochemically monitored. Briefly, this TLC detector consisted of a polycarbonate bottom fixture with a recessed area for precise placement of the sensor chip and a PVC top fixture containing the fluidic inlet/outlet. The sensor chip was fabricated as previously described, and defined the bottom of the TLC where a 1 mm long (extending the width of the channel) gold working electrode was 200 μm downstream of an identical gold electrode converted to a Ag/AgCl pseudo reference electrode, also as previously described [1, 24]. Atop the sensor chip was a precision patterned Viton rubber gasket containing a 500 μm wide X 250 μm deep channel. The top of the channel was defined by a pyrolytic graphite sheet, which was also used as the counter electrode. A detailed diagram of the detector and additional details regarding its fabrication are available (**Figure 4.7**).

4.3.5 Reference DO Removal Manifold

In order to evaluate the performance of our EDOR device, it was essential to have a proven de-oxygenation system available to serve as a reference. Accordingly, we chose to employ a scheme derived from one initially described by Pedrotti et al. and based on the diffusion of DO from a sample stream across O_2 permeable silicone rubber tubing and into a counter-flowing N_2 stream [17-19]. This system was reported to produce >99 % O_2 removal. The details of its construction and validation of its effective oxygen removal can be found in the Supporting Information (**Figure 4.8**). Evidence of complete DO removal

by the reference manifold was demonstrated by the unvarying TLC detector response for a wide range of flow rates (10 µL/min to 200 µL/min).

4.3.6 Experimental Protocol

Air equilibrated 100 mM KCl was pumped directly to the detector, through the reference manifold or through the EDOR device (**Figure 4.2**). To begin de-oxygenation in the reference manifold, an adjustable valve was opened to allow N_2 from a cylinder into the manifold jacket, and the DO content of the sample stream in the inner tubing was monitored at the TLC detector. The de-oxygenation chamber of the EDOR device was filled with 6.5 M NaOH, and the device was activated by applying a 1 V potential between the cathode and anode to initiate DO reduction. The current flowing between the silver and graphite electrodes was monitored with a digital ammeter. Upon initial startup, the platform reaches s.s. operation in a few hours. In principle, three concentration gradients must reach equilibrium after the device is activated: first, the de-oxygenation chamber must be fully de-oxygenated; second, a concentration gradient must presumably form in the silicone rubber separator; and finally a flow rate dependent oxygen concentration gradient must form in the flowing sample stream. A potentiostat was used to monitor O_2 reduction at the downstream TLC detector by CV and amperometry. The CV proceeded between 0 mV to -800 mV at a scan rate of 1000 mV/s, and the potential step amperometry began at 0 mV with a single step to -800 mV. In both cases, the TLC working electrode was held at a pre-conditioning potential of 0 mV prior to the scan or step. In separate offline experiments, 15 ppb Pb^{2+} in 0.1 M acetate buffer pH 5.3 was determined for as prepared sample and effluent collected after passage through EDOR.

Determination was by square wave stripping voltammetry (SWSV: f: 150 Hz, E_p: 25 mV, E_s: 5 mV) on 1.6 mm diameter Au disc electrode vs. Ag/AgCl with Pt. wire as counter electrode while stirring at 400 rpm (E_{dep}: -800 mV, T_{dep}: 300 sec).

4.4 Results and Discussion

4.4.1 Evaluation of EDOR Performance

The fabrication of our electrochemical DO removal device required numerous design choices regarding specifications such as channel dimensions, membrane material, de-oxygenation chamber volume, etc. Accordingly, once these parameters were selected and incorporated into a working platform, the first step was to establish experimentally whether the choices described in the Experimental Section had in fact been appropriate. Our initial evaluation consisted of directing the outflow of the device to a TLC containing a gold working electrode where any O_2 present could be detected by electro-reduction. For comparison purposes, the outflow stream of our reference DO removal system could alternatively be directed into the TLC. Typical results obtained for a 100 mM KCl test sample are shown in **Figure 4.3**. The dissolved O_2 concentration in the initial sample was measured to be 8 ppm with a commercial Clark type probe; and, without any treatment, CV_1 showed the expected O_2 reduction starting at -400 mV. CV_2 and CV_3, obtained after O_2 removal by the reference procedure and by our approach, respectively, both showed essentially the same dramatic decreases in this current. Clearly, the electrochemical removal system was largely successful in its operation.
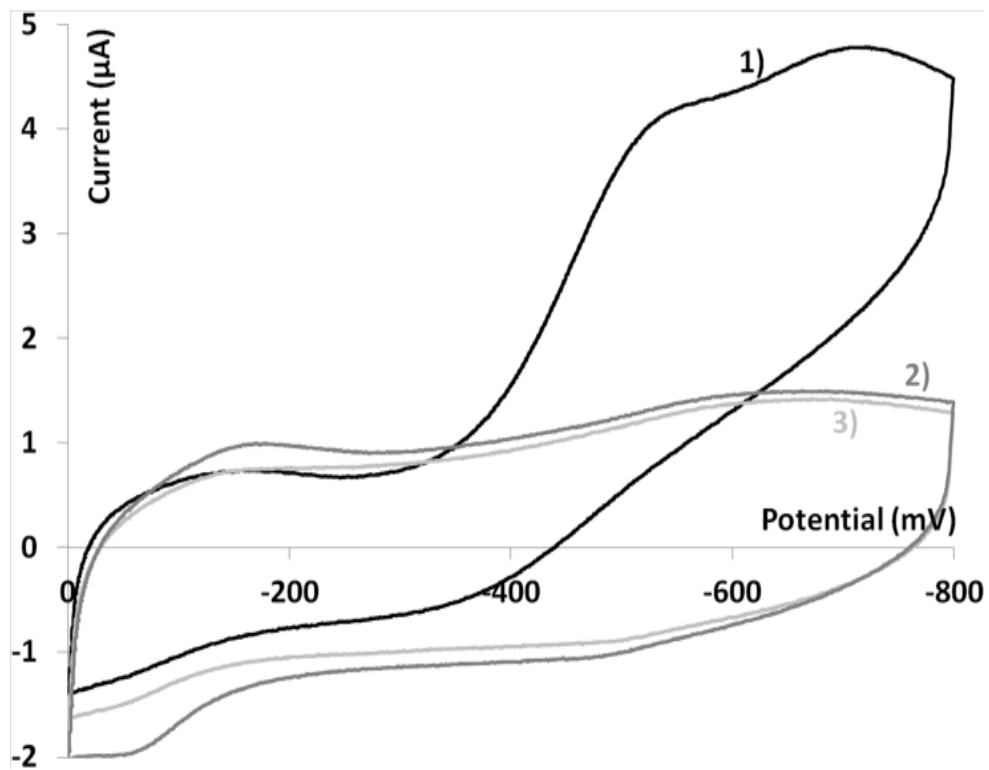
Figure 4.3: Cyclic voltammograms in the TLC DO detector at 10 µL/min for 1) Ambient DO. 2) DO removal by reference manifold. 3) DO removal by EDOR prototype.

Once it had been established that the prototype DO removal device was working well in a qualitative sense, the next step was to evaluate its performance quantitatively. Accordingly, we carried out the same comparison shown in **Figure 4.3** but examined the DO levels via amperometry - an approach that allowed us to look at much lower DO levels than CV. These experiments were initiated by applying a suitable DO reduction potential (i.e., -800 mV) while the sample was passed continuously through the TLC. The corresponding amperograms, obtained downstream in the TLC for the untreated sample stream as well as after passage through both the reference DO removal system and our DO removal device, are shown in **Figure 4.4A**. In each case, there was a very rapid jump in current when the experiment was initiated by stepping to -800 mV (from 0 mV). Subsequently, the currents reached steady-state levels that persisted unchanged throughout the 30-sec measurement period. As expected, a large reduction current, 2550 nA, was observed in the absence of DO removal (curve 1) with dramatically decreased currents after DO removal by either the reference (58 nA +/- 12, curve 3) or the electrochemical (108 nA +/- 12, curve 2) systems. These values were obtained by averaging the steady state current (15-30 sec) for many individual amperometric experiments (as indicated in **Figure 4.5**'s legend) during DO removal. Assuming that the reference method was able to remove all DO and the 58nA current response was largely due to background processes, the electrochemical procedure would appear to be removing at least 98 % under the conditions in effect. Downstream amperometric monitoring showed that this degree of O_2 removal could be sustained continuously for several hours.
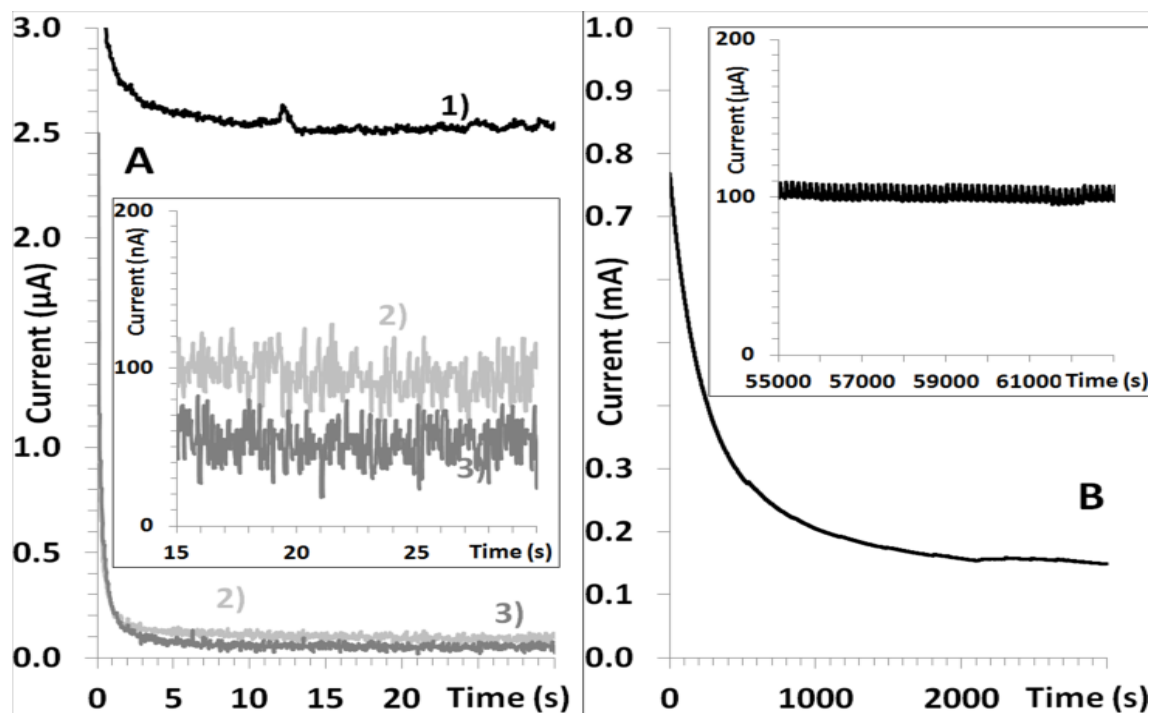
Figure 4.4: Comparison of EDOR prototype and reference manifold. A: Chronoamperometry in the TLC detector for 1) Ambient DO at 10 µL/min. 2) DO removal by reference manifold at 200 µL/min. 3) DO removal by EDOR prototype at 10 µL/min (Inset: Expanded view for traces 2 and 3). B: Measured current for O_2 reduction on Ag cathode at applied potential of 1 V (Inset: Expanded view of current after 16 hours of continuous operation at 10 µL/min).

The capability of this in-line electrochemical approach to eliminate DO is expected to be directly dependent on numerous experimental and system parameters. Chief among these might be the sample stream flow rate. To a limited extent, it is possible to model some aspects of the cell behavior. Complete depletion of an analyte from a fully laminar thin-layer sample stream – so that bulk analyte concentration, $C_o^*=0$, at the outlet – in a rectangular duct with the electrode positioned as one wall of the duct has been previously described [25]. Using the method of reference 25 where all DO is depleted along one wall of our prototype's rectangular channel dimensions, exhaustive diffusion based depletion of DO ought to be possible at flow rates as high as 82 μL/min (diffusion coefficient of DO $= 2 \times 10^{-5}$ cm^2/s) [26]. This is only an approximation since the O_2 concentration at the surface of the silicone rubber separator is unlikely to be zero and the sample flow may not be fully laminar due to wall roughness. The operating principle of the device is such that the limiting process at high flow rates is either the diffusion of DO in the flowing sample stream to the O_2 exchange membrane or the exchange of O_2 across the membrane. Accordingly, the residual DO in the sample stream is expected to increase as the flow rate is increased beyond the limiting process of the cell. As shown in **Figure 4.5A**, this is in fact the case when as the flow-rate increased from 10 μL/min to 187 μL/min. The current at the O_2 reducing silver electrode also increases with flow rate (as shown in **Figure 4.5B**), but this increase occurs at a lower rate than the sample stream. Taken together, these data suggest the limiting process is O_2 diffusion across the membrane (i.e., excess O_2 at higher flow rates does not cross the membrane and is simply carried along the sample stream and detected at the TLC). Nevertheless, a high level of DO removal was maintained at flow rates approaching the

123

expected 80 µL/min. However, the choice of a different membrane material with higher O_2 permeability and different channel dimensions (both of which are to be investigated in future work) would be expected to further improve the O_2 removal capability.

Another performance criterion that might be critical for some applications is the power consumption required for O_2 elimination. For this approach, this is readily evaluated from the potential applied to the Ag electrode for O_2 reduction (1 V). As shown in **Figure 4.4B**, the maximum O_2 reduction current occurs immediately after the 1 V potential is applied and steadily declines to a steady state (s.s.) value of 100 µA for an 8 ppm O_2 sample stream at 10 µL/min. Thus, the energy needed for continuous DO removal is 165 mW hr L^{-1} which is compatible with battery or photovoltaic power sources and is certainly much lower than would be required to operate a vacuum pump. Also, this approach does not require the storage of consumable chemicals or gases on-site. Of course, there remains the issue of transporting the sample in an energy efficient manner; a challenge that is shared by all portable DO removal approaches. In that regard, integrated sample transporting electro-osmotic and capillary micro pumps appear to be fundamentally compatible with our microfluidic approach **[27-28]**.
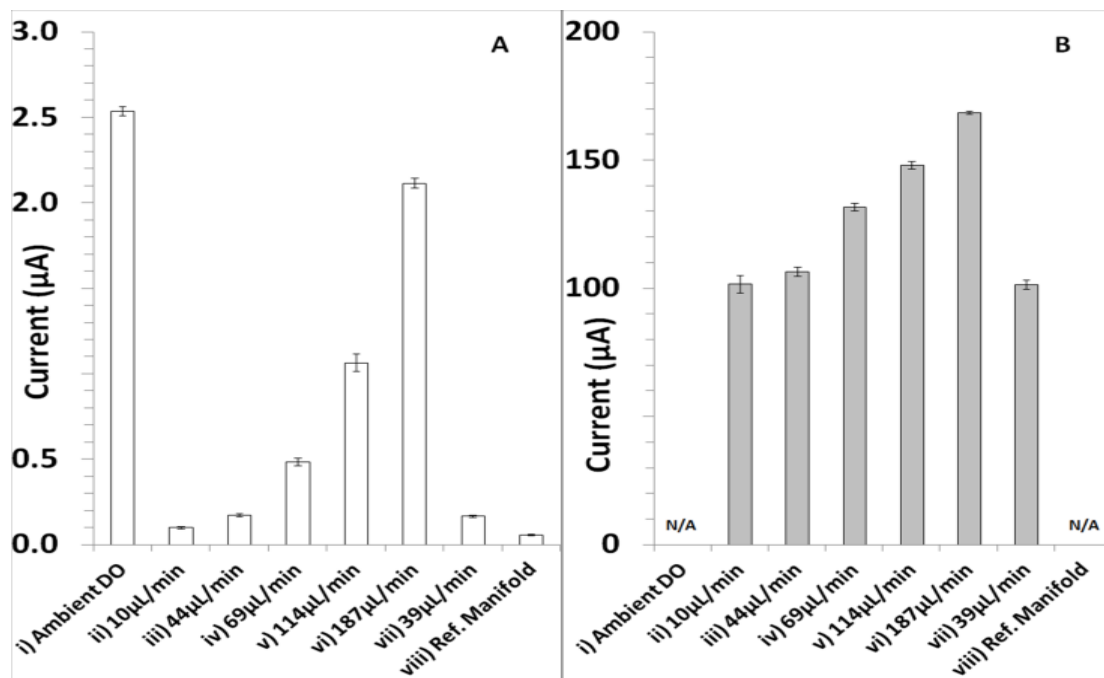
Figure 4.5: EDOR prototype performance at various flow rates. A: Average current recorded in TLC detector for i: Ambient DO at 10 μL/min, ii-vii: EDOR at the indicated flow rates, and viii: DO removal by Reference manifold at 200 μL/min. B: Corresponding measured current for O_2 reduction on silver cathode of EDOR at indicated flow rates. A: bars represent steady state current from 15-30 sec of Figure 4.4 and error bars show standard deviation for n trials over t minutes (i: n=8, t=22; ii: n=138, t=171; iii: n=51, t=62; iv: n=22, t=26; v: n=34, t=42; vi: n=16, t=19; vii: n=34, t=41; viii: n=24, t=28). B: bars represent current recorded (once per sec) at Ag electrode of EDOR prototype over the same time span as A (e.g., ii: n=138*60, t=171 min, etc.).

4.4.2 Practical Considerations

In view of the diverse applications possible for EDOR, it is useful to pay some attention to selectivity issues. For the EDOR device presented here, the selectivity should be determined primarily by the membrane employed to allow entry into the O_2 reduction chamber and its permeability to the different species present in the sample stream. For the current study, the membrane material selected was silicon rubber because of its relatively high permeability toward O_2. In addition, this material was expected to exhibit very low permeability to metal ions such as Pb^{2+} which are potential analytes in our own intended application of the EDOR device. This expectation was confirmed experimentally by passing a test solution containing 15 ppb Pb^{2+} (the EPA recommended action/treatment level for Pb in drinking water) in 0.1 M pH 5.3 acetate buffer through the EDOR platform and collecting the effluent. Subsequently, conventional anodic stripping voltammetry was carried out on both the initial Pb^{2+} solution and the EDOR effluent. As anticipated, no Pb^{2+} appeared to be lost to the device as the Pb stripping peak currents were essentially unchanged for these two solutions (38.9 +/- 1.1 μA vs. 38.4 +/- 0.4 μA). This is consistent with recent findings that diffusion of metal salts across silicone rubber encapsulants for implanted microelectronic devices is negligible **[29]**.

A second selectivity consideration of interest is related to dissolved gases other than O_2 that in fact are much more likely to diffuse through the silicone rubber material. As it was not feasible to test all possible gases, preliminary studies were carried out for CO_2 which has greater aqueous solubility than O_2 as well as higher permeability in silicone rubber **[23, 30]**. In addition, sustained CO_2 removal might cause a change in the acidity of the deoxygenated solution and thereby produce an unintended alteration in

sample pH. Accordingly, we intentionally enriched an aqueous solution with CO_2 and passed this solution continuously through the EDOR device. Subsequently, no CO_2-related current was noted in the O_2 reduction chamber, and no change in the effluent pH was detected. These results suggest that the EDOR device is not responsive to CO_2 even though this gas in all likelihood is able to diffuse through the silicone rubber membrane from the sample stream.

4.5 Supplementary Information

4.5.1 Electrochemical Dissolved Oxygen Remover

A diagram of the complete 14 layer device and some details regarding its fabrication are shown in **Figure 4.6** and **Table 4.1**. The device consisted of PVC fixtures at top and bottom with fluidic inlet/outlets for the de-oxygenation chamber and sample stream, rubber gasket layers, an insulating membrane, silver sheet electrode, and a graphite block anode. Drawings for the PVC fixtures were prepared using Computer Aided Design (CAD) software (Solidworks, Dassault Systèmes SolidWorks Corp., Waltham, MA). The fixtures were machined from polyvinyl chloride blocks by a commercial prototyping service (FirstCut, Proto Labs Inc, Maple Plain, MN). The drawings for the rubber gasket and membrane layers were also made using CAD software (AutoCAD, Autodesk, Inc., San Rafael, CA) and precision patterned with a 40W CO_2 mini laser cutter/engraver (Epilog Laser, Golden, CO). Holes for twelve alignment pins (short 2 mm stainless steel rods) in the PVC fixtures served as guides for precise placement of the remaining layers during assembly. Other holes through all layers of the assembly ended with threads in the bottom fixture for screws to tighten the assembly.

Assembly of the 'stack' resulted in a membrane separated, dual compartment cell with independent flow paths for each compartment (**Figure 4.6**).

Hereafter we refer to the lower compartment as the sample chamber and the upper compartment containing the silver cathode and graphite anode as the de-oxygenation chamber. The bottom of the sample chamber was composed of a Viton rubber layer (Layer B of **Figure 4.6**). The sides of the sample chamber were comprised of a serpentine channel in a Viton rubber layer that was 250 μm deep, 400 μm wide and 345 mm long (Layer C). As previously noted, these dimensions were chosen so that the sample residence time was >10 times the diffusion time based on $\sqrt{2Dt}$ at a flowrate of 10 μL/min. The oxygen exchange membrane defined the top of the sample chamber and was composed of a 125 μm thick ultra-pure silicone rubber silicone rubber sheet (Layer D). The choice of silicone rubber sheet was based on its practicality for device construction and high oxygen permeability coefficient, 19685 $cm^3 \cdot mm/m^2 \cdot day \cdot atm$ for un-wetted silicone rubber **[23]**. On the other side of the silicone rubber separator was an elliptical chamber which 'contained' the perforated silver cathode and a graphite anode separated by an insulating membrane incorporated as additional layers between rubber sheet layers to ensure a fluidic seal.

The de-oxygenation chamber was functionally subdivided into three elliptical thin-layer sub-chambers with independent inlet/outlet ports with valves (Layers E, G, and I). This design was chosen so that opening/closing of the six valves in different combinations allowed complete filling of each thin-layer sub-chamber by syringe. The dimensions of these ellipses were 15 mm X 65 mm X 0.5 mm, 15 mm X 55 mm X 0.5 mm, and 15 mm X 45 mm X 0.5 mm. The spacing between the inlet/outlets of these three

chambers at the top of the cell (Layer L) did not allow for mechanical clearance for fluidic connectors (described below). Therefore, a simple manifold consisting of two additional layers was added so as to increase the spacing between inlet/outlets (Layers M and N). The 200 MWCO (molecular weight cut-off) insulating membrane (SelRO MPF-34, Koch Membrane Systems, Inc., Wilmington, MA) incorporated as Layer H was used to prevent a short circuit between cathode and anode and may have also limited diffusion of anode byproducts to the silver cathode, but its inclusion was precautionary and, to our knowledge, not critical for effective device operation.

The perforated silver cathode (Layer F) was composed of a 99.95% silver foil which was 150 mm X 25 mm X 75 μm foil (Alfa Aesar, Ward Hill, MA). The foil was aligned so that it was offset from center and extended out the side of the stack where an alligator clip was used to make electrical contact. The perforations in the foil were made using a precision laser patterned polycarbonate stencil and a needle to make a few dozen through-holes in the silver foil. These perforations were necessary to allow the graphite anode to be in electronic contact with the solution contained in the bottom-most elliptical chamber (Layer E). The graphite anode itself (Layer J) was machined from a solid block of graphite (McMaster Carr, Aurora, OH) to its final shape also using a precision laser patterned polycarbonate stencil. Electrical contact to the anode was made by affixing a length of copper foil to one corner between Layers J and K which became firmly held in place when the assembly was tightened (Measured ohmic contact of $<1\Omega$).

At the top of the stack (Layer N), six nylon 10-32 UNF threaded to luer adapter fittings were used to connect to PVDF luer stopcocks which could be opened and closed independently when filling the de-oxygenation chamber with 6.5 M NaOH as noted

129

above. Once the three elliptical sub-chambers were filled, these stopcocks were kept closed during use of the device to ensure stopped flow and hence DO depletion within the de-oxygenation chamber. On the bottom side of the stack, fluidic connections to the sample chamber were made using acetal 10-32 UNF threaded Standard Fingertight II™ high-pressure HPLC fittings. To ensure air (and oxygen) tight connections, PEEK (polyetheretherketone) Tubing (0.020" ID, 1/16"OD) was inserted through the center of the fittings with Viton O-rings used as ferrules. Fittings, PEEK tubing, rubber gaskets, O-rings, syringes, and valves for sample handling were all composed of inert plastics and rubbers and were obtained from Cole-Parmer (Vernon Hills, IL), McMaster Carr (Aurora, OH), and/or AAAcme Rubber (Tempe, AZ).
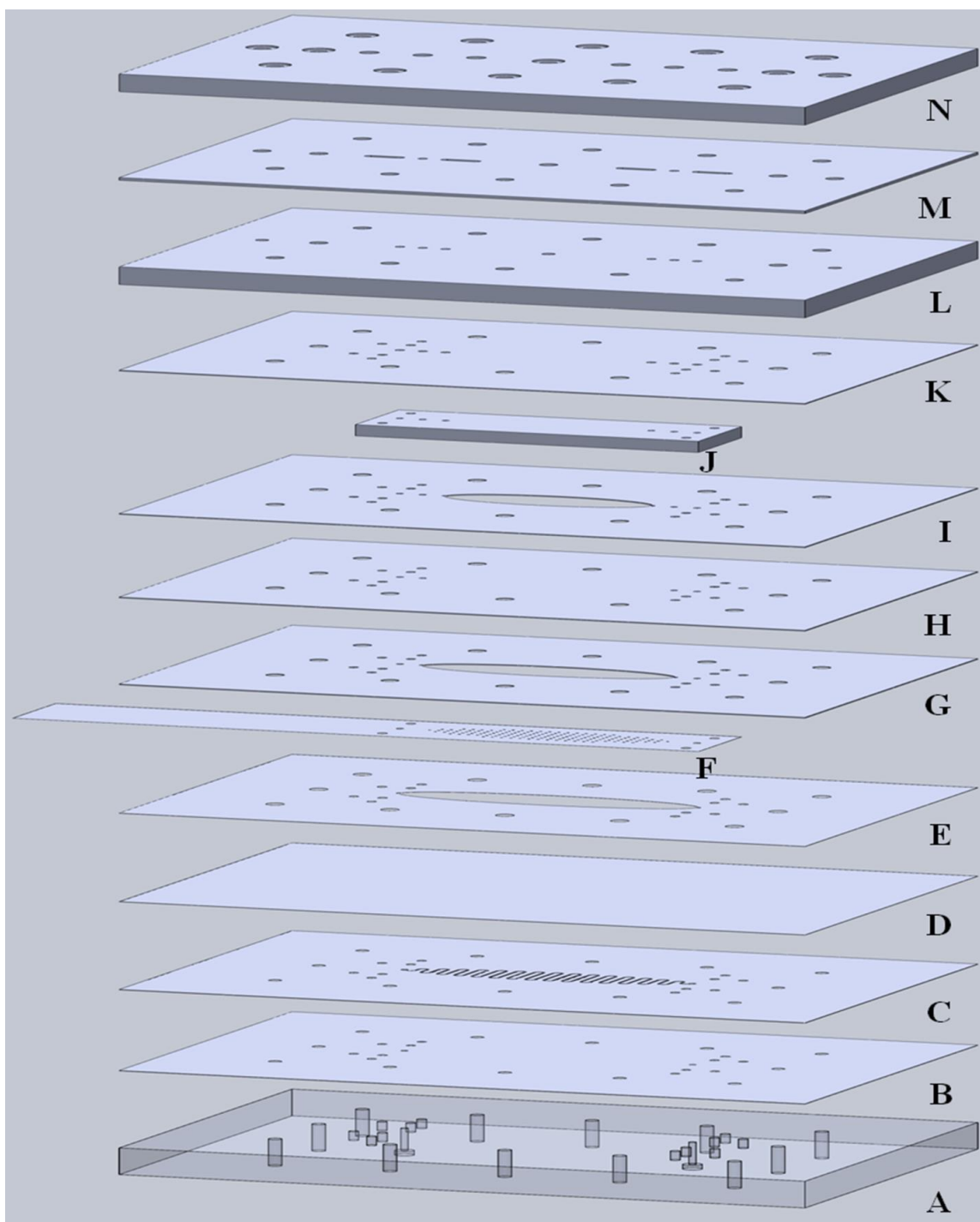
Figure 4.6: Schematic of the complete EDOR prototype. Layer A is displayed as transparent to show the fluidic inlet/outlet of the sample stream. See Table 4.1 and the text for more detailed descriptions of each layer.

Layer	Material	Exterior Dimension	Critical Feature Dimension
A	PVC	150 mm X 100 mm X 15 mm [a]	Threads: 10-32 UNF Fluidic through-holes: 1.5 mm diameter
B	Viton	150 mm X 100 mm X 0.010" [b]	Fluidic through-holes: 1.5 mm diameter
C	Viton	150 mm X 100 mm X 0.010" [b]	Channel: 250 µm deep X 400 µm wide X 345 mm long
D	Silicone Rubber	150 mm X 100 mm X 0.005" [c]	Ultra-thin (~125 µm)
E	Silicone Rubber	150 mm X 100 mm X 0.020" [c]	Elliptical chamber: 15 mm X 65 mm X 0.5 mm
F	Silver Foil	150 mm X 25 mm X 75 µm [d] (offset from center)	Perforations : 0.1 mm to 0.5 mm Fluidic through-holes: 1.5 mm diameter
G	Silicone Rubber	150 mm X 100 mm X 0.020" [c]	Elliptical chamber: 15 mm X 55 mm X 0.5 mm Fluidic through-holes: 1.5 mm diameter
H	Membrane	150 mm X 100 mm X 500µm [e]	Fluidic through-holes: 1.5 mm diameter
I	Silicone Rubber	150 mm X 100 mm X 0.020" [c]	Elliptical chamber: 15 mm X 45 mm X 0.5 mm Fluidic through-holes: 1.5 mm diameter
J	Graphite Sheet	75 mm X 25 mm X ¼" [c]	Fluidic through-holes: 1.5 mm diameter
K	Silicone Rubber	150 mm X 100 mm X 0.020" [c]	Fluidic through-holes: 1.5 mm diameter
L	PVC	150 mm X 100 mm X 10 mm [a]	Fluidic through-holes: 1.5 mm diameter
M	Butyl Rubber	150 mm X 100 mm X 1/16" [c]	Fluidic through-holes: 1.5 mm diameter
N	PVC	150 mm X 100 mm X 10 mm [a]	Threads: 10-32 UNF Fluidic through-holes: 1.5 mm diameter

Table 4.1: List of materials used in fabrication of EDOR prototype along with the important feature dimensions. The thickness of the materials are based on manufacturer/supplier specifications ([a] Firstcut, [b] AAAcme Rubber, [c] McMaster Carr, [d] Alfa Aesar, [e] Koch Membrane)

4.5.2 Custom Built TLC O$_2$ Detector

The detector consisted of a polycarbonate bottom fixture with a recessed groove for precise alignment of the sensor chip, two Viton rubber gasket layers, a pyrolytic graphite sheet, and PVC top fixture with fluidic inlet/outlet. A diagram of the detector and details regarding its fabrication are shown in **Figure 4.7** and **Table 4.2**. The fabrication process of the individual layers was similar to that described above for the EDOR prototype. Assembly resulted in a three electrode single compartment flow cell. The channel was cut from the same Viton material described above and had dimensions of 250 μm deep, 500 μm wide and 2 cm long (Layer C). The working and reference electrodes were based on two lithographically patterned thin film Au electrodes with an exposed length of 1 mm each separated by a 200 μm gap at the bottom of the channel (**Inset of Figure 4.7**). The upstream Au electrode was converted to a Ag/AgCl pseudo reference electrode by deposition of a Ag layer, followed by electrochemical oxidation in Cl- containing medium (a 100 μm electrode between the Working and reference electrodes (WE and RE) along with the remaining electrodes on the sensor chip were not used in this work). The fabrication of the sensor chip and conversion of Au thin-film electrodes to Ag/AgCl pseudo reference electrodes are described in detail elsewhere **[references 1 and 24, respectively]**. The counter electrode consisted of a flat 100μm thick pyrolytic graphite sheet (Panasonic Electronic Components, Secaucus, NJ) incorporated as an additional layer atop the channel. This custom cut pyrolytic graphite sheet (PGS) included holes for the alignment pins and flow paths of the layers above and beneath it. Air tight fluidic connections were made as described above.
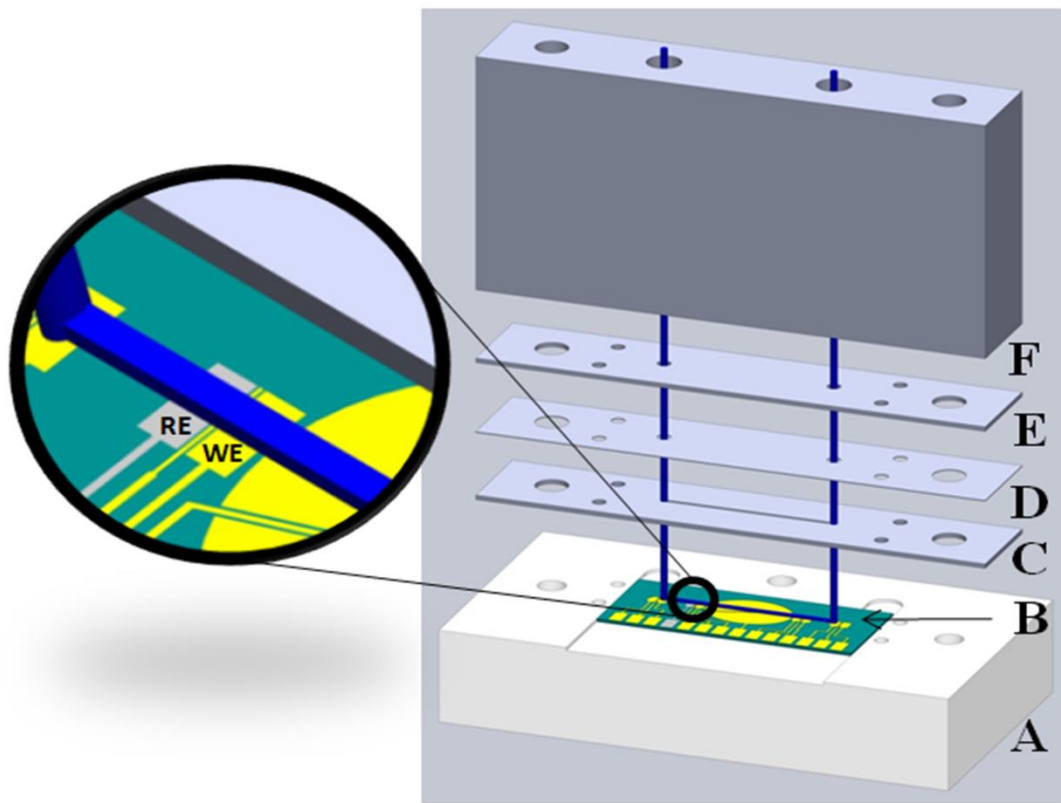
Figure 4.7: Schematic of the complete TLC DO detector. Sample stream defined by layers B-F is shown in blue. See Table 4.2 and the text for detailed descriptions.

Layer	Material	Exterior Dimension	Critical Feature Dimension
A	Polycarbonate	6.0 cm X 3.25 cm X 1 cm [a]	Recessed groove for sensor chip: 3.02 cm X 2.25 cm X 350 μm
B	SiO_2 / Au / AgCl	3.0 cm X 1.3 cm X 500 μm [g]	Exposed Au at channel base: 1 mm Ag/AgCl pseudo ref electrode: 1 mm
C	Viton	6.0 cm X 1.15 cm X 0.010" [b]	Channel: 250 μm deep X 500 μm wide X 2 cm long
D	Pyrolytic Graphite	6.0 cm X 1.15 cm X 100μm [f]	Fluidic through-holes: 1.5 mm
E	Viton	6.0 cm X 1.15 cm X 0.010" [b]	Fluidic through-holes: 1.5 mm
F	PVC	6.0 cm X 1.15cm X 2.54cm [c]	Threads: 10-32 UNF Fluidic through-holes: 1.5 mm

Table 4.2: List of materials used in fabrication of TLC DO detector along with the important feature dimensions. The thickness of the materials are based on manufacturer/supplier specifications or measured ([a] Firstcut, [b] AAAcme Rubber, [c] McMaster Carr, [f] Mouser Electronics, [g] Measured)

4.5.3 Construction and Use of Reference Manifold

In view of using a custom built DO detector for initial evaluation of the EDOR prototype, it was useful to compare the detector response to a proven de-oxygenation platform. The reference de-oxygenation manifold used here follows the same principle reported by Pedrotti et al., who described a system based on the diffusion of DO from a sample stream flowing inside O_2 permeable silicone rubber tubing [17]. Pedrotti et al. used a N_2 atmosphere, a vacuum, or a combination of the two on the outside of the silicone rubber tubing to remove DO from the sample stream, and showed >99% O_2 removal for all cases after optimization. Colombo and Van den Berg investigated the performance of several O_2 permeable tubing materials in a N_2 atmosphere and found silicone rubber tubing and poreflon to be suitable for these devices [18]. Billing et al. later improved on this manifold by jacketing the O_2 permeable silicone rubber tubing with polyethylene tubing where N_2 was counter-flowing to maintain the O_2 concentration gradient along the entire length of the tubing [19].

The reference manifold utilized in this work utilized a 3.5m length of jacketed tubing as illustrated in **Figure 4.8**. The inner tubing was high-purity silicone rubber tubing (0.025" ID, 0.047" OD) and the outer tubing was Polyethylene Tubing (4 mm ID, 6 mm OD). The sample stream was pumped from a reservoir which had been allowed to equilibrate with air for at least 24 hours into the manifold inlet. The manifold outlet was directly connected to the TLC detector as previously described for the EDOR prototype. In order to avoid atmospheric O_2 re-entry into the sample stream between the manifold outlet and the detector, an adapter from the silicone tubing to PEEK tubing (0.020" ID, 1/16"OD) was placed inside the N_2 jacket so that only a short length (<10 cm) of PEEK

tubing extended from the manifold outlet to the detector. To begin de-oxygenation, an adjustable valve was opened to allow N_2 to flow from a cylinder into the manifold jacket, and the DO content of the sample stream was monitored at the TLC detector. Evidence of complete DO removal by the reference manifold was demonstrated by the independence of TLC detector for a wide range of sample flow rates (10 μL/min to 200 μL/min), when N_2 was used in the outer jacket. Conversely, the TLC detector response increased with increasing sample flow rate when the reference manifold was inactive or when O_2 was flowing in the outer jacket.
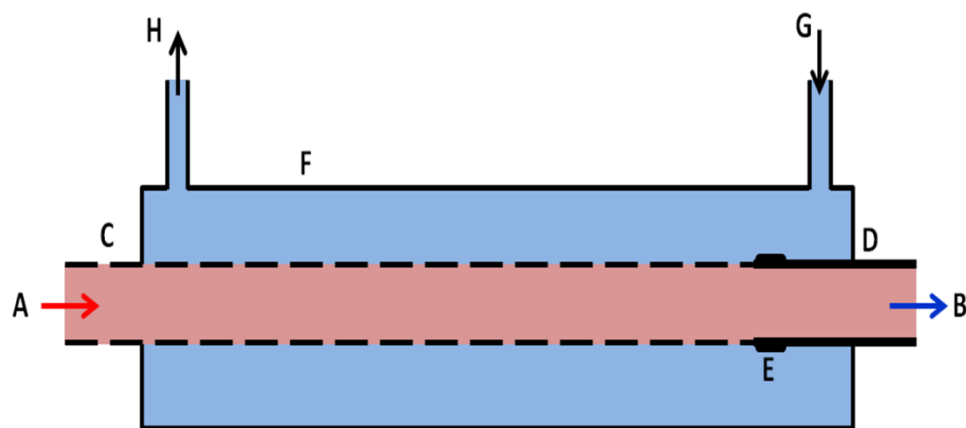
Figure 4.8: Schematic of the reference manifold. A: Sample stream inlet from pump, B: Sample stream outlet to detector, C: O_2 permeable silicone rubber tubing (0.025" ID, 0.047" OD), D: O_2 impermeable PEEK tubing (0.020" ID, 1/16"OD), E: Adapter from silicone to PEEK tubing, F: Polyethylene jacket tubing for counter flowing N_2 (4 mm ID, 6 mm OD), G: N_2 gas inlet from cylinder, H: N_2 vent to atmosphere.

4.6 Conclusions

An indirect electrochemical dissolved oxygen removal device is proposed, and its design and proof of concept are described. The current device is capable of removing 98 % of DO (8 ppm O_2 sample stream flowing at 10 µL/min) and requires 165 mW hr L^{-1}. This is consistent with our intended aim for a continuous flow-by oxygen removal system for our micro anodic stripping coulometry application which analyzes a 2-4 µL volume cell per minute. The device is simple to operate, and the only hook-ups necessary for continuous operation are the sample inlet/outlet and a voltage controlled DC current source. Besides the micro fluidic sample pretreatment applications, the inherent energy efficiency of this approach may eventually attract development of massively parallel preparative de-oxygenation processes (e.g., water for the semiconductor industry, ship ballast water, boiler water, or even jet fuel for the aviation industry).

The next stage of development will involve addressing the limitations of the current prototype. Specifically, future work will be directed at finding more resistant O_2 exchange membranes and/or a milder O_2 reduction electrochemistry. Silicone rubber is not compatible for long term operation in the presence of 6.5 M NaOH due to OH^- hydrolysis of Si-O-Si bonds. Most importantly, the passive nature of DO removal by diffusion in the current scheme ought to be greatly aided by miniaturization of the device. Future investigations are also planned to determine the potential for longer term operation.

CHAPTER V

CONCLUSIONS AND PERSPECTIVES

5.1 Foreword

Having introduced this dissertation within the context of practical, sensitive, and selective measurements, it is appropriate to conclude by addressing the current status of the TLC coulometric sensor along each of these lines and, where possible, to describe future work and make reasoned predictions of future improvements. The proposed sensor for decentralized remote heavy metal monitoring is not intended to compete with or replace the analyses of the central laboratory. It rather seeks to enhance these analytical tools by applying them to where the most interesting measurements can be obtained.

The current generation of the TLC coulometric sensor is capable of the determination of minute amounts of dissolved metals in micro-liter sized sample volumes. For instance, <500 ppb levels of metals such as As^{III} and Cu^{2+} in a 1.85 µL sample can be measured to better than 10% Accuracy and with excellent reproducibility (RSD's generally <5%). Importantly, these measurements can be carried out in about 1-2 minutes and are possible without any calibration steps. The demonstrated detection of Pb and Cd is a work in progress, but the sensor performance discussed in this section provides a general estimate of the results that can be expected. Additionally, the most

difficult challenge for the analysis of Pb and Cd is addressed elsewhere in this work; the development of a highly energy efficient (165 mW hr L^{-1}) means for remote removal of dissolved oxygen (which interferes with Pb and Cd ASC).

5.2 Sensitivity of the Current Heavy Metal Sensor

The discussion of sensitivity has, to this point, proceeded in general terms with the implicit understanding that it also effectively includes considerations regarding the detection limit. In these closing remarks to this work, however, it is appropriate to examine closely the sensitivity (and detection limit) of anodic stripping coulometry by a single potential step (SPS-ASC), the proposed double potential stripping anodic stripping coulometry (DPS-ASC) method, and its sequential multi-potential variant (SEQ-MP-DPS-ASC) for evaluating a single metal in the presence of interferents.

The C_{min} value reflects the smallest discernible concentration increment (e.g., the relative power of the method to discern samples containing 120 ppb vs. 121 ppb arsenite for instance, or 1 ppb vs. 2 ppb). As shown in this hypothetical example, a C_{min} of 1 ppb is quite satisfactory at high concentrations but is clearly much less so as the analyte concentration approaches C_{min}. Accordingly, it is useful to represent C_{min} as a percentage of the measured concentration. The resulting C_{min} values for a few test cases (see **Appendix A** for detailed calculations) indicate that the uncertainty in all measurements performed by SPS-ASC and DPS-ASC is below 12%, whereas measurements by SEQ-MP-DPS-ASC were typically below 21%.

Although C_{min} is a valuable indicator of performance, the most relevant criterion in the context of heavy metal measurements is perhaps the lowest concentration which

can be detected and quantified (C_{LOD} and C_{LOQ}, respectively) since even trace metal levels may be of concern. Evaluating the detection limit of stripping coulometry should, in principle, include components such as the reproducibility of the blank (i.e., $3\sigma_{blank}$), the electrode area (which is often a source of noise in electrochemical measurements), the volume sampled (since the low LODs of stripping analysis arises from the pre-concentration effect usually achieved by sampling bulk solutions while stirring to enlarge the sampled volume), and finally the number of electrons in the redox process (since the sensitivity ought to be greater for a $2e^-$ stripping process vs. a $1e^-$ process because the signals are larger in the former case).

Due to the variations in the metals analyzed, the use of several individual Au electrodes with different histories, and the presence of different interferents, the resulting C_{LOD} values for a few test cases (see **Appendix B** for detailed calculations) are 38 ppb for Cu^{2+} and 19-135 ppb for As^{III}. Further improvements of the detection limits ought to obviously seek favorable alterations to the area to volume (A/V) ratio, since this is in fact the same term responsible for the sensitivity of conventional stripping analysis where a relatively small electrode area pre-concentrates metals from an effectively infinite bulk volume. In the case of the TLC coulometry platform described in this work, relatively modest and technically feasible alterations can have a significant impact on the A/V ratio. For instance, future generations of the current TLC platform employing 100 fold smaller microelectrode arrays (MEA) and 3 times thicker cells would seem to offer useful detection limits. Assuming that the experimentally measured noise in the blank per unit of electrode area remains constant, the predicted C_{LODs} and C_{LOQs} are below the EPA MCL level for drinking waters. In conclusion, the sensitivity of ASC cannot rival that of

traditional stripping voltammetry where essentially unlimited improvements of the A / V term are possible. However, C_{LOD} and C_{LOQ} values suitable for heavy metal detection in drinking waters appear to be achievable with appropriate design and optimization. This is especially plausible since drinking water ought to be a sufficiently stable matrix requiring minimal sample pretreatment. Although natural waters and wastewater effluents may be highly variable matrices with consequently larger Q_{LOD} and Q_{LOQ} values, the C_{LOD} and C_{LOQ} requirements in these cases are also less stringent.

5.3 Selectivity

The use of stripping analysis offers an important advantage in terms of selectivity. The electroactive interferents of most concern are those that are accumulated on the electrode surface prior to the analytical stripping step. Therefore, the most likely interferents in the measurement of metals are other metals. The conventional approach to anodic stripping analysis seeks to deposit all metals present which can be reduced at the deposition potential. The stripping step is performed sequentially so that the removal of each metal at its characteristic oxidation potential is temporally separated from its neighbors. The literature contains many instances where the stripping of two metals occurs at sufficiently close potentials, or even chemically react on the electrode surface, so that their individual stripping signals are indistinguishable. Over the long history of this approach, many special procedures and sample pretreatments have been adopted for application specific problems.

In double potential step anodic stripping coulometry (DPS-ASC), it is necessary to strip all metals simultaneously to obtain the bare electrode surface necessary for blank

subtraction. Hence, the selectivity must instead be applied during the deposition step. The use of selective deposition in conjunction with simultaneous stripping as in PS-ASC is much less developed in the literature. The only cases where it can be said with certainty that an interferent can be tolerated are limited to the results obtained in this work. These show that under the conditions used, MP-DPS-ASC and SEQ-MP-DPS-ASC allow measurement of the individual concentrations of Cu^{2+} and Hg^{2+} in a mixture, Cu^{2+} and As^{III} in a mixture, and that As^{III} can be measured accurately in the presence of Cu^{2+}, Pb^{2+}, Cd^{2+}, and Zn^{2+} (as long as the Pb and Cd ppb levels are at most half the As ppb level). In the long term only time can tell the extent to which these methods may be applicable to increasingly challenging sample matrices.

Despite the presently limited extent to which any predictions regarding selectivity can be made, there are at least two considerations which would seem to indicate that widespread utility of the sensor is possible. The first of these is that heavy metals are themselves the most concerning interferents in anodic stripping coulometry. Since heavy metals are often present at trace levels, it is plausible that the contribution of one metal as an interferent to another may have a minimal impact on the overall measurement. The second of these is that even incomplete selectivity does not necessarily constitute a failure of the sensor to detect heavy metals. If in the course of arsenic monitoring, for instance, the sensor begins to mistakenly report a spike in arsenic concentration due to a spike of another heavy metal, the changing response could actually have the positive effect of directing snapshot monitoring by centralized laboratories to where conditions have changed.

5.4 Practicality

The discussion of practicality cannot proceed to any significant extent without thorough consideration of all the components and challenges for the remote heavy metal monitoring system. The whole system, as currently envisioned, is represented in **Figure 5.1**. The realization of the overall system requires inter-disciplinary collaboration and careful design to minimize cost and complexity. Many of the individual components remain as works in progress, however, few of the challenges appear to pose fundamental technical challenges and several involve the customization of currently available technologies. For instance, several of the functions in the figure can be adequately performed by even the simplest first generation so called smart phones, since these are essentially a packaged microprocessor, battery, and communications platform. Similarly, the design and microfabrication of miniature and inexpensive components such as pumps, microfluidic manifolds including automatic valves, control circuitry, and potentiostats have all been previously described **[1]**. For our application, preliminary work towards the development of customized versions based on assembly of inexpensive, off-the-shelf components appears to also offer a promising avenue.

One major challenge which remains is the issue of sensor durability. In this regard, there are already some promising aspects of the current sensor, and other planned developments which may increase sensor lifetime. Current features of the sensor which are supportive of long term stability include the exhaustive deposition in a thin layer cell, which in the event of partial electrode fouling, would simply take longer to achieve. Secondly, the application of the DPS-ASC method for *in situ* background correction appears promising for proper blank subtraction at the changing electrode surface. Planned

144

developments aim to take advantage of the microfabricated nature of the sensor which, in principle, also allows for a built in redundancy for self-verification and/or increasing periods between maintenance. Future developments also under consideration include the use of alternative materials which are resistant to fouling during extended use including electrode materials such as boron doped diamond and fluoropolymer membranes, and regeneration of the reference electrode.
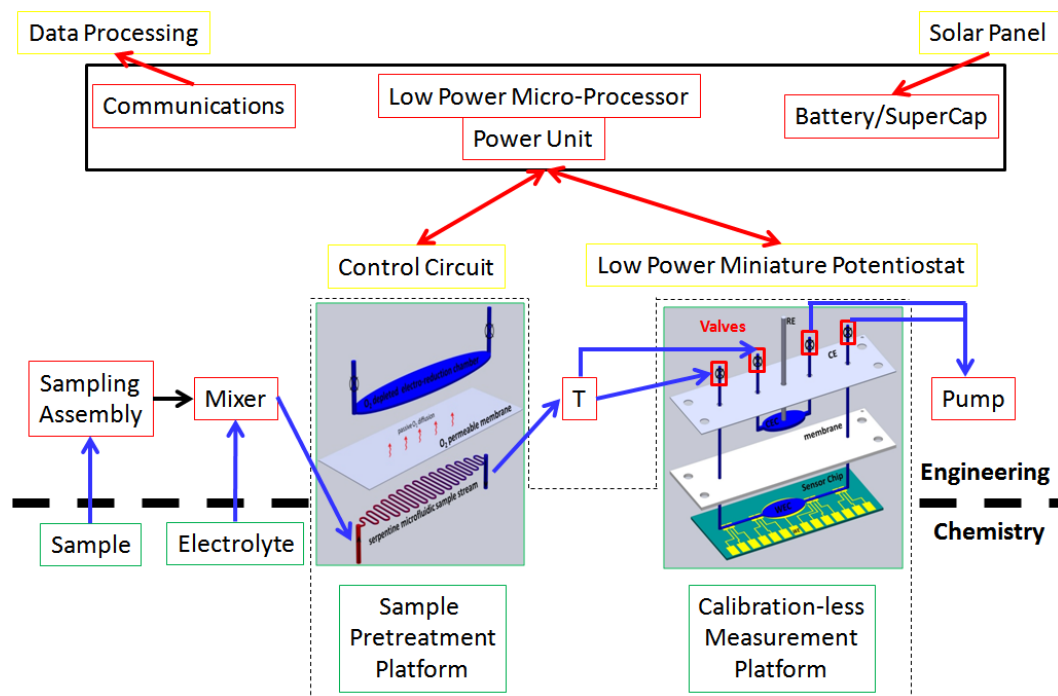
Figure 5.1: Overview of the remote heavy metal sensor. The portions contained within the dashed lines indicate the focus of this dissertation. Green outlines indicate major progress of a component, yellow outlines indicate preliminary work, and red outlines indicate as yet to be addressed components.

REFERENCES

Chapter I References

(1) Walt, D.R. Optical Methods for Single Molecule Detection and Analysis. *Anal. Chem.* **2013**, *85*, 1258-1263.

(2) Fu-Ren F. Fan, F.F.; Kwak, J.; Bard, A.J. Single Molecule Electrochemistry. *J. Am. Chem. Soc.* **1996,** *118,* 9669-9675.

(3) Jenison, R.D.; Gill, S.C.; Pardi,A.; Polisky, B. High-Resolution Molecular Discrimination by RNA. *Science* **1994**, *263*, 1425-1429.

(4) Niazi, J.H.; Lee, S.J.; Kim, Y.S.; Gu, M.B. ssDNA aptamers that selectively bind oxytetracycline. *Bioorganic & Medicinal Chemistry* **2008**, *16*, 1254-1261.

(5) Bakker, E.; Pretsch, E. Potentiometric sensors for trace-level analysis. *TrAC*. **2005**, 24, 199-207.

(6) Pretsch, E. The new wave of ion-selective electrodes. *TrAC*, **2007**, 24, 46-51.

(7) Vessman, J.; Stefan, R.I.; van Staden, J.F.; Danzer, K.; Lindner, W.; Burns, D.T.; Fajgelj, A.; Muller, H. Selectivity in analytical chemistry (IUPAC Recommendations 2001). *Pure Appl. Chem.* **2001**, *73*, 1381-1386.

(8) Danaei, G.; Finucane, M.M.; Lu, Y.; Singh, G.M.; Cowan, M.J.; Paciorek, C.J.; et al.; National, regional, and global trends in fasting plasma glucose and diabetes prevalence since 1980: systematic analysis of health examination surveys and epidemiological studies with 370 country-years and 2.7 million participants. *Lancet*. **2011**, *378*, 31-40.

(9) Abbott Point of Care. Clinical and Laboratory Studies: FreeStyle™ Blood Glucose Test Strip Performance. © 2005 Abbott PRT06911 Rev A. Available on the web at (accessed Aug 1, 2014): https://www.abbottdiabetescare.co.uk/_resources/media/documents/hcps/clinical_papers/CP013_freeStyle_white_paper.pdf

(10) Heller, A.; Feldman, B. Electrochemical glucose sensors and their applications in diabetes management. *Chem. Rev.* **2008**, *108*, 2482-2505.

(11) Wang, J. Electrochemical Glucose Biosensors. *Chem. Rev.* **2008**, *108,* 814-825.

(12) Economou, A. Recent Developments in on-line electrochemical stripping analysis – An overview of the last 12 years. *Anal. Chim. Acta* **2010**, *683*, 38-51.

(13) Wang, J.; Tian, B.; Wang, J.; Lu, J.; Olsen, C.; Yarnitzky, C.; Olsen, K.; Hammerstrom, D.; Bennet, W. Stripping Analysis into the 21st Century: faster, smaller, cheaper, simpler, and better. *Anal. Chim. Acta* **1999**, *385*, 429-435.

(14) Gross, T. M. Efficacy and reliability of the continuous glucose monitoring system. *Diabetes Technol. Ther.* **2000**, *2*, S19-26.

(15) Medtronic MiniMed. MiniMed 530G User Guide, Paradigm REAL-Time Revel System Insulin Pump User Guide. © Medtronic MiniMed, Inc. 2012. Available on the web at (accessed Aug 1, 2014): https://s3.amazonaws.com/medtronic-hcp/MiniMed%20530G%20System%20User%20Guide.pdf

(16) Comprehensive Environmental Response, Compensation, and Liability Act. Title 42 U.S.C. § 9601-9675.

(17) Priority List of Hazardous Substances. Agency for Toxic Substance and Disease Registry. Available on the web at (accessed Aug 1, 2014): http://www.atsdr.cdc.gov/spl/

(18) Detailed Data Table of Priority List of Hazardous Substances. Agency for Toxic Substance and Disease Registry. Available on the web at (accessed Aug 1, 2014): http://www.atsdr.cdc.gov/spl/resources/ATSDR_2013_SPL_Detailed_Data_Table.pdf

(19) Onondaga Lake SuperFund Site. Environmental Protection Agency. Available on the web at (accessed Aug 1, 2014): http://www.epa.gov/r02earth/superfund/npl/onondagalake/index.html

(20) National Priority List Map. Environmental Protection Agency. Available on the web at (accessed Aug 1, 2014): http://www.epa.gov/superfund/sites/products/nplmap.bmp

(21) National Primary Drinking Water Regulations. Environmental Protection Agency. Available on the web at (accessed Aug 1, 2014): http://water.epa.gov/drink/contaminants/upload/mcl-2.pdf

(22) Analytical Methods Approved for Drinking Water Compliance Monitoring of Inorganic Contaminants and Other Inorganic Consistuents. Revised December 2009. Environmental Protection Agency. Available at (accessed Aug 1, 2014): http://www.epa.gov/ogwdw/methods/pdfs/methods/methods_inorganic.pdf

(23) Louisville Water Company. Available on the web at (accessed Aug 1, 2014): http://www.louisvilleky.gov/LWC

(24) Information about Lead. Louisville Water Company. Available on the web at (accessed Aug 1, 2014): http://www.louisvilleky.gov/NR/rdonlyres/305F0641-4355-427E-A917-06D683574278/0/LeadInformation.pdf

(25) Lead and Copper Rule: A Quick Reference Guide. Environmental Protection Agency. Available on the web at (accessed Aug 1, 2014): http://www.epa.gov/ogwdw/lcrmr/pdfs/qrg_lcmr_2004.pdf

(26) 2010 Water Quality Report. Louisville Water Company. Available on the web at (accessed Aug 1, 2014): http://www.louisvilleky.gov/NR/rdonlyres/79FD1F35-D45F-46E6-9600-CAA8BBC2F944/0/2011PureTapReport.pdf

(27) 2013 Water Quality Report. Louisville Water Company. Available on the web at (accessed Aug 1, 2014): http://www.louisvilleky.gov/NR/rdonlyres/679E34E1-4557-4495-8EFD-98403FC896EE/0/CCR2012LRforweb.pdf

(28) Woolf, A.D.; Goldman, R.; Bellinger, D.C. Update on the clinical management of childhood lead poisoning. *Pediatr. Clin. North Am.* **2007**, *54*, 271-94.

(29) U.S. Census Bureau. Current Housing Reports, Series H150/07, American Housing Survey for the United States: 2007, U.S. Government Printing Office, Washington, D.C.: 20401, Printed in 2008. Available at http://www.census.gov/prod/2008pubs/h150-07.pdf

(30) Mandal, B.K.; Suzuki, K.T. Arsenic round the world: a review. *Talanta*. **2002**, *58*, 201-235.

(31) Arsenic in groundwater of the United States. United States Geological Survey. Available on the web at (accessed Aug 1, 2014): http://water.usgs.gov/nawqa/trace/arsenic/

(32) Mukherjee, A.B.; Bhattacharya, P. Arsenic in the groundwater in the Bengal Delta Plain: slow poisoning in Bangladesh. *Environ. Rev.* **2001**, *9*, 189-220.

(33) Eating Arsenic. *Chemical and Engineering News.* **2013**, *91*, 36-39. Available on the web at (accessed Aug 1, 2014): http://cen.acs.org/articles/91/i18/Eating-Arsenic.html

(34) Lead and Copper Rule: A Quick Reference Guide for Schools and Child Care Facilities that are Regulated Under the Safe Drinking Water Act. Environmental Protection Agency. Available on the web at (accessed Aug 1, 2014): http://www.epa.gov/ogwdw/schools/pdfs/lead/qrg_lcr_schools.pdf

(35) Method 1001: Lead in Drinking Water by Differential Pulse Anodic Stripping Voltammetry. August 1999. Can be obtained from: Hach Company. Loveland, Colorado.

http://www.hach.com (Accessed May 13, 2013). May also be obtained from Palintest Ltd. 21 Kenton Lands Road, PO Box 18395. Erlanger, Kentucky 41018. 606/341-7423

(36) Kounaves, S.P. Voltammetric Techniques. Handbook of Instrumental Techniques for Analytical Chemistry, Frank A. Settle (Ed.), Prentice Hall, Upper Saddle River, NJ, 1997.

(37) J.Wang, Stripping Analysis: Principles, Instrumentation, and Applications. VCH Publishers, Deerfield Beach, FL, 1985.

(38) Jagner, D.; Graneli, A. Potentiometric Stripping Analysis. *Anal. Chim. Acta.* **1976**, *83*, 19-26.

(39) Estela, J.M.; Tomas, C.; Cladera, A.; Cerda, V. Potentiometric Stripping Analysis: A Review. *Critical Reviews in Analytical Chemistry*. **1995**, *25*, 91-141

(40) Eggli, R. Anodic Stripping Coulometry at a Thin-Film Mercury Electrode. *Anal. Chim. Acta* **1977**, *91*, 129-138.

(41) A.J. Bard, L.R. Faulkner. Electrochemical Methods: Fundamentals and Applications. 2nd ed., John Wiley, New York, 2001.

(42) Carroll, S.; Marei, M.M.; Roussel, T.J.; Keynton, R.S.; Baldwin, R.P. Microfabricated electrochemical sensors for exhaustive coulometry applications. *Sens Actuators B Chem.* **2011**, *160*, 318-326.

(43) Bakker, E.; Bhakthavatsalam, V.; Gemene, K.L. Beyond potentiometry: Robust Electrochemical Ion Sensor Concepts in View of Remote Chemical Sensing. *Talanta.* **2008**, *75*, 629-635.

(44) Tsujimura, S.; Nishina, A.; Kamitaka, Y.; Kano, K. Coulometric D-Fructose Biosensor Based on Direct Electron Transfer Using D-Fructose Dehydrogenase. *Anal. Chem.* **2009**, *81*, 9383-9387.

(45) Marei, M.M.; Roussel, T.J.; Keynton, R.S.; Baldwin, R.P. Electrochemical and microfabrication strategies for remotely operated smart chemical sensors: Application of anodic stripping coulometry to calibration-free measurements of copper and mercury. *Anal. Chim. Acta* **2013**, *803*, 47-55.

(46) Rogers, L.B.; Stehney, A.F. The Electrodeposition Behavior of a Simple Ion. *J. Electrochem. Soc*. **1949**, *95*, 25-32.

(47) Beinrohr, E. Flow-Through Chronopotentiometry in Waste Water Analysis. Waste Water - Evaluation and Management, Fernando S. Garcia Einschlag (Ed.), ISBN: 978-953-307-233-3, InTech, Available on the web at (accessed Aug 1, 2014): http://cdn.intechweb.org/pdfs/14572.pdf

(48) Garai, T.; Nagy, Z.; Mészáros, L.; Bartalits, L.; Locatelli, C.; Fagioli, F. Theory of derivative and differential potentiometric stripping analysis and stripping chronopotentiometry. *Electroanalysis*. **1992**, *4*, 899-904.

(49) Strelec, M.; Cacho, F.; Manova, A.; Hlubikova S.; Beinrohr, E. Calibrationless Determination of Lead in Waste Water Samples by Flow-Through Stripping Chronopotentiometry. *Chem. Anal. (Warsaw)*. **2007**, *52*, 377-385.

(50) Hazelton, S.G.; Pierce, D.T. Ultratrace Determination of Inorganic Selenium without Signal Calibration. *Anal. Chem.* **2007**, *79*, 4558-4563.

(51) Bresnahan, W.T.; Elving, P.J. Measurement of Surface Excess at a Dropping Mercury Electrode by Normal Pulse Polarography with Coulometry. *Anal. Chem.* **1981**, *53*, 1118-1120.

(52) Bonfil, Y.; Brand, M.; Kirowa-Eisner, E. Characteristics of subtractive anodic stripping voltammetry of Pb and Cd at silver and gold electrodes. *Anal. Chim. Acta.* **2002**, *464*, 99–114.

(53) Dai, X.; Compton, R. G. Detection of As(III) *via* oxidation to As(V) using platinum nanoparticle modified glassy carbon electrodes: arsenic detection without interference from copper. *Analyst*. **2006**, *131*, 516-521

(54) Wang, J. Electrochemical Detection for Capillary Electrophoresis Microchips: A Review. *Electroanalysis*. **2005**, *17*, 1133-40.

(55) Puy, J.; Galceran, J.; Huidobro, C.; Companys, E.; Samper, N.; Garcés, J. L.; Mas, F. Conditional Affinity Spectra of Pb^{2+} – Humic Acid Complexation from Data Obtained with AGNES. *Environ. Sci. and Technol*. **2008**, *42*, 9289-9295.

(56) Logan, E. M.; Pulford, I. D.; Cook, G. T.; Mackenzie, A. B. Complexation of Cu^{2+} and Pb^{2+} by peat and humic acid. *European Journal of Soil Science*. **1997**, *48*, 685-696

(57) *CRC Handbook of Chemistry and Physics*, 85th ed.; Boca Raton, FL, 2004.

(58) Lee, K.H.; Ishikawa, T.; McNiven, S.; Nomura, Y.; Sasaki, S.; Arikawa, Y.; Karube, I. Chemical Oxygen Demand Sensor Employing a Thin Layer Electrochemical Cell. *Anal. Chim. Acta.* **1999**, 386, 211-220.

(59) Cossu , R.; Polcaro , A.M.; Lavagnolo , M.C.; Mascia , M.; Palmas, S.; Renoldi, F. Electrochemical Treatment of Landfill Leachate: Oxidation at Ti/PbO2 and Ti/SnO2 Anodes.
Environ. Sci. Technol. **1998**, *32*, 3570-3573.

(60) Bekbolet, M.; Suphandag, A.S.; Uyguner, C.S. An investigation of the photocatalytic efficiencies of TiO_2 powders on the decolourisation of humic acids. *J. Photochem. Photobiol. A: Chem*. **2002**, *148*, 121-128.

(61) Fernando, A.R.; Plambeck, J.A. Effects of Background Electrolyte and Oxygen on Trace Analysis for Lead and Cadmium by Anodic Stripping Voltammetry. *Anal. Chem.* **1989**, *61*, 2609-2611.

(62) A.Prieto, J.Hernandez, E. Herrero, J.M. Feliu. The Role of Anions in Oxygen Reduction in Neutral and Basic Media on Gold Single-crystal Electrodes. *J. Solid State Electrochem.* **2003**, *7*, 599-606.

(63) Hanekamp, H.B.; Voogt, W.H.; Bos, P.; Frei, R.W. An Electrochemical Scrubber for the Elimination of Eluent Background Effects in Polarographic Flow-through Detection. *Anal. Chim. Acta* **1980**, *118*, 81-86.

(64) Colombo, C.; van den Berg, C.M.G. In-line Deoxygenation for Flow Analysis with Voltammetric Detection. *Anal. Chim. Acta* **1998**, *377*, 229-240.

Chapter II References

(1) Analytical Methods Approved for Drinking Water Compliance Monitoring of Inorganic Contaminants and Other Inorganic Consistuents. Revised December 2009. Environmental Protection Agency. Available at (accessed Aug 1, 2014): http://www.epa.gov/ogwdw/methods/pdfs/methods/methods_inorganic.pdf

(2) Skoog, D.A., F.J. Holler, and T.A. Nieman, Principles of instrumental analysis, Fifth ed., Harcourt Brace, Philadelphia, 1998.

(3) Ashley, K. Ultrasonic extraction and field-portable anodic stripping voltammetry of lead from environmental samples. *Electroanal.* **1995**, *7*, 1189-1192.

(4) Wang, J.; Tian, B.; Lu, J.; Wang, J.; Luo, D.; MacDonald, D. Remote Electrochemical Sensor for Monitoring Trace Mercury. *Electroanal.* **1998**, *10*, 399-402.

(5) Huang, H.; Dasgupta, P.K. A field-deployable instrument for the measurement and speciation of arsenic in potable water. *Anal. Chim. Acta* **1999**, *380*, 27-37.

(6) Daniele, S.; Bragato, C.; Baldo, M.A.; Wang, J.; Lu, J. The use of a remote stripping sensor for the determination of copper and mercury in the Lagoon of Venice. *Analyst* **2000**, *125*, 731-735.

(7) Palchetti, I.; Laschi, S.; Mascini, M. Miniaturised stripping-based carbon modified sensor for in field analysis of heavy metals. *Anal. Chim. Acta* **2005**, *530*, 61-67.

(8) Kovarik, M.L.; Ornoff, D.M.; Melvin, A.T.; Dobes, N.C.; Wang, Y.; Dickinson, A.J.; Gach, P.C.; Shah, P.K.; Allbritton, N.L. Micro Total Analysis Systems: Fundamental Advances and Applications in the Laboratory, Clinic, and Field. *Anal. Chem.* **2013**, *85*, 451-472.

(9) Hach Company. Loveland, Colorado. http://www.hach.com (Accessed May 13, 2013)

(10) Frisby, J.; Raftery, D.; Kerry, J.P.; Diamond, D. Development of an autonomous, wireless pH and temperature sensing system for monitoring pig meat quality. *Meat Sci.* **2005**, *70*, 329-336.

(11) Diamond, D.; Lau, K.T.; Brady, S.; Cleary, J. Integration of analytical measurements and wireless communications - Current issues and future strategies. *Talanta.* **2008**, *75*, 606-612.

(12) A.J. Bard, L.R. Faulkner. Electrochemical Methods, Fundamentals and Applications, second ed., John Wiley, New York, 2001.

(13) Bakker, E.; Bhakthavatsalam, V.; Gemene, K.L. Beyond potentiometry: Robust Electrochemical Ion Sensor Concepts in View of Remote Chemical Sensing. *Talanta.* **2008**, *75*, 629-35.

(14) Grygolowicz-Pawlak, E.; Bakker, E. Thin Layer Coulometry with Ionophore Based Ion-Selective Membranes. *Anal. Chem.* **2010**, *82*, 4537-4542.

(15) Sohail, M.; De Marco, R.; Lamb, K.; Bakker, E. Thin layer coulometric determination of nitrate in fresh waters. *Anal. Chim. Acta* **2012**, *744*, 39-44.

(16) Beinrohr, E.; Nemeth, M.; Tschopel, P.; Tolg, G.Anodic stripping coulometry with collection for absolute trace analysis of lead, using flow-through electrochemical cells with porous working electrodes. *Fresenius J. Anal. Chem.* **1992**, *344*, 93-99.

(17) Beinrohr, E.; Cakrt, M.; Dzurov, J.; Jurica, L.; Broekaert, J.A. Simultaneous Calibrationless Determination of Zinc, Cadmium, Lead, and Copper by Flow-Through Stripping Chronopotentiometry. *Electroanal.* **1999**, *11*, 1137-1144.

(18) Jurica, L.; Manova, A.; Dzurov, J.; Beinrohr, E.; Broekaert, J.A.C. Calibrationless flow-through stripping coulometric determination of arsenic(III) and total arsenic in contaminated water samples after microwave assisted reduction of arsenic(V). *Fresenius J. Anal. Chem.* **2000**, *366*, 260-266.

(19) Strelec, M.; Cacho, F.; Manova, A.; Hlubikova S.; Beinrohr, E. Calibrationless Determination of Lead in Waste Water Samples by Flow-Through Stripping Chronopotentiometry. *Chem. Anal. (Warsaw).* **2007**, *52*, 377-385.

(20) Nasraoui, R.; Floner, D.; Paul-Roth, C.; Geneste, F. Flow electroanalytical system based on cyclam-modified graphite felt electrodes for lead detection. *J. Electroanal. Chem.* **2010**, *638*, 9-14.

(21) Nasraoui, R.; Floner, D.; Geneste, F. Improvement in performance of a flow electrochemical sensor by using carbamoyl-arms polyazamacrocycle for the preconcentration of lead ions onto the electrode. *Electrochem. Commun.* **2010**, *12*, 98-100.

(22) Hazelton, S.G.; Pierce, D.T. Ultratrace Determination of Inorganic Selenium without Signal Calibration. *Anal. Chem.* **2007**, *79*, 4558-4563.

(23) Carroll, S.; Marei, M.M.; Roussel, T.J.; Keynton, R.S.; Baldwin, R.P. Micro-fabricated electrochemical sensors for exhaustive coulometry applications. *Sens. Actuators, B.* **2011**, *160*, 318-326.

(24) Lee, K.H.; Ishikawa, T.; Sasaki, S.; Arikawa, Y.; Karube, I. Chemical oxygen demand (COD) sensor using a stopped-flow thin layer electrochemical cell. *Electroanal.* **1999**, *11*, 1172-79.

(25) Condit, D.A.; Herrera, M.E.; Stankovich, M.T.; Curran, D.J. Five-electrode thin-layer cell for spectroelectrochemistry applied to spectrocoulometric titrations. *Anal. Chem.* **1984**, *56*, 2909-2914.

(26) Bonfil, Y.; Brand, M.; Kirowa-Eisner, E. Determination of sub-μg l^{-1} concentrations of copper by anodic stripping voltammetry at the gold electrode. *Anal. Chim. Acta* **1999**, *387*, 85-95.

(27) Bonfil, Y.; Brand, M.; Kirowa-Eisner, E. Determination of mercury and copper in waste water by anodic-stripping voltammetry at the gold electrode. *Reviews in Analytical Chemistry* **2000**, *19*, 201-216.

(28) Bonfil, Y.; Brand, M.; Kirowa-Eisner, E. Trace determination of mercury by anodic stripping voltammetry at the rotating gold electrode. *Anal. Chim. Acta* **2000**, *424*, 65-76.

Chapter III References

(1) Lubin, J.H.; Beane, L.E.; Cantor, K.P. Inorganic arsenic in drinking water: an evolving public health concern. *J. National Cancer Institute*. **2007**, *99*, 906-907.

(2) National Primary Drinking Water Regulations. Environmental Protection Agency. Available on the web at (accessed Aug 1, 2014): http://water.epa.gov/drink/contaminants/upload/mcl-2.pdf

(3) Guidelines for drinking-water quality - Volume 1: Recommendations. Third edition, incorporating first and second addenda. World Health Organization. Available on the web at (accessed Aug 1, 2014):
http://www.who.int/water_sanitation_health/dwq/gdwq3rev/en/

(4) Mukherjee, A.B.; Bhattacharya, P. Arsenic in the groundwater in the Bengal Delta Plain: slow poisoning in Bangladesh. *Environ. Rev.* **2001**, *9*, 189-220.

(5) Arsenic in groundwater of the United States. United States Geological Survey. Available on the web at (accessed Aug 1, 2014):
http://water.usgs.gov/nawqa/trace/arsenic/

(6) Eating Arsenic. *Chemical and Engineering News.* **2013**, *91*, 36-39. Available on the web at (accessed Aug 1, 2014): http://cen.acs.org/articles/91/i18/Eating-Arsenic.html

(7) Analytical Methods Approved for Drinking Water Compliance Monitoring of Inorganic Contaminants and Other Inorganic Consistuents. Revised December 2009. Environmental Protection Agency. Available at (accessed Aug 1, 2014):
http://www.epa.gov/ogwdw/methods/pdfs/methods/methods_inorganic.pdf

(8) T.D. Martin. Method 200.5: Determination of Trace Elements in Drinking Water by Axially Viewed Inductively Coupled Plasma – Atomic Emission Spectrometry. Environmental Protection Agency. Revision 4.2, October, 2003.

(9) J.T. Creed, C.A. Brockhoff, T.D. Martin. Method 200.8: Determination of Trace Elements in Waters and Wastes by Inductively Coupled Plasma – Mass Spectrometry. Environmental Protection Agency. Revision 5.4, 1994.

(10) J.T. Creed, T.D. Martin, J.W. 'Dell. Method 200.9: Determination of Trace Elements by Stabilized temperature Graphite Furnace Atomic Absorption. Environmental Protection Agency. Revision 2.2, 1994.

(11) 3113B, 3114B, 3114B-97, 3113B-99 Standard Test Methods for Arsenic in Water. Standard Methods for the Examination of Water and Wastewater, 21st edition (2005). Available from American Public Health Association, 800 I Street, NW, Washington, DC 20001-3710.

(12) ASTM D2972-03, ASTM D2972-08, ASTM D2972-97 Standard Test Methods for Arsenic in Water. Available from ASTM International, 100 Barr Harbor Drive, West Conshohocken, PA 19428-2959 or http://astm.org

(13) Rodríguez-Lado, L.; Sun, G.; Berg, M.; Zhang,Q.; Xue, H.; Zheng, Q.; Johnson, C.A. Groundwater Arsenic Contamination Throughout China. *Science* **2013**, *341*, 866-868.

(14) Wang, J.; Tian, B.; Wang, J.; Lu, J.; Olsen, C.; Yarnitzky, C.; Olsen, K.; Hammerstrom, D.; Bennet, W. Stripping Analysis into the 21st Century: faster, smaller, cheaper, simpler, and better. *Anal. Chim. Acta* **1999**, *385*, 429-435.

(15) Marei, M.M.; Roussel, T.J.; Keynton, R.S.; Baldwin, R.P. Electrochemical and microfabrication strategies for remotely operated smart chemical sensors: Application of anodic stripping coulometry to calibration-free measurements of copper and mercury. *Anal. Chim. Acta* **2013**, *803*, 47-55.

(16) Ma, J.; Sengupta, M.K.; Yuan, D.; Dasgupta, P.K. Speciation and detection of arsenic in aqueous samples: A review of recent progress in non-atomic spectrometric methods. *Anal. Chim. Acta* **2014**, *831*, 1-23.

(17) Arsenic Factsheet. World Health Organization. Available on the web at (accessed Aug 1, 2014): http://www.who.int/mediacentre/factsheets/fs372/en/

(18) Harvey, C.F.; Ashfaque, K.N.; Yu, W.; Badruzzaman, A.B.M.; Ali, A.M.; Oates, P.M.; Michael, H.A.; Neumann, R.B.; Beckie, R.; Islam, S.; Ahmed, M.F. Groundwater dynamics and arsenic contamination in Bangladesh. *Chemical Geology*. **2006**, *228*, 112-136.

(19) Cullen, W.; Reimer, K. Arsenic speciation in the environment. *Chem. Rev.* **1989**, *89*, 713-764.

(20) Mabuchi, L.;Lilienfeld, A.M.; Snell, L.M. Lung Cancer among Pesticide Workers Exposed to Inorganic Arsenicais. *Arch. Environ. Health* **1979**, *34*, 312-20.

(21) Morita, M. Determination of arsenic species in biological and environmental samples. *Pure Appl. Chem.* **1992**, *64*, 575-590.

(22) Dinan, T.E.; Jou, W.F.; Cheh, H.Y. Arsenic deposition onto a gold substrate. *J. Electrochem. Soc.* **1989**, *136*, 3284-3287.

(23) Dai, X.; Nekrassova, O.; Hyde, M.E.; Compton, R. G. Anodic Stripping Voltammetry of Arsenic(III) using Gold Nanoparticle-Modified Electrodes. *Anal Chem*. **2004**, *76*, 5924-5929.

(24) Yamada, D.; Ivandini, T.A.; Komatsu, M.; Fujishima, A.; Einaga, Y. Anodic stripping voltammetry of inorganic species of As^{3+} and As^{5+} at gold-modified boron doped diamond electrodes. *J. Electroanal. Chem.* **2008**, *615*, 145-153.

(25) Salaun, P.; Gibbon-Walsh, K.B.; Alves, G.M.S.; Soares, H.M.V.M.; van den Berg, C.M.G. Determination of arsenic and antimony in seawater by voltammetric and chronopotentiometric stripping using a vibrated gold microwire electrode. *Anal. Chim. Acta* **2012**, *746*, 53-62.

(26) Bonfil, Y.; Brand, M.; Kirowa-Eisner, E. Characteristics of subtractive anodic stripping voltammetry of Pb and Cd at silver and gold electrodes. *Anal. Chim. Acta* **2002**, *464*, 99-114.

(27) Kounaves, S.P.; O'Dea, J.J.; Chandresekhar, P.; Osteryoung, J. Square Wave Anodic Stripping Voltammetry at the Mercury Film Electrode: Theoretical Treatment. *Anal. Chem.* **1987**, *59*, 386-389.

(28) Feeney, R.; Kounaves, S.P. On-Site Analysis of Arsenic in Groundwater using a Microfabricated Gold Ultramicroelectrode Array. *Anal. Chem.* **2000**, *72*, 2222-2228.

(29) Davis, P.; Dulude, G.; Griffin, R.; Matson, W.; Zink, E. Determination of total arsenic at the nanogram level by high-speed anodic stripping voltammetry. *Anal. Chem.* **1978**, *50*, 137-143.

(30) Fernando, A.R.; Plambeck, J.A. Effects of Background Electrolyte and Oxygen on Trace Analysis for Lead and Cadmium by Anodic Stripping Voltammetry. *Anal. Chem.* **1989**, *61*, 2609-2611.

(31) A.Prieto, J.Hernandez, E. Herrero, J.M. Feliu. The Role of Anions in Oxygen Reduction in Neutral and Basic Media on Gold Single-crystal Electrodes. *J. Solid State Electrochem.* **2003**, *7*, 599-606.

(32) Salaun, P.; Planer-Friedrich, B.; van den Berg, C.M.G. Inorganic arsenic speciation in water and seawater by anodic stripping voltammetry with a gold microelectrode. *Anal. Chim. Acta* **2007**, *585*, 312-322.

(33) Jurica, L.; Manova, A.; Dzurov, J.; Beinrohr, E.; Broekaert, J.A.C. Calibrationless flow-through stripping coulometric determination of arsenic(III) and total arsenic in contaminated water samples after microwave assisted reduction of arsenic(V). *Fresenius J. Anal. Chem.* **2000**, *366*, 260-266.

(34) Hung, D.Q.; Nekrassova, O.; Compton, R.G. Analytical methods for inorganic arsenic in water: a review. *Talanta* **2004**, *64*, 269-277.

(35) Song, Y.; Swain, G.M. Total inorganic arsenic detection in real water samples using anodic stripping voltammetry and a gold-coated diamond thin-film electrode. *Anal. Chim. Acta* **2007**, *593*, 7-12.

(36) Gibbon-Walsh, K.; Salaun, P.; van den Berg, C.M.G. Arsenic speciation in natural waters by cathodic stripping voltammetry. *Anal. Chim. Acta* **2010**, *662*, 1-8.

Chapter IV References

(1) Marei, M.M.; Roussel, T.J.; Keynton, R.S.; Baldwin, R.P. Electrochemical and microfabrication strategies for remotely operated smart chemical sensors: Application of anodic stripping coulometry to calibration-free measurements of copper and mercury. *Anal. Chim. Acta* **2013**, *803*, 47-55.

(2) Prieto, A.; Hernandez, J.; Herrero, E.; Feliu, J.M. The Role of Anions in Oxygen Reduction in Neutral and Basic Media on Gold Single-crystal Electrodes. *J. Solid State Electrochem.* **2003**, *7*, 599-606.

(3) Economou, A. Recent Developments in on-line electrochemical stripping analysis – An overview of the last 12 years. *Anal. Chim. Acta* **2010**, *683*, 38-51.

(4) Beinrohr, E.; Cakrt, M.; Dzurov, J.; Jurica, L.; Broekaert, J.A. Simultaneous Calibrationless Determination of Zinc, Cadmium, Lead, and Copper by Flow-Through Stripping Chronopotentiometry. *Electroanalysis*. **1999**, *11*, 1137-1144.

(5) Tercier-Waeber, M.L.; Buffle, J. Submersible Online Oxygen Removal System Coupled to an in Situ Voltammetric Probe for Trace Element Monitoring in Freshwater. *Environ. Sci. Technol.* **2000**, *34*, 4018-4024.

(6) Kirowa-Eisner, E.; Brand, M.; Tzur, D. Determination of sub-nanomolar concentrations of lead by anodic-stripping voltammetry at the silver electrode. *Anal. Chim. Acta* **1999**, *385*, 325-335.

(7) Bonfil, Y.; Brand, M.; Kirowa-Eisner, E. Determination of nanomolar concentrations of lead and cadmium by anodic-stripping voltammetry at the silver electrode. *Anal. Chim. Acta* **2002**, *457*, 285-296.

(8) Bonfil Y.; Brand, M.; Kirowa-Eisner, E. Characteristics of subtractive anodic stripping voltammetry of Pb and Cd at silver and gold electrodes. *Anal. Chim. Acta* **2002**, *464*, 99-114.

(9) Bi, Z.; Salaün, P.; van den Berg, C.M.G. Determination of lead and cadmium in seawater using a vibrating silver amalgam microwire electrode. *Anal. Chim. Acta* **2013**, *769*, 56-64.

(10) Quintana, J.C.; Arduini, F.; Amine, A.; van Velzen, K.; Palleschi, G.; Moscone, D. Part two: Analytical optimisation of a procedure for lead detection in milk by means of bismuth-modified screen-printed electrodes. *Anal. Chim. Acta* **2012**, *736*, 92-99.

(11) Fernando, A.R.; Plambeck, J.A. Effects of Background Electrolyte and Oxygen on Trace Analysis for Lead and Cadmium by Anodic Stripping Voltammetry. *Anal. Chem.* **1989**, *61*, 2609-2611.

(12) Wang, J.; Polsky, R.; Tian, B.; Chatrathi, M.P. Voltammetry on Microfluidic Chip Platforms. *Anal. Chem.* **2000**, *72*, 5285-5289.

(13) Skolimowski, M.; Nielsen, M.W.; Emneus, J.; Molin, S.; Taboryski, R.; Sternberg, C.; Dufva, M.; Geschke, O. Microfluidic dissolved oxygen gradient generator biochip as a useful tool in bacterial biofilm studies. *Lab Chip* **2010**, *10*, 2162–2169.

(14) Thomas, P.C.; Raghavan, S.R.; Forry, S.P. Regulating Oxygen Levels in a Microfluidic Device. *Anal. Chem.* **2011**, *83*, 8821-8824.

(15) Sandia National Laboratories. A MicroBio Reactor for Hydrogen Production. SANDSAND2003-8794, December 2002; Available at: http://prod.sandia.gov/techlib/access-control.cgi/2003/038794.pdf

(16) Plumere, N.; Henig, J.; Campbell, W.H. Enzyme-Catalyzed O_2 Removal System for Electrochemical Analysis under Ambient Air: Application in an Amperometric Nitrate Biosensor. *Anal. Chem.* **2012**, *84*, 2141-2146.

(17) Pedrotti, J.J.; Angnes, L.; Gutz, I.G.R. A fast, highly efficient, continuous degassing device and its application to oxygen removal in flow-injection analysis with amperometric detection. *Anal. Chim. Acta* **1994**, *298*, 393-399.

(18) Colombo, C.; van den Berg, C.M.G. In-line Deoxygenation for Flow Analysis with Voltammetric Detection. *Anal. Chim. Acta* **1998**, *377*, 229-240.

(19) Billing, C.; Groot, D.R.; van Staden, J.F. Determination of arsenic in gold samples using matrix exchange differential pulse stripping voltammetry. *Anal. Chim. Acta* **2002**, *453*, 201–208.

(20) Hanekamp, H.B.; Voogt, W.H.; Bos, P.; Frei, R.W. An Electrochemical Scrubber for the Elimination of Eluent Background Effects in Polarographic Flow-through Detection. *Anal. Chim. Acta* **1980**, *118*, 81-86.

(21) Adanuvor, P.K.; White, R.E. Oxygen Reduction on Silver in 6.5M Caustic Soda Solution. *J. Electrochem. Soc*. **1988**, *135*, 2509-2517.

(22) Littauer, E.L.; Tsai, K.C. Catalytic Decomposition of Hydrogen Peroxide in Alkaline Solution. *J. Electrochem. Soc*. **1979**, *126*, 1924-1927.

(23) *Permeability Properties of Plastics and Elastomers - A Guide to Packaging and Barrier Materials*, 2nd ed.; Massey, L.K., Ed.; Plastics Design Library Series; William Andrew Publishing: Norwich, NY, 2003. (ISBN 9781884207976)

(24) Carroll, S.; Marei, M.M.; Roussel, T.J.; Keynton, R.S.; Baldwin, R.P. Micro-fabricated electrochemical sensors for exhaustive coulometry applications. S*ens. Actuators, B.* **2011**, *160*, 318-326.

(25) Vaireanu, D.I.; Ruck, N.; Fielden, P.R. Predictive model for coulometric operation in a thin-layer amperometric flow cell. *Anal. Chim. Acta* **1995**, *306*, 115-122.

(26) Han, P.; Bartels, D.M. Temperature Dependence of Oxygen Diffusion in H_2O and D_2O. *J. Phys. Chem*. **1996**, *100*, 5597-5602.

(27) He, C.; Lu, J.J.; Jia, Z.; Wang, W.; Wang, X.; Dasgupta, P.K.; Liu, S. Flow Batteries for Microfluidic Networks: Configuring An Electroosmotic Pump for Nonterminal Positions. *Anal. Chem.* **2011**, *83*, 2430-2433.

(28) Horiuchi, T.; Hayashi, K.; Seyama, M.; Inoue, S.; Tamechika, E. Cooperative Suction by Vertical Capillary Array Pump for Controlling Flow Profiles of Microfluidic Sensor Chips. *Sensors* **2012**, *12*, 14053-14067.

(29) Donaldson, N.; Baviskar, P.; Cunningham, J.; Wilson, D. *J.* The permeability of silicone rubber to metal compounds: Relevance to implanted devices. *Biomed. Mater. Res., Part A* **2012**, *100A*, 588-598.

(30) *CRC Handbook of Chemistry and Physics*, 85th ed.; Boca Raton, FL, 2004.

Chapter V and Appendices References

(1) Zou, Z.; Jang, A.; MacKnight, E.T.; Wu, P.M.; Do, J.; Shim, J.S.; Bishop, P.L.; Ahn, C.H. An On-Site Heavy Metal Analyzer With Polymer Lab-on-a-Chips for Continuous Sampling and Monitoring. *IEEE Sensors Journal* **2009**, *9*, 586-594.

(2) Eggli, R. The detection limit of anodic stripping coulometry at mercury-film glassy carbon electrodes. *Anal. Chim. Acta* **1978**, *97*, 195-198.

Appendix A

The Minimum Measurable Concentration Increment:

C_{min}

In analytical chemistry, the term analytical sensitivity is defined according to **Equation A1**

$$\gamma = m\ /\ \sigma_{signal} \qquad \textbf{(Equation A1)}$$

where m is the calibration sensitivity (i.e., slope) and σ_{signal} is the standard deviation. The smallest measurable concentration difference (C_{min}) is defined as the inverse of the analytical sensitivity according to **Equation A2**

$$C_{min} = \gamma^{-1} \qquad \textbf{(Equation A2)}$$

The C_{min} value reflects the smallest discernible concentration increment (e.g., the relative power of the method to discern samples containing 120 ppb vs. 121 ppb arsenite for instance, or 1 ppb vs. 2 ppb). As shown in this hypothetical example, a C_{min} of 1 ppb is quite satisfactory at high concentrations but is clearly much less so as the analyte

concentration approaches C_{min}. Accordingly, it is useful to represent C_{min} as a percentage

of the measured concentration.

In order to report quantitative values for C_{min}, a few test cases were selected from

the data previously shown in Chapters 2 and 3. These data sets include the determination

of 50 ppb to 7.5 ppm Cu^{2+} and 100 ppb to1 ppm As^{III} in carefully prepared standard

solutions. In order to evaluate the effect of interferents on C_{min}, the same calculations

were performed for experiments where the carefully prepared standards also contained

selected interferents (100 ppb – 1 ppm As^{III} as measured by SEQ-MP-DPS-ASC in the

presence of 1.3 ppm Cu^{2+}, 500 ppb Pb^{2+}, 500 ppb Cd^{2+}, and 5 ppm Zn^{2+}). Similarly,

measurements of arsenite spiked river waters allowed estimation of C_{min} in natural

samples. The specific experimental details for these test cases have been compiled in

Table A1. The resulting C_{min} values for each of the test cases, tabulated in **Table A2**,

indicate that the uncertainty in all measurements performed by SPS-ASC and DPS-ASC

is below 12%, whereas measurements by SEQ-MP-DPS-ASC were typically below 21%.

The only case where C_{min} exceeded 21% was for the determination of arsenite in

the presence of interferents (1.3 ppm Cu^{2+}, 500 ppb Pb^{2+}, 500 ppb Cd^{2+}, and 5 ppm Zn^{2+}).

A closer examination of this data shows that C_{min} was 12, 15, 22, 28, and 87% for

arsenite concentrations of 100, 250, 500, 750, and 1000 ppb, respectively. Hence, C_{min}

was below 22% when the As ppb level was less than Pb and Cd ppb levels. The

interferent levels in that particular study were purposely chosen to be much higher than

would be encountered in any actual sample. The high C_{min} for the 100 ppb and 250 ppb

arsenite solutions (28% and 87%, respectively) noted above caused overestimation of the

actual arsenite concentration. The extent of this overestimation was 29 and 36%,

respectively which indicates imperfect selectivity against Pb and Cd when these metals

are present at high levels, and further discussion of this can be found in that Selectivity

section below. Overall however, these calculations demonstrate the range of C_{min} values

for several metals determined at different times under different conditions using several

variants of potential step ASC. Accordingly, it seems reasonable to expect that most

measurements would have an associated +/- 20% uncertainty. This level of uncertainty is

useful for remote monitoring devices and would hopefully aid in directing the random

sampling by central laboratories to sites where metals are near or above the levels of

concern.

Test Case	Method	Metal Analyzed / Concentration Range	Interferent / Concentration Range	Matrix	Sepatarely Measured Blank Solution or *In Situ* Blank Correction	Potential window of blank (E_{dep}/E_{strip})	Potential Window of Metal Analysis (E_{dep}/E_{strip})
1	SPS-ASC	Cu^{2+} / 50 ppb - 7.5 ppm	none	10 mM HNO_3 & 10 mM NaCl	Separate	0 mV / 500 mV	0 mV / 500 mV
2	DPS-ASC	As^{III} / 100 ppb -1 ppm	none	10 mM HNO_3 & 10 mM NaCl	*In Situ*	-500 mV / 500 mV	-500 mV / 500 mV
3	SEQ-DPS-ASC	As^{III} / 100 ppb -1 ppm	1.3 ppm Cu^{2+} 500 ppb Pb^{2+} 500 ppb Cd^{2+} 5 ppm Zn^{2+}	10 mM HNO_3 & 10 mM NaCl	*In Situ**	-300 mV / 500 mV	-500 mV / 500 mV
4	SEQ-DPS-ASC	As^{III} / 100 ppb -1 ppm	Unknown	As Spiked Ohio River Water (Added HNO_3 to pH 2 and NaCl to 10 mM)	*In Situ**	-300 mV / 500 mV	-500 mV / 500 mV

Table A1: A Summary of select experiments used to calculate the C_{min} and C_{LOD} values within this chapter. **In situ* blank correction utilized a separate aliquot of sample than used for the analysis.

Metal / Concentration / # samples	C_{min} for ideal standards	C_{min} for Interferents spiked standards	C_{min} for real sample
Cu^{2+} / 50 ppb - 7.5 ppm / 17	1-12% [a]	N/A	N/A
As^{III} / 100 ppb -1 ppm / 5	2-5% [b]	12-87%* [c]	1-21% [d]

Table A2: Calculated C_{min} as a percentage of the measured concentration. Superscripts denote the experiment of Table A1 used for the calculation: [a] Test Case 1, [b] Test Case 2, [c] Test Case 3, [d] Test Case 4.

Appendix B

Limits of Detection and Quantification: C_{LOD} and C_{LOQ}

Part 1) Current C_{LOD} and C_{LOQ}

Although C_{min} is a valuable indicator of performance, the most relevant criterion in the context of heavy metal measurements is perhaps the lowest concentration which can be detected and quantified (C_{LOD} and C_{LOQ}, respectively) since even trace metal levels may be of concern. Evaluating the detection limit of stripping coulometry should, in principle, include components such as the reproducibility of the blank (i.e., $3\sigma_{blank}$), the electrode area (which is often a source of noise in electrochemical measurements), the volume sampled (since the low LODs of stripping analysis arises from the pre-concentration effect usually achieved by sampling bulk solutions while stirring to enlarge the sampled volume), and finally the number of electrons in the redox process (since the sensitivity ought to be greater for a 2e⁻ stripping process vs. a 1e⁻ process because the signals are larger in the former case). Combination of all these variables to evaluate the detection limit of anodic stripping coulometry (of which SPS-ASC, DPS-ASC, and SEQ-MP-DPS-ASC are variants) has been previously proposed by Eggli according to

Equation B1 [2]

$$C_{LOD} = (Q_{LOD}) \cdot (A/V) \cdot (1/nF) \qquad \textbf{(Equation B1)}$$

where C_{LOD} is the lowest detectable concentration, Q_{LOD} is the lowest measurable charge per unit area under a particular set of conditions, A is the electrode area, V is the volume sampled, n is the number of electrons in the redox process, and F is the Faraday constant. The evaluation of Q_{LOD} is dependent on the reproducibility of the blank charge and is related to the standard deviation of the blank according to **Equation B2**

$$Q_{LOD} = 3\sigma_{blank} \qquad \textbf{(Equation B2)}$$

Similarly, the lowest concentration which can be quantified (C_{LOQ}) can be evaluated by **Equations B3 and B4**

$$C_{LOQ} = (Q_{LOQ}) \cdot (A/V) \cdot (1/nF) \qquad \textbf{(Equation B3)}$$

$$Q_{LOQ} = 10\sigma_{blank} \qquad \textbf{(Equation B4)}$$

where the blank charge and its standard deviation may be obtained by measurements in a separate blank (metal free) solution as in SPS-ASC, in the same solution after a brief deposition causing negligible metal pre-concentration as in DPS-ASC, or even by a separate DPS-ASC experiment conducted at an entirely different potential as in SEQ-MP-DPS-ASC.

The same data sets used to determine C_{min} above were used to estimate the values of Q_{LOD}. As previously noted, these experiments consisted of multiple types of ASC experiments (including SPS-ASC, DPS-ASC, or SEQ-MP-DPS-ASC variants) for several metals which were determined at a variety of potentials (As: E_{dep} = -500 mV, E_{strip} = 500 mV. Cu: E_{dep} = 0 mV, E_{strip} = 500 mV). The various experimental details are tabulated in **Table A1**. Due to the variations in the metals analyzed, the use of several individual Au electrodes with different histories, and the presence of different interferents, the Q_{LOD} values ranged from 0.6 $\mu C/cm^2$ at best to 3.9 $\mu C/cm^2$ at worst. The electrode area was 0.25 cm^2 and the volume was 1.85 μL for a constant A / V ratio of 135 cm^{-1}, since 4 mm by 8 mm elliptical gold electrodes were used in the same TLC platform for all experiments. The resulting C_{LOD} values are shown in **Table B1** for Cu and As since the calculations were based on ASC experiments for these two metals.

$C_{LOD}=(Q_{LOD})\cdot(A/V)\cdot(1/nF)$		C_{LOD} (ppb)	
Q_{LOD} (C/cm^2)	Area / Volume (cm-1)	Cu (n=2) EPA MCL = 1.3 ppm	As (n=3) EPA MCL = 10 ppb
8.7E-07	135	**38** [a]	N/A
3.9E-06	135	N/A	**135** [b]
3.2E-06	135	N/A	**113** [c]
5.6E-07	135	N/A	**19** [d]

Table B1: Calculated C_{LOD} values based on select experiments shown in bold. Other values are projected based on the Q_{LOD}. Superscripts denote the experiment of Table A1 used for the calculation: [a] Test Case 1, [b] Test Case 2, [c] Test Case 3, [d] Test Case 4.

Part 2) Predicted Enhancement of C_{LOD} and C_{LOQ}

Further improvements of the detection limits ought to obviously seek favorable alterations to the terms of **Equation B1**. The term A / V appears to offer the most direct means of enhancement and is in fact the same term responsible for the sensitivity of conventional stripping analysis where a relatively small electrode area pre-concentrates metals from an effectively infinite bulk volume. In the case of the TLC coulometry platform described in this work, relatively modest and technically feasible alterations can have a significant impact on the A / V term. For instance, the microelectrode array (MEA) shown in **Figure B1** consists of 10 μm diameter openings with 60 μm center to center spacing. This particular MEA offers a 50 fold reduction of the effective electrode surface area while covering the same geometric area as the elliptical 4 mm by 8 mm electrode. Similarly, the TLC platform currently in use offers a cell thickness of about 75 μm. Modestly thicker cells could, in principle, be used without significant increases of the time required for complete deposition (e.g., 225 μm cell would require approximately 200 seconds).

Assuming that the experimentally measured, normalized Q_{LOD} values remain constant per unit area of active electrode surface, future generations of the current TLC platform employing 100 fold smaller area electrodes and 3 times thicker cells would seem to offer useful detection limits. Using the range of experimentally measured Q_{LOD} values under a variety of circumstances along with such a 300 fold reduced A / V ratio allows prediction of the C_{LOD} and C_{LOQ} values. The predicted C_{LOD}s along with the predicted C_{LOQ}s (based on $Q_{LOQ} = 10\sigma_{blank}$) are shown in **Table B2**. These predicted values are, with the lone exception of the Hg C_{LOQ}, below the EPA MCL level for each of

the metals chosen. In conclusion, the sensitivity of ASC cannot rival that of traditional

stripping voltammetry where essentially unlimited improvements of the A / V term are

possible. However, C_{LOD} and C_{LOQ} values suitable for heavy metal detection in drinking

waters appear to be achievable with appropriate design and optimization. This is

especially plausible since drinking water ought to be a sufficiently stable matrix requiring

minimal sample pretreatment. Although natural waters and wastewater effluents may be

highly variable matrices with consequently larger Q_{LOD} and Q_{LOQ} values, the C_{LOD} and

C_{LOQ} requirements in these cases are also less stringent.
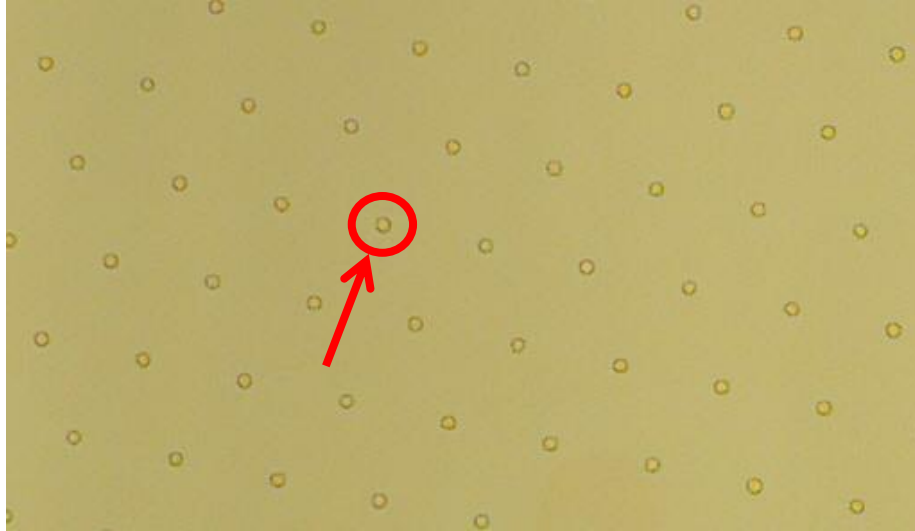
Figure B1: A portion of the Au 4 mm by 8 mm ellipse showing deposited and patterned silicon nitride to expose microelectrode array of 10 μm diameter openings which are 60 μm center to center. Red arrow highlights one of the 10 μm diameter openings.

Metal	EPA MCL (ppb)	Predicted C_{LOD} Range (ppb)	Predicted C_{LOQ} Range (ppb)
As	10	0.06 - 0.45	0.22 - 1.50
Cd	5	0.15 - 1.02	0.49 - 3.39
Cu	1300	0.08 - 0.57	0.27 - 1.91
Pb	15	0.27 - 1.87	0.9 - 6.24
Hg	2	0.26 - 1.81	0.87 - 6.04
Se	50	0.07 - 0.48	0.23 - 1.59
Zn	5000	0.08 - 0.59	0.28 - 1.97

Table B2: Predicted C_{LOD} and C_{LOQ} values based on a 300 fold improvement of the A/V term of Equations B1 and B2 and experimentally measured Q_{LOD}/Q_{LOQ}*values from Table B1. Q_{LOQ} is 10/3 Q_{LOD} according to Equations B3 and B4.

CURRICULUM VITAE

Mohamed M. Marei

Graduate Research Assistant
Department of Chemistry
University of Louisville

2320 S. Brook Street	**862 Ash Street**
Louisville, KY 40292	**Louisville, KY 40217**
(lab) 502.852.6975	**(cell) 513.545.0092**
mmmare01@louisville.edu	mareimm1@gmail.com

www.linkedin.com/pub/mohamed-marei/37/638/41a/

Education

2009-2014   **Ph.D., Analytical Chemistry (August, 2014)**
University of Louisville, Louisville KY
Advisor: Richard Baldwin
Dissertation: Electrochemical and Microfabrication Strategies for Remotely Operated Heavy Metal Sensor Networks for Water Analysis: The Dual Challenges of Calibration-less Measurement and Sample Pretreatment
- Concentration – Electrochemical Measurements, Micro-Electro-Mechanical Systems (MEMS) Design and Fabrication, Microfluidics

2007-2009   **M.S., Biochemistry (August, 2009)**
University of Cincinnati, Cincinnati, OH
Advisor: Pearl Tsang
Thesis: The use of pLysB19, a New Plasmid, for in vitro Transcription of Milligram Quantities of Human Lysyl tRNA and Purification by Urea Denaturing PAGE
- Concentration – Biosynthesis, Purification, and Characterization of Proteins and Nucleic Acids, Enzymatic Activity and Binding Assays

2006   **B.S., Chemistry (June, 2006)**
University of Cincinnati, Cincinnati, OH
Capstone: A Review of the Structural and Functional Domains of HIV-1 Reverse Transcriptase
- Concentration – Biochemistry Degree Option

Research Experience

University of Louisville; Louisville, KY
Graduate Research Assistant

Electrochemistry
- Solved microfluidic flow behavior by fluorescent particle imaging and electrochemically confirmed the achievement of a stopped-flow thin layer cell for coulometric analysis
- Investigated a rarely reported double potential step anodic stripping coulometry (DPS-ASC) technique and established its applicability to calibration-less analysis of heavy metals such as arsenic, copper, and mercury
- Conceptualized and demonstrated successful and passive (sample non-altering) specific removal of dissolved oxygen by indirect electro-reduction in flowing microfluidic sample streams
- Solid understanding of fundamental theory and practical uses of a wide variety of electrochemical techniques including CV, amperometry, coulometry, step and sweep voltammetry, and chronopotentiometry

Microfabrication
- Microfabricated and characterized custom metal on wafer electrodes and microelectrode arrays
- Engineered and realized two generations of platforms for the continuous removal of dissolved oxygen from flowing sample streams along with a custom built dissolved oxygen sensor (amperometric TLC) to evaluate performance
- Capable of original process design and characterization; possess the ingenuity to flexibly adapt available resources to achieve desirable attributes and performance in the final device
- Experienced with a wide variety of microfabrication and characterization techniques including: photolithographic patterning, thin-film depositions, dry/wet etching, ultra-thin membranes

University of Cincinnati; Cincinnati, OH
Graduate Research Assistant

Biochemistry and Microbiology
- Systematized a protocol for bio-synthesis of multi-milligram quantities of human lysyl tRNA by in-vitro transcription
- Developed a simple gel based assay for quantitative evaluation of the charging efficiency of synthesized tRNA with lysine and compared to ^{3}H label based charging assays
- Experienced with a wide variety of bench techniques including bacterial transfections, cell culturing, isolation of DNA and proteins, nucleic acid production by in vitro transcription, PCR, and characterization of nucleic acids and proteins by a variety of gel electrophoresis methods

Awards and Honors

- 2013   **Society for Electroanalytical Chemistry (SEAC) Student Travel Award**
- 2013   **Graduate Student Council Travel Award** (University of Louisville)
- 2008   **Robert M. Koppenhoefer Research Associate Award for Outstanding First Year Graduate Student in Biochemistry** (Chemistry Department, University of Cincinnati)

Grants

- 2013   **Electrochemically Mediated Passive Dissolved Oxygen Removal**
  Intramural Research and Creative Activities Grant (Successfully funded-$500)
  (College of Arts & Sciences, University of Louisville)
- 2012   **Calibration-less Remote Monitoring of Arsenic in Drinking Water**
  Science to Achieve Results Fellowship (Not funded)
  (U.S. Environmental Protection Agency)

Software Skills

- **Extensive experience with 2D (AutoCAD) and 3D (SolidWorks) Computer Assisted Design (CAD); proficient with** Microsoft Office; exposure to labVIEW and MathCAD

Teaching Experience

University of Louisville; Louisville, KY
Graduate Teaching Assistant

200 level Analytical Chemistry Lab Series
- Supervised and encouraged students to understand and execute techniques learned in lecture including titrations, extractions, UV/Vis spectroscopy, and gas chromatography
- Contributed to the conception and method development of honors labs; guided students through their first use of a variety of analytical instrumentation including GC-MS, AAS, CE, and ISE potentiometry

University of Cincinnati; Cincinnati, OH
Graduate Teaching Assistant

200 level Organic Chemistry Lab Series
- Assigned to organic chemistry laboratory by faculty request; coached students as they learned about and used a variety of techniques and instruments including

syntheses, bench-top column chromatography, extractions, re-crystallizations, and characterization by TLC, NMR and FT-IR

500-600 level Biochemistry Lab Series
- Designed and authored an experiment based on in vitro transcription of short tRNA oligomers using T7 RNA polymerase (topic of M.S. Thesis) for upper level biochemistry laboratory

Peer Reviewed Publications

1. **M.M. Marei**, T.J. Roussel, R.S. Keynton, R.P. Baldwin
    A Novel Approach for Electrochemical Dissolved Oxygen Removal from Micro Fluidic Streams for LOC Sample Pretreatment. Analytical Chemistry. <u>Manuscript Accepted July 30, 2014, In Press.</u>

2. **M.M. Marei**, T.J. Roussel, R.S. Keynton, R.P. Baldwin.
    Electrochemical and Microfabrication Strategies for Remotely Operated Smart Chemical Sensors: Application of Anodic Stripping Coulometry to Calibration-free Measurements of Copper and Mercury. Anal. Chim. Acta **803** (2013) 47-55.

3. S. Carroll, **M.M. Marei**, T.J. Roussel, R.S. Keynton, R.P. Baldwin.
    Microfabricated Electrochemical Sensors for Exhaustive Coulometry Applications. Sensors and Actuators B: Chemical **160** (2011) 318-326.

Patent Disclosures

1. 'Electrochemical Removal of Dissolved Oxygen from Sample Streams.' Provisional application. U.S.P.O. #62000267.

Presentations (as Presenting Author)

1. T.J. Roussel, **M.M. Marei**, R.S. Keynton, R.P. Baldwin
    Solar Powered Deoxygenation for Remotely Deployed Coulometric Detection of Heavy Metals
    May 26-30, 2014
    European Materials Research Society Spring Meeting 2014
    Lille, France

2. **M.M. Marei**, T.J. Roussel, R.S. Keynton, R.P. Baldwin
    Electrochemical Determination of As(III) by Subtractive Anodic Stripping Coulometry in a Micro-fabricated Platform
    March 2-6, 2014
    PITTCON Conference & Expo
    Chicago, IL USA

3.   **M.M. Marei**, T.J. Roussel, R.S. Keynton, R.P. Baldwin
        Electrochemical and Microfabrication Strategies for Remotely Operated Smart
        Chemical Sensors: The Dual Challenges of Sample Preparation and Calibration-
        less Measurements
        September 8-12, 2013
        246th ACS National Fall Meeting 2013
        Indianapolis, IN USA

4.   **M.M. Marei**, T.J. Roussel, R.S. Keynton, R.P. Baldwin
        Calibration-free Micro-fabricated Electrochemical Sensor for Heavy Metal
        Determination
        March 19-23, 2013
        PITTCON Conference & Expo
        Philadelphia, PA USA

Presentations (as Co-Author)

1.   R.P. Baldwin, **M.M. Marei**, T.J. Roussel, R.S. Keynton
        Calibration-free Microfabricated Electrochemical Sensor Based on Coulometry
        December 11-14, 2012
        20th Annual Research and Development Conference 2012
        Melbourne, Australia

2.   R. P. Baldwin, S. Carroll, **M. Marei**, T.J. Roussel1, R.S. Keynton
        A Calibration-Free Coulometric Detection System for Remote Sensing
        Applications
        May 8-11, 2011
        9th spring Meeting of the International Society of Electrochemistry
        Turku, Finland

3.   T.J. Roussel, S. Carroll, **M. Marei**, R.S. Keynton, R. P. Baldwin
        A Calibration-Free Coulometric Detection System for Remote Monitoring
        August 28th - September 3rd, 2010
        2010 IEEE International Conference
        Honolulu, HI USA

4.   J.O. Melby, P. Tsang, S. Liu, **M. Marei**, C. Robinson, M. Howell
        Probing the tRNA Binding Properties of Lysyl tRNA Synthetase Anticodon
        Binding Domain
        March 22-26, 2009
        237th ACS National Meeting
        Salt Lake City, UT USA

5.   S.B. Obafemi, C. Robinson, **M. Marei**, M. Howell, P. Tsang
        Investigative Studies of Cognate and Noncognate tRNA Binding by Intact Human
        Lysyl tRNA Synthetase
        April 6-10, 2008
        235th ACS National Meeting
        New Orleans, LA USA

6.   R. Siddiqui, **M. Marei**, P. Tsang
        Optimization and Validation of the in vitro Production of Human Lysyl tRNA
        May 20-23, 2007
        39th Central Regional Meeting of the American Chemical Society
        Covington, KY USA

7.   M.K. Bates, R. Kennedy, K. Musier-Forsyth, M. Howell, P. Tsang, **M. Marei**
        Human Lysyl Aminoacyl tRNA Synthetase and tRNA Binding
        March 25-29, 2007
        233rd ACS National Meeting
        Chicago, IL USA

Leadership and Service

- 2010-2012   **Treasurer**, UofL Chemistry Graduate Student Association
- 2010-Present **Reviewer**, Analytica Chimica Acta

Affiliations

- 2010-Present **Member**, American Chemical Society
- 2010-Present **Member**, The Electrochemical Society
- 2010-Present **Member**, The Society for Electroanalytical Chemistry

Languages

- Native bilingual fluency in English (U.S.) and Arabic (Egypt)

References

Available Upon Request